Titre: Title:	Short-term and long-term experimental response and finite element modelling of partially encased composite columns
Auteur: Author:	Thierry Chicoine
Date:	2001
Type:	Mémoire ou thèse / Dissertation or Thesis
Référence: Citation:	Chicoine, T. (2001). Short-term and long-term experimental response and finite element modelling of partially encased composite columns [Thèse de doctorat, École Polytechnique de Montréal]. PolyPublie. https://publications.polymtl.ca/7053/

UNIVERSITÉ DE MONTRÉAL

SHORT-TERM AND LONG-TERM EXPERIMENTAL RESPONSE AND FINITE ELEMENT MODELLING OF PARTIALLY ENCASED COMPOSITE COLUMNS

THIERRY CHICOINE
DÉPARTEMENT DES GÉNIES CIVIL, GÉOLOGIQUE ET DES MINES
ÉCOLE POLYTECHNIQUE DE MONTRÉAL

THÈSE PRÉSENTÉE EN VUE DE L'OBTENTION
DU DIPLÔME DE PHILOSOPHIAE DOCTOR (Ph.D.)
(GÉNIE CIVIL)

SEPTEMBRE 2001

UNIVERSITÉ DE MONTRÉAL

ÉCOLE POLYTECHNIQUE DE MONTRÉAL

Cette thèse intitulée:

SHORT-TERM AND LONG-TERM EXPERIMENTAL RESPONSE AND FINITE ELEMENT MODELLING OF PARTIALLY ENCASED COMPOSITE COLUMNS

présentée par: CHICOINE Thierry

en vue de l'obtention du diplôme de: Philosophiae Doctor

à été dûment acceptée par le jury d'examen constitué de:

M. LÉGER Pierre, Ph.D., président

M. TREMBLAY Robert, Ph.D., membre et directeur de recherche

M. MASSICOTTE Bruno, Ph.D., membre et co-directeur de recherche

M. CORTHÉSY Robert, Ph.D., membre

M. LÉON Roberto, Ph.D., membre

À ma femme

À ma mère et mon frère

ACKNOWLEDGEMENTS

The author wish to thank its research supervisors, professors Robert Tremblay and Bruno Massicotte, and the technical personnel at Ecole Polytechnique of Montreal, McGill University, and Lehigh University structures laboratories. Funding was provided by Canam Steel Inc. and the Natural Sciences and Engineering Research Council of Canada (NSERC).

The author also wants to acknowledge the financial support of the Steel Structures Education Foundation, and the continuous moral support of his family and friends.

ABSTRACT

A comprehensive study has been conducted to investigate the short-term and long-term behaviour and strength of a new type of partially encased composite (PEC) column made with thin-walled, welded I-section, stiffened with transverse links. Concrete is poured between the flanges of the steel section and the transverse link spacing typically varies from 0.5 to 1 times the depth and the width-to-thickness ratio of the flanges ranges from 23 to 35.

A first series of specimens tested in the scope of this thesis included five large 600 x 600 x 3 000 mm stub-column specimens, to assess any size effect with previously tested smaller specimens of this type. The dimension of these large specimens were close to the size of columns in a real multi-storey building, and marks a clear contrast with the usual size of composite column tests reported in the literature. This series of tests is an important contribution to the existing experimental database on composite stub-columns.

A second series of tests was performed to study the long-term behaviour of four 300 x 300 x 1 500 mm and one 450 x 450 x 2 250 mm stub-column specimens, four of which were loaded for 150 days, following a typical construction sequence. Long-term behaviour of composite columns is less documented because of the technical difficulties involved with the experimental setup. Furthermore, no previous tests to ultimate load were ever done, in the author best knowledge, after applying both a sequence of loading

and a sustained load on composite specimens. The characterization of these specimens long-term and ultimate behaviour also represents an important contribution.

Long-term axial deformations due primarily to creep of the concrete were recorded in long-term specimens and were compared to a prediction model. The relatively higher stresses in the steel shape due to creep and shrinkage of the concrete, and the sequence of loading, had no significant effect on the failure mode and ultimate capacity for this type of column. Failure of all 10 specimens tested to ultimate capacity was due to local buckling of the flanges along with concrete crushing. Tensile transverse stresses measured in the steel section and caused by the expansion of the concrete were found to be small and did not impair the axial compressive strength of the steel section. High stresses, however, developed in the transverse links as a result of the lateral expansion of the concrete. The study also shows that a closer link spacing and the use of additional reinforcements can improve the post-ultimate load behaviour.

Comparison with previous tests revealed that 450 mm and 600 mm specimens behaved in a similar manner. When compared to larger specimens with the same characteristics, a 300 mm specimen did not experience local buckling before peak load, had a more progressive failure, but exhibited the same post-peak response.

The specimens tested were also examined using finite element program ABAQUS. The numerical model accounted for non linear stress-strain behaviour of

materials, residual stresses in the steel shape, initial local imperfections of the flanges, and allowed for large rotations in the solution. The results of the numerical simulations were compared to the experimental response. Non linear analyses on the composite models reproduced accurately the capacity of the specimens, the failure mode, the axial strain at peak load, the transverse stresses in the web, and the axial stresses in the transverse links. The influence of applying a typical construction loading sequence was also well predicted numerically. The successful analysis and validation of a non linear finite element model combining solid elements for the concrete and plate elements for the steel, together with the interaction between the two materials, is considered to be an important achievement.

Based on the experimental and finite element results, a design equation for predicting the axial load capacity, and accounting for local flange buckling, the variation of the concrete strength with column size and quality of structural concrete, is proposed for PEC columns.

CONDENSÉ EN FRANÇAIS

Une étude approfondie a été réalisée pour étudier le comportement structural à court et à long-terme d'un nouveau type de poteau mixte partiellement enrobé, fait de trois plaques d'acier élancées soudées et raidies par des liens transversaux reliant les ailes. Le béton est coulé entre les ailes seulement. L'espacement des liens transversaux peut varier de 0.5 à 1 fois la profondeur du poteau, alors que le rapport d'élancement des ailes d'acier varie de 23 à 35.

Une première série d'essais a été réalisée, dans le cadre de cette thèse, sur 5 poteaux courts de grande dimension, 600 x 600 x 3 000 mm, pour étudier l'effet d'échelle en comparant les résultats avec ceux d'essais effectués précédemment sur des spécimens semblables mais de plus petite dimension. La taille des 5 spécimens testés se rapproche de celle qui serait utilisée dans un vrai bâtiment multi-étagé, et se démarque par leurs dimensions des essais de poteaux mixtes généralement testés et publiés. La réalisation de ces essais constitue une contribution importante à la base de données déjà existante sur les poteaux mixtes.

Une deuxième série d'essais a été réalisée pour étudier le comportement à long-terme de quatre poteaux courts de section 300 x 300 x 1 500 mm et un poteau de 450 x 450 x 2 250 mm, dont quatre furent soumis à une séquence de chargement typique d'un bâtiment et eurent une charge permanente appliquée pendant une période d'environ 150

jours. Le comportement à long-terme des poteaux mixtes est un phénomène qui est peu documenté à cause des difficultés techniques qu'entraîne le montage expérimental. De plus, aucun essai n'avait encore été fait sur des poteaux mixtes soumis à la fois à une séquence de construction et une charge à long-terme. L'étude du comportement à long-terme et à l'ultime de ces spécimens représente aussi une contribution importante.

Les déformations à long-terme des spécimens furent causées principalement par le retrait et le fluage du béton. Ces déformations ont été comparées à des modèles théoriques existants. L'augmentation des contraintes dans l'acier, causée par la séquence de chargement et la redistribution des efforts du béton sur l'acier due aux déformations à long-terme, n'a pas influencé de façon significative le mode de rupture et la capacité axiale des poteaux. Le mode de rupture des 10 spécimens testés dans le cadre de la présente étude s'est produit simultanément par le voilement local des ailes et l'écrasement du béton en compression entre deux liens transversaux adjacents. Les contraintes transversales de traction dans la section d'acier, due à l'expansion du béton, n'ont pas réduit de façon significative la capacité axiale des spécimens. De grands efforts de traction ont toutefois été enregistrés dans les liens transversaux à cause de l'expansion du béton plus accentuée vers la rupture.

La comparaison entre les spécimens testés dans le cadre de cette étude et d'autres poteaux du même type mais de dimensions plus petites testés auparavant a démontré que le comportement des poteaux avec des profondeurs de 450 mm et de 600 mm est très

similaire. Les poteaux avec une profondeur de 300 mm n'ont pas subi quant à eux de voilement local des ailes avant la rupture qui s'est produite de façon plus progressive. Toutefois, le comportement post-pic de tous les poteaux a été semblable. L'étude a aussi montré que des liens transversaux plus rapprochés et l'utilisation de barres d'armature et d'étriers supplémentaires peuvent augmenter la ductilité post-pic des poteaux de ce type.

Le comportement des spécimens testés a aussi été étudié à l'aide de la méthode des éléments finis avec le logiciel ABAQUS. Le modèle d'éléments finis incluait le comportement élasto-plastique des matériaux, les contraintes résiduelles dans la section d'acier, les défauts de rectitude initiaux des ailes, et permettait les grandes rotations. Les résultats des analyses ont été comparés au comportement expérimental des poteaux. Les analyses non linéaires sur le modèle de poteau mixte ont reproduit avec exactitude la capacité axiale, le mode de rupture, la déformation axiale à la rupture, les contraintes transversales dans l'âme de la section d'acier et les contraintes axiales dans les liens transversaux. Les effets de la séquence de chargement et du comportement à long-terme du poteau ont aussi été bien modélisés. L'élaboration et la validation d'un modèle non linéaire de poteau mixte par la méthode des éléments finis, incorporant des éléments de solides pour le béton, des éléments de plaques pour l'acier et des éléments d'interaction entre les deux matériaux, représente une réalisation importante.

En s'appuyant sur les résultats obtenus des essais et des analyses par éléments finis, une nouvelle équation de calcul a été proposée pour déterminer la capacité axiale de

ce type de poteau mixte partiellement enrobé. L'équation de calcul prend en compte le voilement des ailes, la variabilité de la capacité du béton en fonction de la taille du spécimen et la qualité du béton structural comparativement au béton des cylindres.

TABLE OF CONTENT

LIST OF FIGURES

LIST OF TABLES

LIST OF SYMBOLS

A_c = concrete area (mm^2);

A_r = longitudinal reinforcement area (mm^2);

A_s = steel flange area (mm^2);

A_{se} = steel flange effective area (mm^2);

b = flange half-width (mm);

b_e = flange effective width (mm);

b_f = flange width (mm);

d = column depth (mm);

E = elastic modulus (MPa);

E_{ce}= concrete effective elastic modulus (MPa);

f'_c = concrete strength (MPa);

f'_{ce} = concrete effective strength (MPa);

F_y = steel yield strength (MPa);

f_{yr} = longitudinal reinforcement yield strength (MPa);

k = plate buckling coefficient (-);

L = column length (mm);

P_0 = plastic capacity of the composite section (kN);

$P_{u,pred.}$ = predicted ultimate load (kN);

$P_{u,exp.}$ = experimental ultimate load (kN);

r_y = radius of gyration about the weak-axis (mm);

s = transverse link spacing (mm);

t = plate thickness (mm);

δ_0 = local flange out-of-straightness (mm);

ε_a = average longitudinal strain (mm/mm);

λ = plate slenderness ratio (-);

ν = Poisson's ratio (-);

σ_1 = longitudinal stress (MPa);

σ_2 = transverse stress (MPa);

σ_c = average stress in the concrete of the finite element model (MPa);

σ_{fl} = average stress in the flange of the finite element model (MPa);

σ_r = longitudinal residual stress (MPa);

σ_w = average stress in the web of the finite element model (MPa);

ψ = concrete strength modification factor (-).

LIST OF APPENDICES

CHAPTER I

INTRODUCTION

1.1 Background

1.1.1 Existing composite column systems and proposed new design

The name composite column refers to a structural column system made up of two components : a steel shape embedded in or enclosing a concrete volume. Experimental research on composite columns started at the beginning of the 20th century (Talbot and Lord; 1912) but their use in engineering practice really expanded in the 1960's, in the construction of multi-storey buildings.

Using composite columns offers several advantages over traditional reinforced concrete (RC) or steel only columns:

- An increased speed of erection compared to RC columns, because the steel shape is able to carry construction loads and also serves as formwork for the concrete;
- A more cost-effective design, as concrete is a more economical material than steel to carry axial loads;
- Smaller cross-section dimensions for similar axial resistance;
- A better resistance to fire and local buckling than for steel only columns;

Common types of composite column design include concrete filled tubes (CFT) and steel reinforced concrete columns (SRC), as respectively illustrated in Fig. 1.1b and 1.1c. However, these composite column concepts have limitations that may restrict their use in practice. For instance, the cross-section dimensions for small CFTs are limited to available standard steel tube shapes, and larger columns must be custom made. On the other hand, SRC columns require extensive formwork, especially at beam-column connections. The new partially encased composite (PEC) column studied in this thesis (Fig. 1.1a) aims at alleviating these restrictions, as the steel shape is made from plates flame-cut to the desired dimensions, and the beams connect directly to the flanges about the strong axis, or to a plate welded to the flange tips about the weak axis (Vincent, 2000).

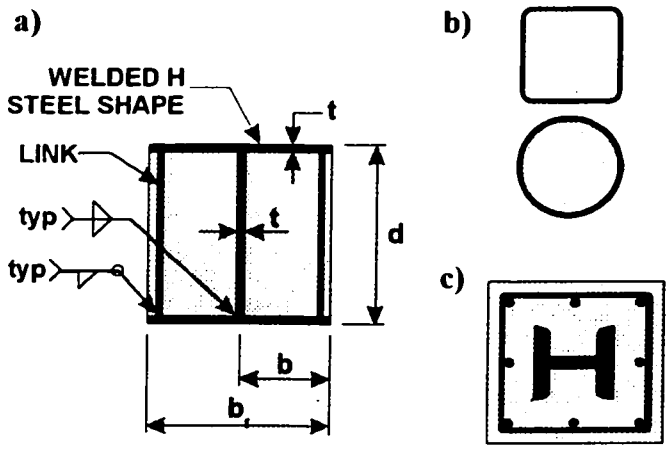

Figure 1.1 Composite Columns: (a) Proposed New Design; (b) CFT; (c) SRC.

This new type of steel and concrete composite column consisting of thin-walled, I-shaped steel section with concrete being poured between the flanges of the steel section has recently been developed and patented by the Canam Manac Group. The steel section features very slender plates exceeding the width to thickness ratio limits for non-compact sections. Transverse links between the flanges are spaced at regular intervals to enhance the resistance of the flanges to local buckling. The proposed composite column is intended to carry only axial loads in multi-storey buildings, the lateral loads being resisted by other structural systems such as shear walls. The new system is also different from partially encased composite column currently used in European practice (CEN-AFNOR, 1994) as the latter is made with hot-rolled standard W-shapes not prone to local buckling. By using thin steel plates in the new column design, the fraction of the load carried by the concrete is increased, leading to more cost-effective columns.

1.1.2 Sequence of loading and long-term behaviour

Figure 1.2 shows the column system at three different stages during construction. The formwork for the columns only consists in plywood sheeting closing the space between the column flange tips. The concrete is poured in the columns one level at a time, while pouring the slab at the level above. For simplicity, the same concrete mix is used for the columns and the slab. According to typical construction sequence, the steel shape alone must be able to carry, without the contribution of the concrete, the dead load and construction live loads for up to 12 floors, including three floors where the slab is

poured. The composite section will carry other loads that are applied subsequently. This construction sequence results in relatively higher stresses in the steel. The shrinkage and creep of the concrete induce, by friction, axial strains in the steel shape of a composite column. This additional stress in the steel shape will not influence the axial capacity of the column if the full section is capable of yielding. In the proposed new design, however, the steel shape features slender plates that may be prone to local buckling. The effect of long-term deformation in the concrete could, therefore, reduce the overall capacity of the composite column if premature buckling occurs.

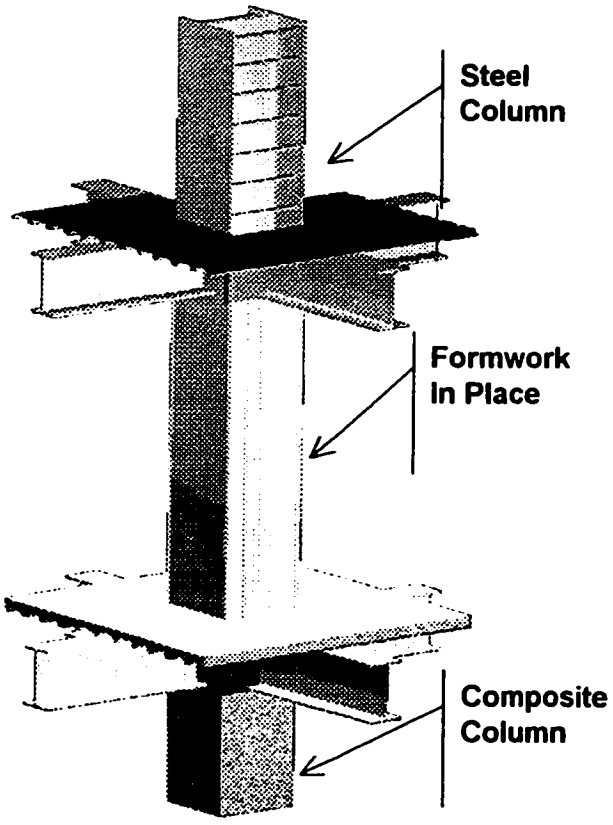

Figure 1.2 Construction Stages for Partially Encased Composite Column

1.1.3 Previous studies on partially encased columns

This study follows up on an experimental programme by Tremblay et al.(1998) who reported on a first series of tests on the new column system and proposed a design equation accounting for local flange buckling. The specimens tested included six composite stub columns with a cross-section of 300 x 300 mm and 450 x 450 mm.

1.2 Project objectives

The objectives of the project may be divided into three parts, each corresponding to the objectives listed in the three articles presented in Appendices A to C.

1.2.1 Paper 1 objectives

The objectives presented in the first paper (Appendix A) were to:

- Evaluate possible size effects on the ultimate load and the failure mode of specimens with larger cross-section and compare with the results from tests on smaller specimens (Tremblay et al., 1998);
- Assess the need for additional reinforcement such as longitudinal rebars and stirrups;
- Obtain experimental data on the magnitude of transverse stresses in the steel shape and the links due to the lateral expansion of the concrete.

1.2.2 Paper 2 objectives

The objectives presented in the second paper (Appendix B) were to:

- Evaluate experimentally the behaviour of the proposed column system under typical construction loading sequence and long-term loading, and obtain data on the effects of creep and shrinkage on the deformations and stresses in the steel and the concrete;
- Check the applicability to predict the long-term deformations in both materials with existing analytical models developed for plain concrete;
- Evaluate the influence of creep and shrinkage of the concrete on the ultimate axial capacity of the columns and on its behaviour near peak load, including the failure mode of the column, the ultimate strain, the steel shape transverse stresses, and the transverse link stresses.

1.2.3 Paper 3 objectives

The objectives presented in the third paper (Appendix C) were to reproduce numerically, using a finite element model, the key results from previously tested specimens, including:

- The peak load of the specimens;
- The strain at peak load;
- The modes of failure;
- The transverse stresses in the web of the steel shape;

- The axial stresses in the transverse links;
- The effects of loading sequence and long-term loading for some specimens.

A new design equation for the axial capacity of the PEC columns was to be derived from the experimental and finite element analyses.

1.3 Project scope

The scope of each paper is presented herein. The characteristics of the specimens in each test programme are presented in more details in Chapter III.

1.3.1 Scope of Paper 1

The first paper describes the test on five composite stub-columns having a 600 mm x 600 mm cross-section, and a height of 3 000 mm. The plate thickness and the transverse links spacing were varied in the series of test. One of the five large stub-columns had additional reinforcement consisting of longitudinal rebars and transverse U-shaped stirrups with the same spacing as the transverse links attached to the flanges of the steel shape.

1.3.2 Scope of Paper 2

The test programme reported in the second paper included a total of seven composite stub-columns. Five specimens were 300 x 300 mm and two had a 450 x 450 mm cross-section. All specimens had a height of 5d. Strain readings were taken on each specimen over a measurement period of approximately 150 days to determine long-term axial deformations. Four of the specimens were loaded according to anticipated construction sequence, and five columns were tested to ultimate capacity.

1.3.2 Scope of Paper 3

The numerical analyses presented in the third paper were performed on finite element models of five specimens presented in the first paper, five specimens from the second paper, and four specimens tested by Tremblay et al. (1998). The finite element program ABAQUS had the capacity of modelling residual stresses, local flange imperfection, and non linear materials behaviour. The parameters studied were the flange slenderness ratio, the transverse link spacing, the specimen size, and the long-term effects.

CHAPTER II

LITTERATURE REVIEW

2.1 Short-term experimental programmes on existing composite column systems

Extensive experimental studies have been performed on concrete-filled tubes, CFT (Furlong, 1967; Gardner and Jacobson, 1967; Knowles and Park, 1970; Tomii et al., 1977) and steel reinforced columns, SRC (Stevens, 1965; Bridge and Roderick, 1978; Johnson and May, 1978; SSRC, 1979; Ricles and Paboojian, 1994) and design procedures have been developed for these systems (Saw and Liew, 2000).

Gardner and Jacobson (1967) first demonstrated experimentally that adding the individual load contributions from the steel and the concrete represents well the capacity of short CFT columns if adjustments are made to account for the confinement effects. The steel shape in a composite column acts as a restraint to the volumetric expansion of the concrete, especially near peak load when the concrete expands rapidly. The confinement pressure, or hoop stresses, exerted by the walls of the steel shape on the concrete creates a favourable triaxial state of stresses in the concrete that improves its axial capacity. The confinement pressure, however, as the opposite effect on the steel shape, creating transverse tensile stresses thus reducing the axial capacity of the steel shape. The global effect on the capacity of the composite column is generally beneficial

since the area of concrete is greater than that of the steel cross-section. The effects of confinement were found to be greater in the CFT columns than in the SRC columns because the concrete is encased on all four sides in the former and only on two sides for the latter. O'Shea and Bridge (2000) proposed several design methods to estimate the strength of thin-walled CFT columns under different loading conditions. The loading conditions examined included axial loading of the steel only, axial loading of the concrete only, and simultaneous loading of the steel and the concrete with and without eccentricity of the load. The tubes tested were short columns, with a length–to-diameter ratio of 3.5 and a diameter-to-thickness ratio between 60 and 220, meeting the definition of thin-walled sections. The concrete cylinders had a nominal strength ranging from 50 to 120 MPa. The tests revealed that the concrete confinement effect was maximum when only the concrete was loaded, while the steel acted as passive lateral restraint. The authors found that the bond between the steel and the concrete was critical in determining the formation of local buckling. In tests where the steel and the concrete were loaded simultaneously, local buckling of the tube did not occur if there was sufficient bond between the two materials. The authors reported that the European Standard Eurocode 4 (1994) matched the most adequately the ultimate strength of their specimens. The predicted capacities was better estimated when including the effects of concrete confinement for concrete strength not exceeding 80 MPa, and with no reduction in the steel shape for local buckling. The authors recommended not to take into account the increase in concrete strength due to confinement for specimens with a concrete strength exceeding 80 MPa because of the lower lateral expansion of the concrete. Moment-axial

load interaction was also well represented using the provisions of Eurocode 4. Knowles and Park (1970) proposed formulas for determining the global buckling load of slender CFT columns. The authors represented the composite column capacity as the summation of the buckling capacities of the steel and the concrete elements acting independently, and compared favourably these predictions with experimental work. This procedure was adopted by Canadian Standard S16.1 (CSA, 1994b) for the design of slender composite columns.

Local buckling in CFT columns has also been studied and documented. Ge and Usami (1992) examined the strength of concrete-filled thin-walled steel box columns, with and without longitudinal stiffeners. Six specimens, with a depth ranging from 200 mm to 350 mm, were tested under cyclic compressive loads, and the effect of plate width-to-thickness ratio and stiffener rigidity was examined. An empirical reduction factor of 0.7 was applied to the cylinder concrete strength, f'_c, to account for the size effect of the filled-in concrete, and the local buckling strength of the plate panel in composite columns was then compared with available empirical design formulas for thin-walled steel member in compression. The authors proposed lower and upper bound equations for the local buckling capacity of the plates, based on the concept of effective width. Significant improvement in the steel column capacity was also observed when increasing the rigidity of the stiffeners. Uy (2000) also conducted an experimental programme on concrete filled thin-walled steel box columns. The capacity of the steel component was found to be well modelled using the effective width concept. The author

also suggested to use the full plastic capacity of the concrete for the concrete component. The plate buckling capacity prediction model proposed by Ge and Usami seems, however, more appropriate because the steel contribution was estimated from the experimental results, while Uy only considered the overall capacity of the composite column. Wright (1993) proposed formulas predicting the buckling strength of plates in contact with a rigid medium, based on energetic methods. Several cases were investigated, such as the local buckling of the flange of an I-beam partially encased in concrete, and the flange of a tube in-filled with concrete.

Experimental programmes on SRC columns are also well documented in the literature. Bridge and Roderick (1978) examined the behaviour of slender built-up composite columns made up of a pair of channels encased in concrete, and loaded as pin-ended members. The authors proposed theoretical analyses of column biaxial bending capacity, taking into account the full range of linear and non linear characteristics of the materials. Tested specimens confirmed the validity of the prediction model. Ricles and Paboojian (1994) studied the experimental behaviour of SRC columns made up of steel rolled W-beam encased in concrete, and loaded under cyclic loading. The composite columns consisted of a W8x40 shape encased in a 400 x 400 mm reinforced concrete column, with different configurations of shear stirrups, longitudinal rebars, and shear studs welded to the flanges. The parameter studied included the degree of concrete confinement, the effectiveness of flange shear studs, and the shear resistance of the column. The results of the study indicated that SRC columns possess good cyclic strength

and ductility if buckling of the longitudinal reinforcement is inhibited. The encased steel shape was found to provide the primary resistance to transverse shear, with the shear studs welded to the flanges were found not to be effective in enhancing the flexural resistance to lateral loading. The authors also that the specimens combined axial and flexural behaviour was conservatively modelled using Standard ACI 318 (1992), based on full composite action.

2.2 Standardised models for predicting the axial capacity of composite columns

Construction Standards in North America and Europe present the axial capacity of a composite column as the summation of the axial capacities of the steel and the concrete components. Two design philosophies exist, however, for taking into account the global slenderness of the column:

- The stiffness of the steel and the concrete components are determined independently to compute independent buckling capacities that are then added together to obtain the buckling capacity of the composite column (CSA S16.1, 1994).
- The stiffness of the steel and the concrete sections are transformed into an equivalent stiffness used in the calculation of the global buckling load (CSA A23.3, 1994; LRFD, 1993; CEN Eurocode 4, 1994).

2.2.1 Canadian Standards CSA S16.1-94 and A23.3-94

Canadian Standards CSA S16.1-94 and A23.3-94 present methods for designing concrete-filled tubes (CFT) and steel reinforced (SRC) composite columns, respectively.

In Standard S16.1-94, the axial capacity of the composite section, C_{rc}, is computed as the summation of the capacities of the steel section, C_r, and the concrete section, C'_r, acting independently, as shown in the following equation,

$$C_{rc} = \tau C_r + \tau' C'_r \tag{2.1}$$

where τ and τ' are coefficients accounting for the effects of concrete confinement.

The axial capacities of the steel and the concrete are determined from Eqs.(2.2) and (2.3) as a function of the slenderness ratio of each component, λ_s and λ_c, respectively,

$$C_r = \phi_s A_s F_y \left(1 + \lambda_s^{2n}\right)^{-\frac{1}{n}} \tag{2.2}$$

where ϕ_s is the performance factor for steel (0.9), A_s is the steel cross-section area, F_y is the yield stress of the steel, λ_s is the slenderness ratio of the steel only column, and n is a parameter taking into account the effects of residual stresses and initial imperfections, which depends on the type of columns. A value of n equals 1.34 is used for hot-rolled I-shapes, Class 1 to 3, and for Category C tubular shapes, and a value of n equal to 2.24 is

used with WWF and Category H tubular sections. For PEC columns, Eq. (2.2) could be modified to account for the local buckling of the Class 4 flanges.

In Standard S16.1-94, the axial capacity of the concrete component is:

$$C_r' = 0.85\phi_c f_c' A_c \lambda_c^{-2}\left(\sqrt{1+0.25\lambda_c^{-4}} - 0.5\lambda_c^{-2}\right) \qquad (2.3)$$

where ϕ_c is the performance factor for the concrete (0.6), f'_c is the concrete ultimate strength, A_c and λ_c are respectively the concrete cross-section area and slenderness ratio (Eq. 2.4),

$$\lambda_c = \frac{KL}{r_c}\sqrt{\frac{f_c'}{\pi^2 E_c}} \qquad (2.4)$$

where KL is the effective length of the column, r_c is radius of gyration of the concrete section, and E_c is the concrete elastic modulus, with $E_c=5000(f'_c)^{1/2}$. Equation (2.3) is based on the one presented in Knowles et Park (1970) for the calculation of the buckling capacity of a concrete column, and based on the concept of the tangential elastic modulus. The procedure was also validated experimentally.

Canadian Standard A23.3-94 presents a design procedure for steel reinforced composite columns. The axial capacity of the column, P_{rmax}, is determined as:

$$P_{r\max} = \gamma e\left\{\alpha_1\phi_c f_c'(A_g - A_{st} - A_t) + \phi_s f_y A_{st} + \phi_a F_y A_t\right\} \qquad (2.5)$$

where γe is a reduction factor accounting for accidental eccentricity of the load and potential of sustained axial load, and is equal to 0.8 or 0.85 for a column with rectangular or spiral shear reinforcement, respectively. The factor α_1 is a stress block coefficient for modelling the concrete stresses at the ultimate limit state. Parameters ϕ_c, ϕ_s, and ϕ_a are materials performance factors for the concrete, the reinforcing steel (rebars) and the embedded steel shape, equal to 0.6, 0.85, and 0.9, respectively. Parameters A_g, A_{st}, and A_t are the cross-section areas for the gross section, the rebars, and the steel section, respectively. Parameters f'_c, f_y et F_y are the ultimate limit stresses for the corresponding materials.

Standard A23.3-94 accounts for the overall slenderness of the column by considering secondary P-delta moments and the elastic buckling load of the transformed cross section.

2.2.2 U.S. Standards LRFD-93

U.S. Standard LRFD-93 presents a procedure to calculate the axial capacity of CFT and SRC columns. The capacity of the column is obtained by considering an transformed equivalent steel section, defined as follows:

$$P_u = \phi_c A_s F_{cr} \tag{2.6}$$

where P_u is the factored axial capacity of the composite column, ϕ_c is a performance factor for the compression (0.85), A_s is the cross section area of the steel shape, and F_{cr} is

the equivalent ultimate stress in the steel accounting for overall buckling of the transformed section. The stress F_{cr} is calculated as follows:

$$0.85F_{cr} = 0.85(0.658^{\lambda_c^2})F_{my} \quad \text{if} \quad \lambda_c \leq 1.5 \tag{2.7}$$

$$0.85F_{cr} = 0.85\frac{0.877}{\lambda_c^2}F_{my} \quad \text{if} \quad \lambda_c > 1.5 \tag{2.8}$$

where λ_c is the composite column slenderness ratio (Eq.2.9) and F_{my} is the steel modified elastic stress (Eq. 2.10) which includes the properties of the concrete component.

$$\lambda_c = \frac{KL}{r_m \pi}\left(F_{my}/E_m\right)^{0.5} \tag{2.9}$$

where r_m is the greater radius of gyration of the steel only section or the gross cross section (AISC, 1979), but lower than 0.3 times de column width, and E_m is the steel modified elastic modulus (Eq. 2.11).

$$F_{my} = F_y + c_1 F_{yr}\left(A_r/A_s\right) + c_2 f_c^{'}\left(A_c/A_s\right) \tag{2.10}$$

where A_r is the area of longitudinal reinforcement, and c_1 and c_2 are non dimensional factors presented in Table 2.1.

$$E_m = E_s + c_3 E_c\left(A_c/A_s\right) \tag{2.11}$$

where c_3 is a non dimensional factor also presented in Table 2.1

TABLE 2.1. Parameters c_1, c_2, and c_3 of LRFD-94 procedure

	c_1	c_2	c_3
CFT columns	1.0	0.85	0.4
SRC columns	0.7	0.6	0.2

Parameters c_1 and c_2 for CFT columns are the same as those used for the design of reinforced concrete columns. Parameter c_2 takes into account the strength difference between cylinder and structural concrete. Parameters c_1 and c_2 for SRC columns are set to 70% of those for the CFT columns. This reduction provides a safety margin since the concrete in SRC columns, which is only confined by the longitudinal reinforcement, is likely to spall and may not reach $0.85f'_c$ at column failure. The concrete stiffness in slender composite column is very dependant on the amount of cracking and creep due to long-term loading. AISC (1979) thus recommends a conservative estimate of the concrete stiffness in Eq. 2.11, as shown with the low values of c_3.

2.2.3 European Standard Eurocode 4-94

Eurocode 4-94 applies to composite construction in Europe and presents design procedures for CFT and SRC composite columns. The factored axial capacity, N_r is obtained using Eq. (2.12) for SRC columns and Eq. (2.13) for CFT columns.

$$N_r = A_a \frac{f_{ya}}{\gamma_{Ma}} + 0.85 A_c \frac{f_c'}{\gamma_c} + A_s \frac{f_{ys}}{\gamma_s} \tag{2.12}$$

$$N_r = A_a \frac{f_{ya}}{\gamma_{Ma}} + A_c \frac{f_c'}{\gamma_c} + A_s \frac{f_{ys}}{\gamma_s} \tag{2.13}$$

where γ_{Ma}, γ_c, and γ_s are materials performance factor for the steel shape, the concrete, and the longitudinal reinforcement, equal to 1.1, 1.5, and 1.15, respectively.

Eurocode 4 limits the concrete stress to 0.85 f'_c in SRC columns due to possible loss of cover, but allows to use the full capacity of the concrete f'_c for CFT columns, because of a better confinement. Therefore, Eurocode 4 is more liberal than Standard LRFD which allows to take only 0.85 times f'_c for CFT columns and 0.6 times f'_c for SRC columns. An additional strength increase due to confinement is permitted in CFT if the slenderness of the column is small.

As in S16.1-94, the global stability of the column is taken into account by multiplying the cross-section capacity by a reduction factor, χ, accounting for the column slenderness, defined in the following equations.

$$N_f \leq \chi \, N_r \tag{2.14}$$

where

$$\chi = \frac{1}{\phi + \sqrt{\phi^2 - \lambda^2}} \leq 1 \tag{2.15}$$

and N_f is the slender column capacity, and ϕ and λ are slenderness parameters computed with Eqs. (2.16) and (2.17).

$$\phi = 0.5\left[1 + \alpha(\lambda - 0.2) + \lambda^2\right] \tag{2.16}$$

$$\lambda = \sqrt{\frac{N_r}{N_{cr}}} \tag{2.17}$$

where α is equal to 0.21 for CFT columns, 0.34 for SRC columns in strong axis bending, and 0.49 for SRC in weak axis bending. In Eq. (2.17), N_r is the cross-section capacity computed in Eqs. (2.12) and (2.13) with the material performance factors set to 1. N_{cr} is the elastic buckling load, calculated using Eq. (2.18).

$$N_{cr} = \frac{\pi^2 (EI)_e}{(KL)^2} \tag{2.18}$$

where $(EI)_e$ is an equivalent moment of inertia of the composite column, as defined in Eq.(2.19).

$$(EI)_e = E_a I_a + 0.8 E_{cd} I_c + E_s I_s \tag{2.19}$$

where I_a, I_c , and I_s are moments of inertia of the steel shape, the uncracked concrete section, and longitudinal reinforcement, respectively. The factored elastic modulus of the concrete, E_{cd} , is equal to $E_{cd} = E_{cm}/\gamma_c$, where E_{cm} is the secant concrete modulus and γ_c a stiffness reduction factor accounting for cracking and long-term effects, and equal to 1.35.

2.3 Short-term experimental programmes on partially encased composite column systems and prediction model for axial capacity

Research has also been carried out on partially encased columns with W-shapes (e.g. Hunaiti and Abdel Fattah, 1994; Elnashai et al., 1995; Plumier et al., 1995). Elnashai et al. (1995) examined the seismic behaviour of W-shape beam-columns with concrete poured between the flanges only. The steel shape also featured steel bars welded to the tip of the flanges and spaced at regular intervals. These transverse links improved the buckling capacity of the steel flanges and allowed the composite column to maintain its structural integrity. The authors observed that this composite system exhibited a ductile behaviour under cyclic loading.

These tests, however, were made with a stocky, hot-rolled steel shape, which did not experience local buckling during static loading. The steel shape of the PEC column studied in this thesis is made up of slender plates prone to local buckling prior to reaching the ultimate capacity of the column. Filion (1998), Tremblay et al. (1998), and Maranda (1999) conducted small scale tests on 7 partially-encased composite columns with built-up steel shapes. The depth of the square cross section ranged from 300 mm to 450 mm, and normal strength concrete (30 MPa) was poured between the flanges only. These columns all had a height-to-depth ratio of five, qualifying as stub-columns. The steel shape featured thin plates with a width-to-thickness ratio ranging from 23 to 35, and with transverse links between the flanges, placed at regular intervals, to improve local buckling capacity, shear transfer and structural integrity between the concrete and the

steel. The specimens failed by local buckling of the steel flanges and crushing of the concrete. Tremblay et al. (1998) proposed a first set of design equations for predicting the ultimate load ($P_{u,pred.}$) of this type of composite column. These equations were based on experimental results and accounted for local buckling of the flanges by the use of an effective width which is a function of b/t and the link spacing:

$$P_{u,pred.} = 0.85 A_c f'_c + A_{se} F_y + A_r f_{yr} \tag{2.20}$$

$$A_{se} = (d - 2t + 2b_e)t \tag{2.21}$$

$$\frac{b_e}{b_f} = \frac{0.6}{\lambda_p} \leq 1.0 \tag{2.22}$$

$$\lambda_p = \frac{b}{t}\sqrt{\frac{12(1-\nu^2)F_y}{\pi^2 Ek}} \tag{2.23}$$

$$k = \frac{4}{(s/b)^2} + \frac{15}{\pi^4}(s/b)^2 + \frac{20}{3\pi^2}(2-3\nu) \tag{2.24}$$

In Eqs. (2.20) to (2.24), A_c is the concrete area, A_{se} is the steel effective area accounting for local buckling, A_r and f_{yr} are the area and the yield strength of the longitudinal reinforcement, b_e is the total effective width of one flange, λ_p is the slenderness ratio for the flanges, and k is the plate buckling coefficient dependant on the s/b ratio. Using Eqs.(2.20) to (2.24), the test-to-predicted ratio for specimens tested was 0.99 with a standard deviation of 0.022.

2.4 Additional research needs on partially encased composite columns

A new series of short-term tests needs to be carried out to assess any scale effects on the column axial capacity of PEC columns. It as been confirmed experimentally (Neville, 1966) that the strength of concrete cylinders decreases as their cross sectional dimensions increase. The previous tests on PEC columns were done on small specimens, with a cross section of 300 x 300 and 450 x 450 mm, while the actual column size in a real building could be 900 x 900 mm or even larger. Furthermore, no study on the cross-sectional scale effect was previously reported in the literature on composite columns.

New tests are also needed on PEC columns to confirm the reduced effect of confinement on the concrete (Filion, 1998) and measure if there is any detrimental effect on the steel section due to hoop stresses. These results should confirm whether PEC columns offer limited confinement as in SRC columns, or if any confinement is introduced with the presence of the transverse links between the flanges in PEC columns. Confinement effects in PEC columns, however, are expected to be less than for CFT columns since the concrete is confined on only three sides.

Additional testing on PEC columns are also needed to better characterise the local buckling of the steel shape. Test results should determine if existing theoretical models for the buckling capacity of the steel shape (Filion, 1998, Tremblay et al., 1998) may be adapted to larger PEC columns. These design equations need to be validated and

modified, if necessary, to account for the effects of column size, concrete confinement, and local buckling of the flanges. Existing standardised procedures for composite columns in Canada, United States, and Europe may provide some guidelines to formulate the new design equations. For the calculation of the axial cross-section axial capacity of PEC columns, the procedure proposed by S16.1, A23.3, and Eurocode 4 seems more appropriate. The contribution of each component, steel shape, concrete core, and longitudinal reinforcement, is calculated independently and summed together. This approach is simpler than the LRFD method using transformed properties for the cross section capacity. The summation method also allows to modify one of the component to account easily for specific modifications, i.e. local buckling of the flanges in the steel shape, confinement effects in the steel shape and the concrete, long-term effect on each materials. A concrete strength of 0.85 f'_c also seems a good estimate for computing the capacity of the concrete component in PEC columns, due to limited confinement expected to be offered by the thin plates. At ultimate limit states, the reduction in capacity for the concrete proposed by the different Standards are: 0.85 x 0.6= 0.51 for S16.1, 0.8 x 0.6 = 0.48 for A23.3, 0.85 x 0.6 = 0.51 for LRFD, and 0.85/1.5 =0.53 for Eurocode 4. Similar values should be used for the design of PEC columns.

In Standard S16.1 (CSA,1994), the buckling load is determined based on the inertia of individual materials acting independently, as if no interaction existing between the two. This approach is deemed too conservative since the composite column is stiffer than the summation of a steel and a concrete column acting separately. For computing the

buckling capacity of slender composite columns, the transformed moment of inertia method proposed by Eurocode 4 seems the appropriate and would be therefore considered for the design of slender PEC columns.

2.5 Long-term behaviour of composite columns

This section complements the literature review presented in the second paper (Appendix B). Despite the wide range of experimental data on the short-term strength and behaviour of composite columns (e.g. Gardner and Jacobson, 1967; Knowles and Park, 1970; Bridge and Roderick, 1978; Elnashai et al., 1995), and the literature on the long-term behaviour of plain concrete (Ghali and Favre, 1994; Neville et al., 1983; ACI, 1992), few references document the long-term behaviour of composite columns.

Furlong (1967) noted the effect of concrete relaxation on the axial capacity of a CFT when the load decreased by 10 to 15 % while the displacement was held constant, after the steel had yielded. Bode (1976) suggested that the concrete in CFT columns is subjected to shrinkage and creep, but to a lesser extent than in conventional reinforced concrete columns because the steel shape would offer more restraint to the deformations and because the exchange of humidity with the external environment is mostly prevented. Bode notes that creep and shrinkage of concrete may reduce the axial capacity of slender columns and that a correction should be made to reduce the elastic modulus of the concrete in the design equations. Bradford and Gilbert (1990) proposed a method to

determine the time-dependant behaviour of composite columns subjected to an eccentric axial load. The age-adjusted effective modulus method was used to reduce the concrete elastic modulus in the calculations of the buckling load and a stiffness reduction factor of 0.35 was found to be adequate. Stelco (1981) proposed to modify the uniaxial stress-strain relationship of the concrete to account for the long-term behaviour of concrete. The strain may be doubled at a given load level, up to the ultimate strength of the concrete, effectively halving its elastic modulus.

Existing standards for the design of the axial capacity of composite columns account for long-term behaviour of the concrete exclusively by modifying its elastic modulus, thus affecting the buckling load of more slender columns. In the Canadian Standard S16.1 (CSA, 1994) and European Standard Eurocode-4 (CEN,1994) the elastic modulus of the concrete by a factor of $(1 + S / T) / 2$, where S and T represent the short-term and total loads, respectively. The LRFD method also reduces the elastic modulus of the concrete, by multiplying it by 0.4 for CFT columns and 0.2 for SRC columns, to account for the effects of creep and cracking on the buckling load (factor c_3 in Table 2.1).

Nakai et al. (1991) conducted an experimental study on the creep of concrete filled steel pipes. They noted that while the long-term deformations in the concrete does not affect the ultimate strength, they may become important for serviceability limit states. A total of six specimens, which had a height of 1 m and a 165 mm diameter were tested by applying a long-term concentric axial load. Three of these specimens were loaded with

a prestressing bars setup for a period of 160 days, during which the load was not readjusted and strain measurements were taken to measure the column strain caused by the creep and shrinkage of the concrete. The other three specimens were not loaded and were used to record the strain caused by the shrinkage of the concrete. After 160 days, it was found that the shrinkage strain in the concrete of the CFT column was about 30 με, while that in a reference concrete-only column was about 300 με. The final creep strain, measured in the concrete and the steel shape, were respectively 100 and 50 με. The ratio of total (elastic and creep) to elastic strain ranged from 1.4 to 1.6, compared to 2.8 for the tested concrete reference specimens. The authors concluded that the creep phenomenon in CFT columns is smaller than that in plain concrete structures, and that the concrete shrinkage strain may be neglected for this composite system.

Uy (2001) conducted an experimental programme to assess the shrinkage and creep effects in short concrete-filled steel box columns under sustained loading. High-strength concrete was used in the experiments. The maximum shrinkage strain after 140 days was 160 με in the composite columns, and 600 με in the companion concrete cylinders. These shrinkage strains for the CFT specimens were larger than those obtained in CFT columns tested by Nakai et al. (1991) and Terrey et al. (1994), both reporting values of 30 με at 130 days, while the strain in reference concrete-only specimens ranged from 300 με to 500 με. De Larrard (1999) noted that the shrinkage strain of plain concrete is composed of two components: drying and autogenous shrinkage. The first type of shrinkage is negligible in CFT columns since the encased concrete is not exposed

to ambient environment. The latter type results from the chemical reaction of the cement paste with water, and is typically higher for high-strength concrete. The ratio of creep strain to elastic strain was found to be 0.7 for the CFT specimens (Uy, 2000), values comparable to those obtained by Nakai et al. (1991), Terrey et al. (1994), and Morino et al. (1996) under similar loading conditions, respectively 1.5, 1.1 and 0.5. The ratio of creep-to-elastic strains ranged from 2.7 to 2.8 for plain concrete reference columns (Nakai et al., 1991). Fintel et al. (1987) describe the strain measurements made on a large reinforced concrete column of a tall building. They reported long-term strains on the order of 104 με for shrinkage and 65 με for creep.

The experimental results on CFT columns, however, may not be compared directly to those presented in this paper since shrinkage and creep strains are dependent upon the type of concrete used, and the ratio of volume to exposed surface. Unlike for CFT columns, two concrete faces are exposed to the ambient environment in the new PEC columns. The ACI (1992) shrinkage and creep models for plain concrete take into account these parameters, and will therefore be adapted to PEC columns for comparison with the long-term experimental results presented herein.

2.6 Finite element modeling of steel and concrete composite structures

This section complements the literature review presented in the third paper (Appendix C). Finite element modelling is used in this thesis to reproduce the

experimental results, better understand the behaviour of PEC columns, and expand the range of the experimental parameters. Finite element models of composite columns presented herein provided useful information in the construction of the PEC model elaborated in the third paper.

A finite element model of partially encased composite columns was presented by Maranda (1999) using finite element program MEF. Using the double symmetry of the column, only a quarter of the cross section was modeled, with shell elements for the steel shape, solid elements for the concrete core and beam elements for the transverse links. The model included local imperfection of the steel flange, obtained by scaling the displacements from the buckled elastic shape. The residual stresses were modeled by modifying the yield plateau of the steel stress-strain curve, for the shell elements. The model presented by Maranda (1999) represented adequately the experimental axial capacity of tested specimens, with an average ratio of experimental to numerical peak loads of 0.95, and a standard deviation of 0.03. In most of the analyses, however, the post-peak response could not be obtained. In fact, the model still had some stiffness at the last converged solution point, indicating that the load had not reached the peak load. Furthermore, the local imperfections were modelled outward, away from the concrete, in the opposite direction of those measured experimentally. For these reasons, the actual average ratio of experimental to numerical peak load could be lower than that reported.

Broderick and Elnashai (1994) studied the seismic behaviour of partially encased composite columns with a compact steel shape and transverse links. The specimens were tested under dynamic and pseudo-dynamic procedure, and for different axial load levels. The authors proposed a numerical model, using the program ADAPTIC, that featured three types of concrete confinement: unconfined concrete between the open face and the transverse links, fully-confined near the web of the steel shape, and partially confined between the two other confinement regions. The model was in good agreement with the experimental results for predicting the displacement and rotation ductility, the ultimate moment, and confirmed the seismic efficiency of this type of composite system.

Finite element program ABAQUS was used by Sugiura et al. (2000) in modeling a composite sandwich beam, tested in flexure. The interface between the concrete and the reinforcing material at the tensile face was modeled using a set of nonlinear springs in the three principal directions of the coordinate system. The concrete part was modeled using 20-node quadratic brick element with reduced integration (C3D20R). ABAQUS was also reported to be used by Wheeler and Bridge (2000) to model a concrete filled steel tube in flexure. The concrete inside the tube was modeled with stiff spring elements to avoid distortion of the cross section.

CHAPTER III

EXPERIMENTAL and FINITE ELEMENT RESULTS

This chapter summarizes the results presented in the 3 papers in appendices.

3.1 Test programme

3.1.1 Test specimens

Table 3.1 presents the specimens designed to meet the objectives described in the first and the second papers, Series 2 and 3 respectively. The table also presents Series 1 specimens tested by Tremblay et al. (1998). The finite element (FE) analyses have been carried out for most of the specimens from Series 1 to 3.

TABLE 3.1. Properties of Test Specimens

Test Series	Design.	b_f x d x t (mm)	L (mm)	b / t ()	s (mm)	Link ϕ (mm)	F_y (MPa)	f'_c (MPa)
Series 1 (Small Specimens	C-2	450x450x9.7	2 250	23.2	225	12.7	370	32.7
	C-3	450x450x9.7	2 250	23.2	338	12.7	370	32.4
	C-4	450x450x9.7	2 250	23.2	450	12.7	370	31.9
	C-5	450x450x9.7	2 250	23.2	225	22.2	370	34.3
	C-6	450x450x6.4	2 250	35.4	338	12.7	374	32.7
	C-7	300x300x6.4	1 500	23.6	300	12.7	374	31.9
Series 2 (Large Specimens	C-8	600x600x12.9	3 000	23.3	600	16.0	360	34.2
	C-9	600x600x12.9	3 000	23.2	600	16.0	360	34.2
	C-10	600x600x12.8	3 000	23.4	300	16.0	360	34.2
	C-11	600x600x9.7	3 000	30.9	600	16.0	360	34.2
	C-12*	600x600x12.9	3 000	23.3	300	16.0	360	34.2
Series 3 (Long-Term Specimens	P-1	300x300x6.5	1 500	23.6	300	12.7	390	36.8
	P-2	300x300x6 .5	1 500	23.6	300	12.7	390	36.8
	P-3	300x300x6. 5	1 500	23.6	300	12.7	390	36.8
	P-4	300x300x6.5	1 500	23.6	300	12.7	390	36.8
	P-5	450x450x9.6	2 350	23.2	450	12.7	345	28.0
	P-6	450x450x9.6	900	23.2	450	12.7	345	28.0
	P-7	300x300x6.5	1 500	23.6	300	12.7	390	36.8

* With additional reinforcements: 4-20M longitudinal rebars, and pairs of U-stirrups 15M@300 mm.

The designation of the geometrical properties is illustrated in Fig. 3.1. F_y and f'_c in Table 3.1 are the steel yield stress and the concrete ultimate strength (MPa), respectively.

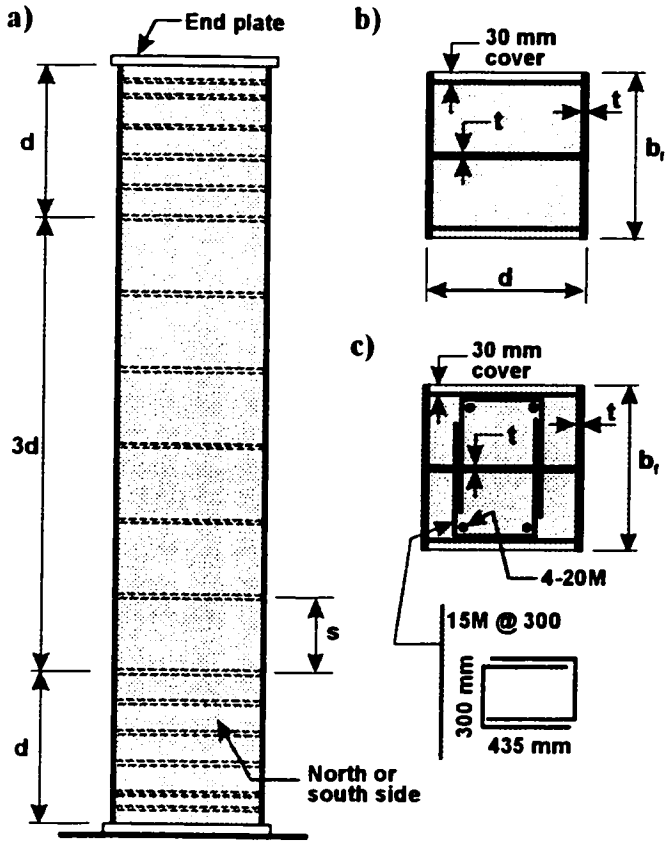

Figure 3.1. Geometry of Stub Columns: (a) Elevation View; (b) Cross-Section without Additional Reinforcement; (c) Cross-Section with Additional Reinforcement

All the specimens met SSRC (1998) requirements for stub columns. For each specimen, the same plate thickness was used for the web and flanges. The transverse links of the specimens were round bars. Each specimen had extra transverse links and higher strength concrete over a height of d at each end to prevent local failure at these locations due to possible uneven loading (Fig.3.1). End plates were also welded to each specimen to obtain a more uniform load distribution in the column.

3.1.2 Mix properties and loading sequence for Series 3 specimens

The composition of the concrete mix is given in Table 3.2. For determining the creep and shrinkage response of PEC columns in test Series 3, the volume to exposed surface ratio (V/S) was taken as d/2, the slump of the plastic concrete was 5 mm, as measured after mixing, the fine aggregate ratio was of 46%, based on concrete mix composition, and the air content was measured as 1.8% in the plastic concrete after mixing.

TABLE 3.2. Concrete Mixes for Test Specimen, in kg/m^3

	25 MPa	40 MPa
Water	160	160
Cement, type 10	265	410
Fine aggregates	900	780
Coarse aggregates (20 mm)	1060	1060

An axial loading sequence that included a total of three stages was developed for specimens P-2 to P-5 of Series 3 (Paper 2). At Stage 1, an axial load was applied to the steel shape only, before concreting, to induce a nominal compressive stress of 100 MPa, which corresponds to the maximum anticipated effects of typical construction loading carried by the steel shape alone. At Stage 2, 14 days after pouring the concrete, the applied load was increased to reach the anticipated axial load corresponding to the long-term service load: D + 0.5L. This load increased the stress in the steel up to approximately 170 MPa and produced a stress of 10 MPa in the concrete. The day when Stage 2 loads were applied is referred to herein as "Day 0". The load at this stage was maintained during approximately 150 days. These construction and service loads induced stresses in both materials were determined from a parametric analysis performed on a typical 36-floor building (Chicoine et al., 2000). Mechanical strain targets (Demec®) and a micrometer were used to measure the axial strains in both materials during Stages 1 and 2 loading (150 days). At Stage 3, the applied load on the composite column was increased further up to failure. The setup for preloading Specimens P-2 to P-5 is illustrated in Fig.3.4 and described in more details in Paper 2.

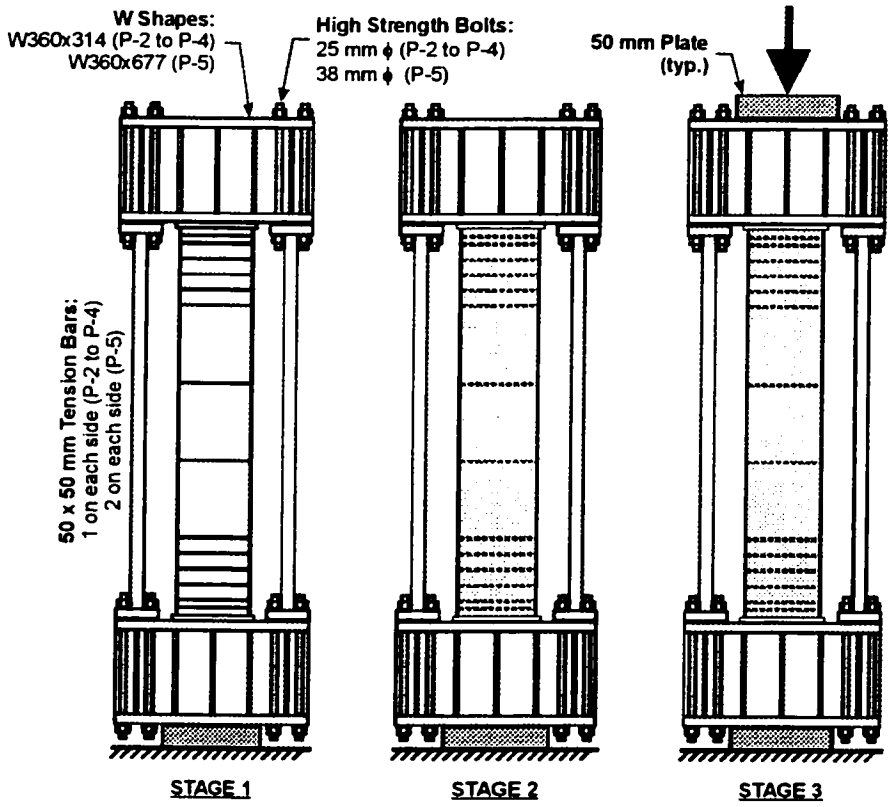

Figure 3.2. Loading Stages 1 to 3 for Specimens P-2 to P-5

3.1.3 Residual stresses

Residual stresses and flange imperfections were measured in all specimens (Papers 1 and 2). The residual stresses in the flanges and web were mostly compressive except at the weld, where high tensile stresses developed. The flange local imperfections were directed inwards due to the fabrication process.

3.1.4 Testing equipment

The tests to ultimate capacity were axial compression tests. The specimens from Series 1 were placed into a 11 MN universal testing machine and the tests from Series 2 were performed with a 22 MN machine. The specimens from Series 3 together with the preloading setup, were placed into a 11 MN universal tasting machine and the load was applied to the cross-beams. During the test, the axial shortening of the column was measured using Linear Variable Displacement Transducers (LVDTs) installed at the four corners having a gauge length of 2 600 mm. Longitudinal and transverse strains were recorded with strain gauges located on the steel flanges and web, in the mid-height region of the column. Strain gauges were also put on the transverse links and concrete, at the same elevation as those on the steel.

3.2 Finite element modelling

3.2.1 Finite element model validation

Preliminary analyses on reduced models were executed to validate the performance to local buckling under compressive stress of shell elements S8R used for the steel and the axial capacity of concrete brick elements C3D20R used for the concrete.

For the shell element, a rectangular plate with fixed cross section (b x t) of 450 mm x 9.5 mm, was analyzed with different length-to-width ratio. The plate had a fixed number of S8R elements, 9, an elastic modulus, E, equal to 200 GPa, and a Poisson's ratio, ν, equal to 0.3. As illustrated in Fig.3.3, three classic boundary configurations were considered, representing various degrees of plate stiffness: low stiffness, with three sides fixed, intermediate stiffness, with four sides simply supported, and high stiffness, with four sides fixed. The figure plots the ratio of the first mode elastic buckling load obtained from ABAQUS to the theoretical elastic buckling load, with respect to the plate length-to-width ratio (a/b). The elastic buckling theoretical load was computed with Eq. (3.1).

$$P_{cr} = A_s \frac{k\pi^2 E}{12(1-\nu^2)(b/t)^2} \tag{3.1}$$

where A_s is the cross-section (mm^2), k is the plate buckling in Fig. 3.4 (Salmon and Johnson, 1996).

For all three boundary configurations, the load ratio is close to unity when the a/b ratio is less or equal to 2. For an ratio a/b greater than one, the accuracy of the model decreases progressively as the length increases, particularly for the very stiff plate. It is therefore suggested to use square elements with an aspect ratio equal to one.

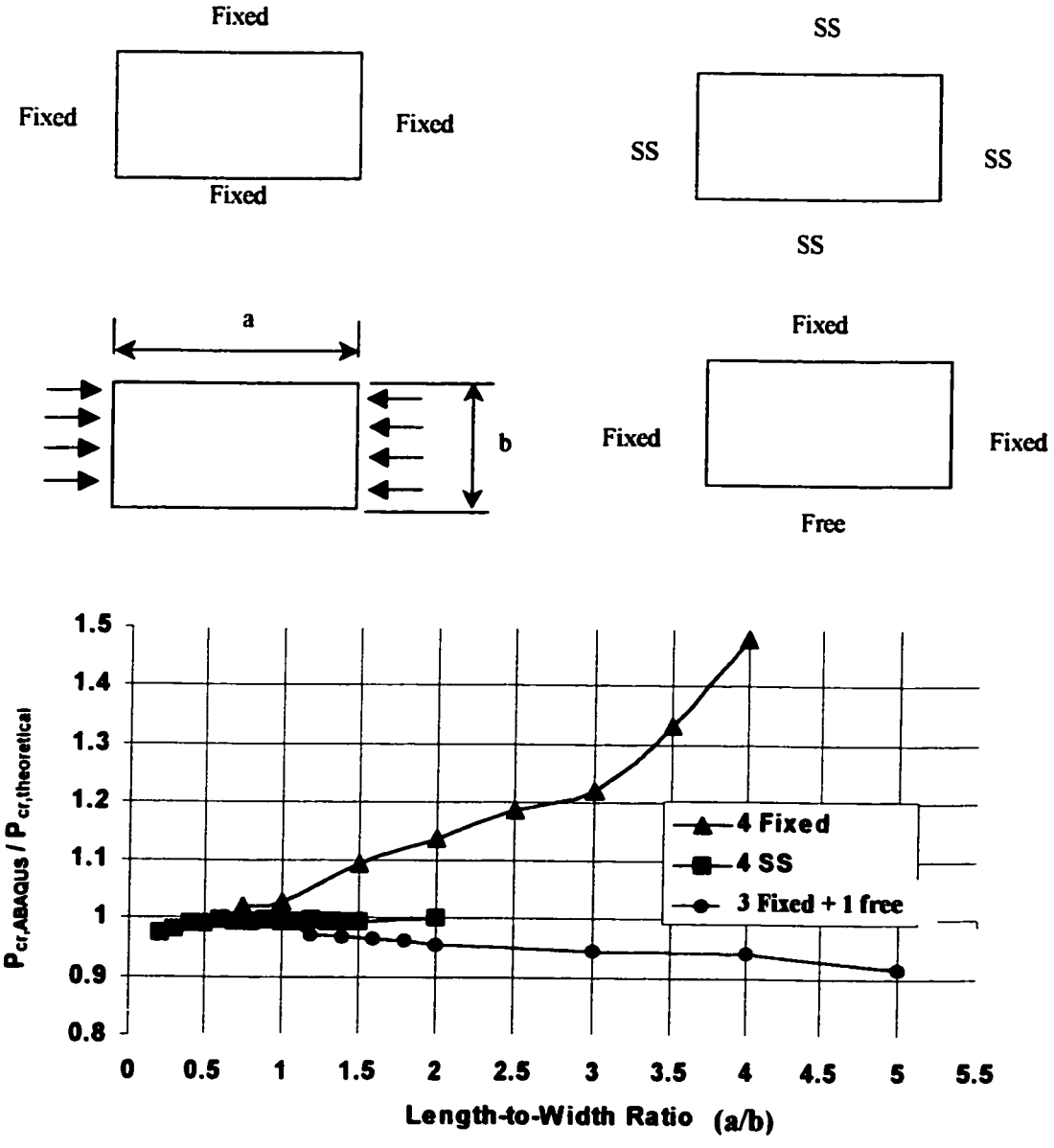

Figure 3.3. Buckling Model with Different Aspect Ratio and Boundary Conditions

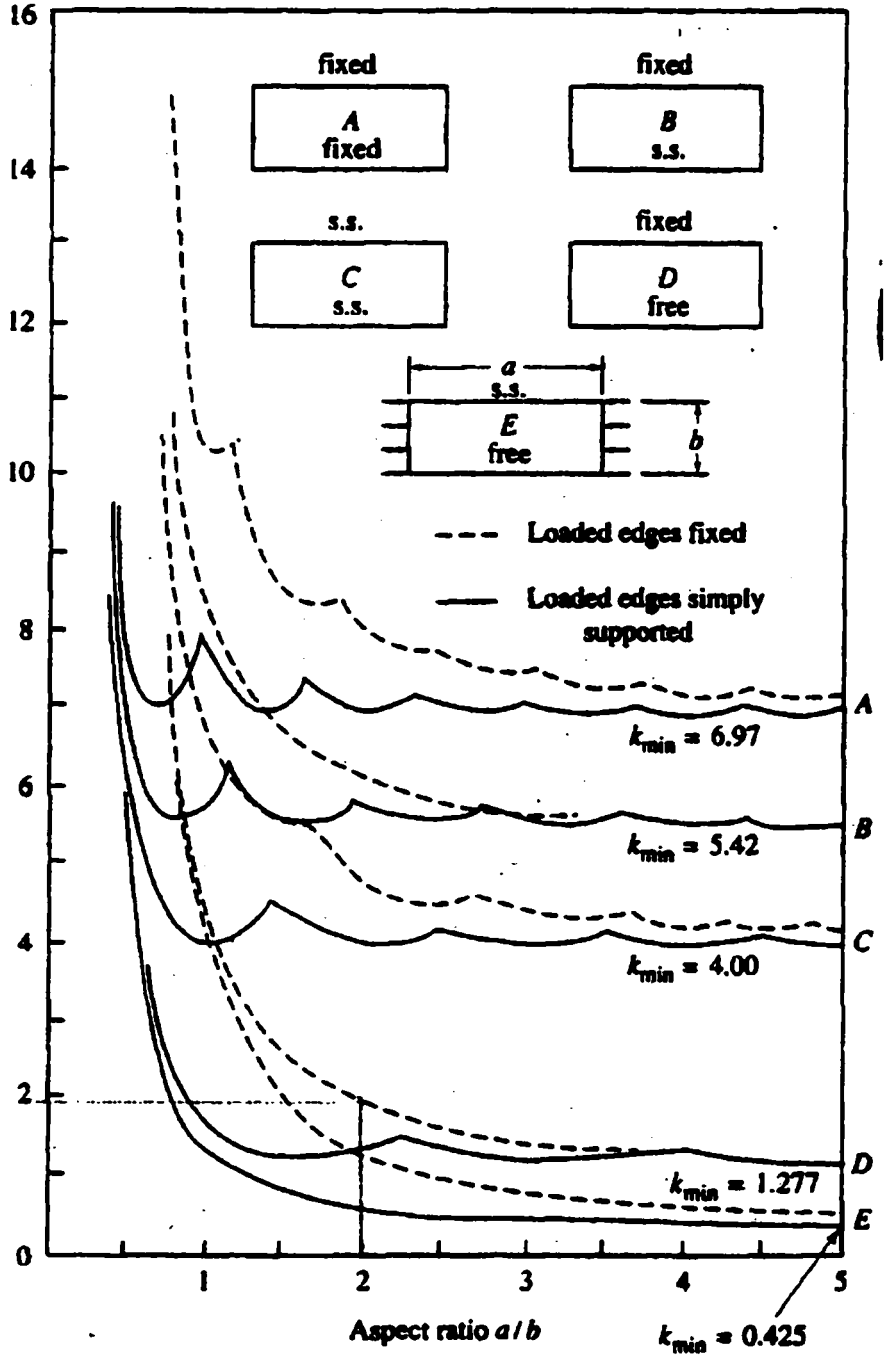

Figure 3.4. Variation of Plate Buckling Coefficient k with a/b Ratio (Salmon and Johnson, 1996)

The concrete elements were validated in uniaxial and biaxial compression. In ABAQUS, the uniaxial stress-strain curve of the concrete is defined in two steps: an elastic branch and a plastic branch. The biaxial behaviour of the concrete in compression is defined by specifying the value of three parameters in the case of equal stresses in both directions: the ratio of the longitudinal biaxial strength to the uniaxial strength at peak load (default value of 1.16), the ratio of ultimate uniaxial tensile to ultimate uniaxial compressive stress (default value of 0.09), and the ratio of longitudinal biaxial strain to uniaxial strain at peak load (default value of 1.28). The default values were calibrated to the test results by Kupfer and Hilsdorf (1969), who tested square concrete plates of 200 mm x 200 mm x 50 mm under biaxial stresses. In their test program, the lateral stresses (f_{22}) were proportional to the longitudinal stresses (f_{11}) with f_{22}/f_{11} ratio of 0.5 and 1.0. The concrete in uniaxial compression had a strength f'_c of 30.7 MPa at a strain of 2 200 $\mu\varepsilon$, and an elastic modulus estimated at : $5\,000(f'_c)^{1/2} = 27\,700$ MPa.

These tests were reproduced numerically with ABAQUS using a 3 x 3 mesh of C3D20R elements, under displacement control (Riks method). The analysis results are presented in Figs.3.5 and 3.6, and the experimental results in Fig.3.7. The input stress-strain curve for the concrete was given at every 100 $\mu\varepsilon$, using the Tsai (1988) formulation for the plastic branch, and the previously determined materials properties. Figure 3.5 shows that the ultimate longitudinal stress in uniaxial compression follows exactly the input data, with a peak stress of 30.7 MPa at about 2 170 $\mu\varepsilon$. The ultimate longitudinal stress in biaxial compression, with a ratio f_{22}/f_{11} of 1.0, is equal to 1.16 f'_c at a strain of

2 480 με, values very close to the experimental ones shown in Fig.3.7: 1.16 f'_c at about 2 600 με. The ultimate longitudinal stress in biaxial compression, with a ratio f_{22}/f_{11} of 0.5, is equal to 1.27 f'_c at a strain of about 3 740 με, values very close to the experimental ones shown in Fig.3.7: 1.27 f'_c at about 3 000 με. The difference in strain arise from the fact that the analysis strategy was in displacement control and that the peak load could therefore not be identified exactly. The transverse strains obtained from FE analysis (Fig. 3.6) are also very close to those obtained experimentally (Fig.3.7).

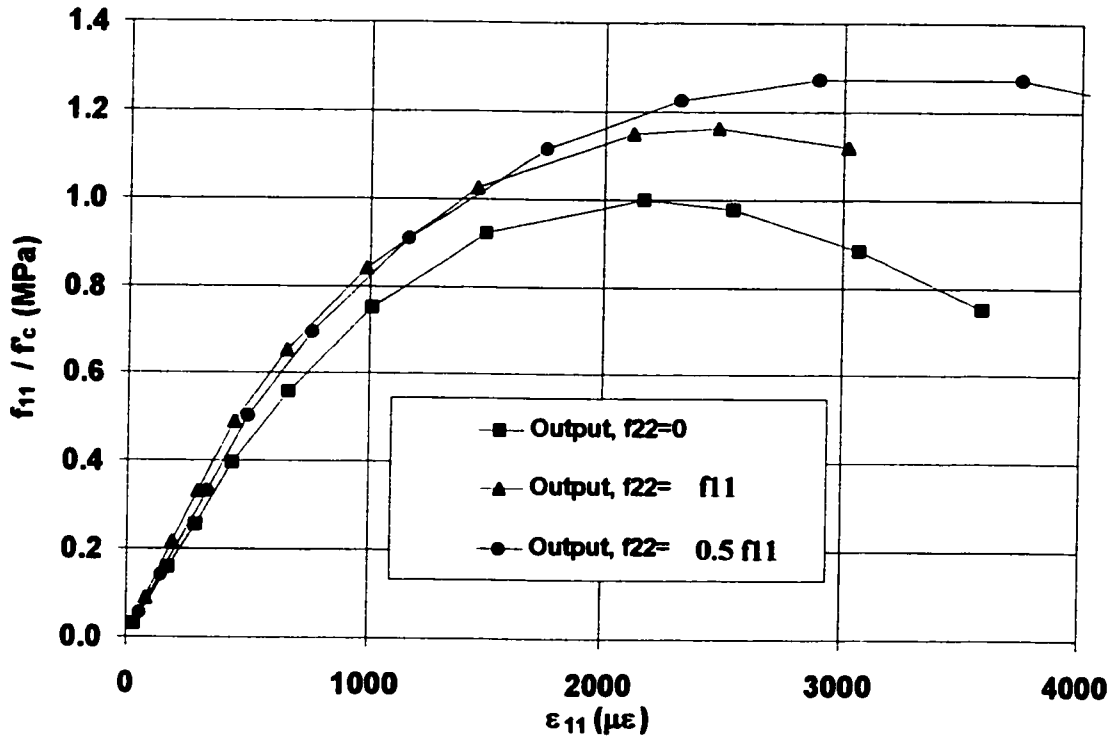

Figure 3.5. Normalized Longitudinal Stresses with Longitudinal Strain

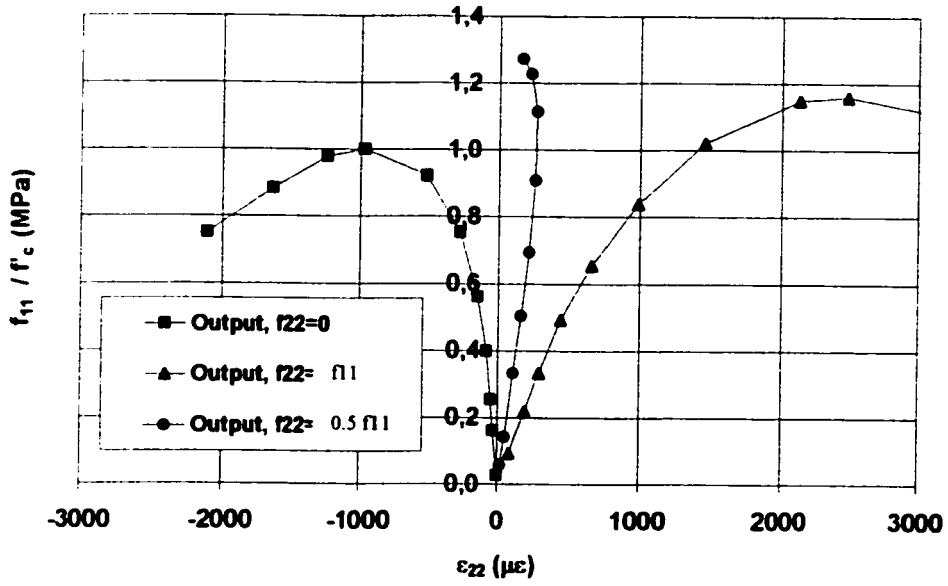

Figure 3.6. Normalised Longitudinal Stresses with Lateral Strain

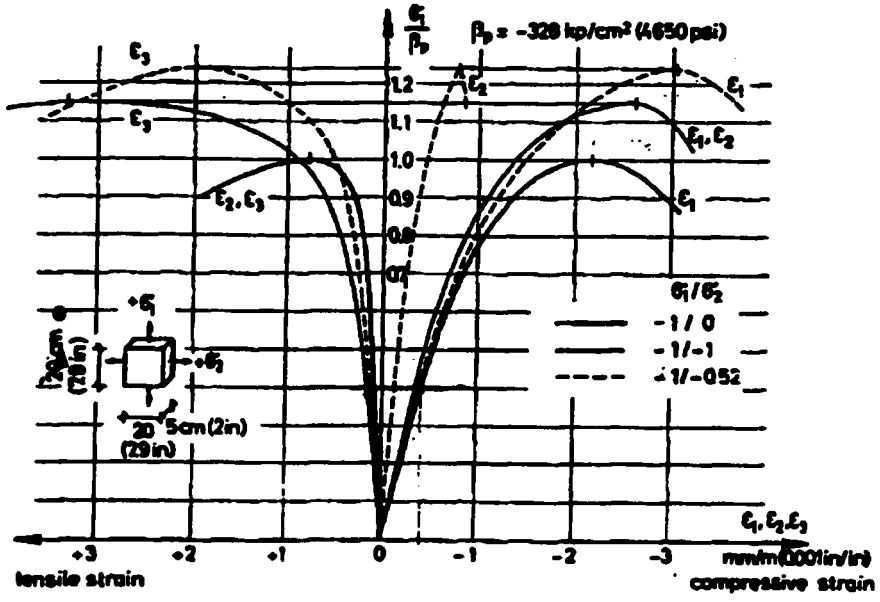

Figure 3.7. Longitudinal and Transversal Stress-Strain Relationship for Biaxial Test (Kupfer and Hilsdorf, 1969)

3.2.2 Finite element model of PEC column

By taking advantage of the cross section symmetry and of the failure mode observed in the tests, the FE model only included a quarter of the cross section, over a height equal to one transverse link spacing (Fig.3.8a). The complete models are presented in Figs.3.8b and 3.8c for link spacing of s = d/2 and s = d, respectively. An example of input file is presented in Appendix D for Specimen P-3 with loading sequence.

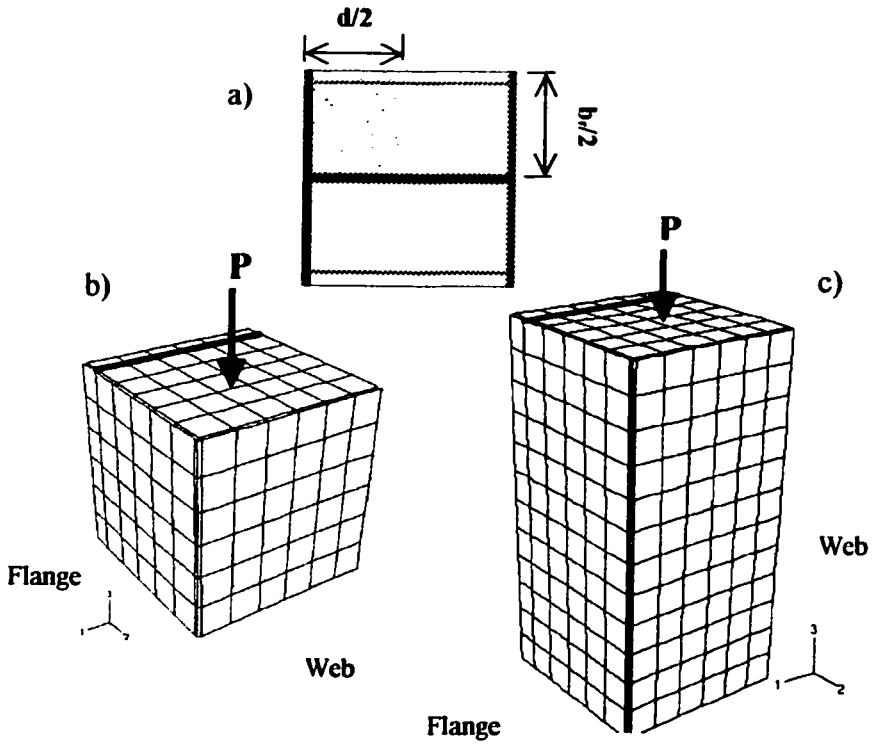

Figure 3.8 Finite element models of the column: (a) Quarter cross section; (b) Specimen with s = d /2; and (c) Specimen with s = d.

The boundary conditions of the model are presented in Fig.3.9a and 3.9b. Boundary conditions are identified by a letter, followed by the DOF that are blocked for the corresponding node set: numbers 1, 2, and 3 represent the displacement DOF and numbers 4, 5, and 6 the rotation DOF, respectively, along global axis X, Y, and Z.

A: 2	$0 < z \leq s$	I : 2,3,4,5,6	$z = 0$
B: 1,2	$0 < z \leq s$	J : 1,2,3,4,5,6	$z = 0$
C: 2,3	$z = 0$	K : 4,5	$z = s$
D: 1,2,3	$z = 0$	L : 3,4,5	$z = 0$
E: 1,3	$z = 0$	M : 3	$z = 0$
F: 1	$0 < z \leq s$	N_{top}: 1,4,5,6	$z = s$
G: 2,4,5,6	$0 < z \leq s$	N_{bottom}: 1,3,4,5,6	$z = 0$
H : 1,2,4,5,6	$0 < z \leq s$		

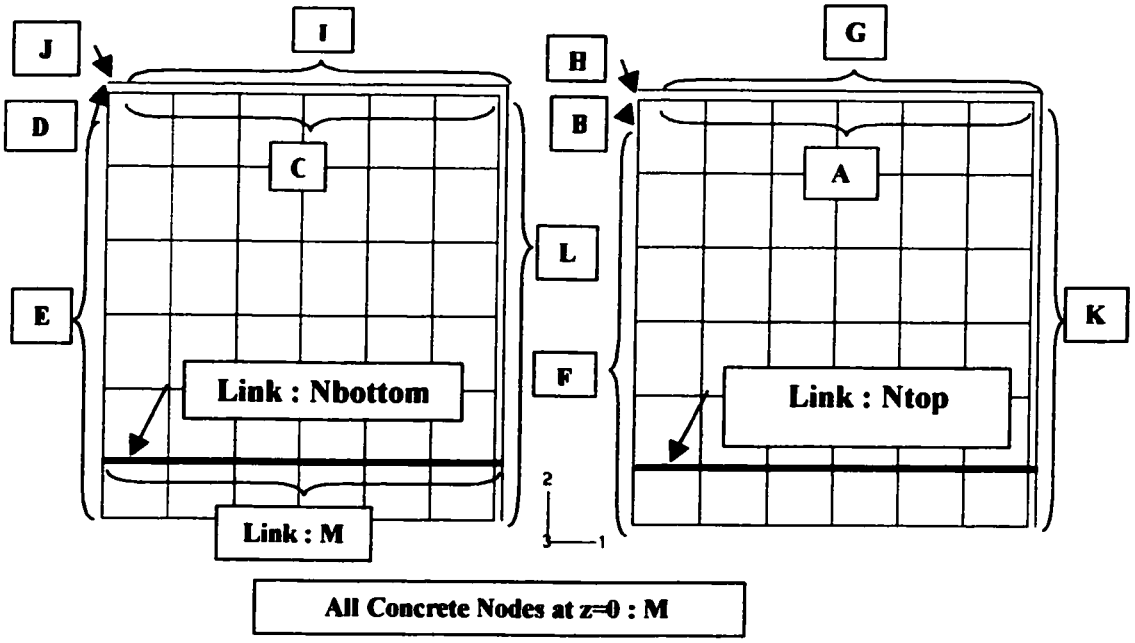

FIG. 3.9. Boundary Conditions at : (a) z = 0; (b) z > 0

The following DOF were coupled using very stiff springs elements. The displacements of the nodes of the concrete block, the flange and the web at z = s were coupled in the longitudinal direction (dir-3) to ensure that the load is applied uniformly on both materials. The load was applied as a concentrated load on one of the nodes on the upper face.

Interface elements do exist in ABAQUS but are not easy to use and often lead to problems of solution convergence, even with simple interaction laws. It was considered that the use of springs to model the interaction between the steel and the concrete was easier and effective. The displacements of the nodes of the concrete block facing the web and all those of the web were coupled with springs, one by one, in dir-1 and dir-3, to simulate the assumed perfect contact between the concrete and the steel web. Springs were installed in dir-1, one by one, between all of the flange nodes and the facing concrete nodes. The springs had a very high compressive stiffness to simulate the presence of the concrete and prevent the flange to buckle inwards, and a very low tensile stiffness to allow the flange to buckle outward freely. No springs were installed in dir-2 to simulate the friction between the flange and the concrete as this interaction would reduce to zero when the plate buckles. All displacement and rotations at the junction of the flange and the web were coupled, to simulate the continuity between the two plate provided by the weld. All the displacements and rotations at the junction of the flange and each transverse link were coupled, also to simulate the continuity provided by the weld. The displacement of the transverse link nodes, at z = 0 and z = s, were coupled with

the adjacent concrete nodes in dir-1, to simulate perfect bond and determine the stress in the links due to transverse expansion of concrete.

A bilinear strain-stress behaviour was assumed for steel, with an elastic modulus of 200 GPa, a yield stress of F_y, given in Table 3.1, and a strain hardening slope of 800 MPa, based on typical stress-strain curves obtained from tensile tests on steel coupons. The analyses were made with the concrete effective strength, f'_{ce}, and the effective elastic modulus, E_{ce}, computed from Eq. (3.2) and (3.3), respectively.

$$f'_{ce} = 0.92\Psi f'_c \tag{3.2}$$

$$E_{ce} = \sqrt{0.92\Psi}\, E_c \tag{3.3}$$

where f'_c and E_c are respectively the concrete strength and elastic modulus measured from cylinders at the day of column testing. Parameter Ψ was proposed by Chicoine et al. (2000c) to model adequately size effects on the concrete strength in PEC columns, based on experimental data reported by Neville (1966):

$$\psi = 0.85\left(0.96 + \frac{22}{b}\right) \quad \begin{cases} \geq 0.85 \\ \leq 0.97 \end{cases} \tag{3.4}$$

The additional reduction factor of 0.92 mainly accounts for the lower quality of the concrete used in structural elements compared to the concrete in test cylinders. This factor was adjusted at 0.92 so that the ultimate loads obtained from the finite element analysis matched the experimental values. The models also accounted for the residual stresses and local imperfections of the steel shape. Actual imperfections were measured inward, toward the web. Due to limitations of the model to properly simulate the

expansion of the concrete beyond 0.4 f'_c, the pushing effect of concrete on the flange could not be reproduced. It was therefore decided to model the flange imperfections outwards, in the opposite direction as the measured imperfection, to better simulate the experimental buckling mode of the flange.

3.3. Experimental results and discussion

3.3.1 Long-term results for Series 3 specimens (Paper 2)

Long-term deformations in specimens loaded in Stages 1 and 2 were due to the creep and shrinkage of the concrete. The restrained shrinkage strains, measured in the load free Specimens P-1, P-2, and P-7, were very low, with an average value of 35 με at the end of Stage 2, represents approximately 20% of the total strain increase in Specimens P-3 to P-5, while the creep strains were in the order of 150 to 200 με. This low average shrinkage strain value was due in part because the concrete was drier than expected at pouring, with a slump of only 5 mm. The experimental creep strains may be higher than in an actual building because the load applied to Specimens P-3 to P-5, DL+0.5LL, was relatively higher than what would be expected in an actual structure, DL+0.1LL. The ratio of creep to elastic strains for the concrete was 0.5 for specimens P-3 and P-4. Table 3.3 shows the elastic and long-term stresses in the steel and the concrete of Specimens P-2 to P-5, loaded in Stages 1 and 2. The total stress increases in the steel shape of Specimens P-3 to P-5, at the end of loading stage 2, are respectively: 41 MPa, 44 MPa, and 37 MPa, for a total stress of 215 MPa, 219 MPa, and 223 MPa. The stresses in

the concrete had decreased after 150 days, from 9.7 to 6.8 MPa, 9.8 to 6.5 MPa, and 9.0 to 6.5 MPa, for Specimens P-3 through P-5, respectively.

TABLE 3.3. Summary of Stress Variation

Specimen no.	$f_{s,\,el}$ (MPa)	f_{s}, 150d (MPa)	f_{cycl} (MPa)	f_{c} , 150d (MPa)
P-2	100	111	-	-
P-3	174	215	9.7	6.8
P-4	175	219	9.8	6.5
P-5	186	223	9.0	6.5

The column axial strain due to creep of the concrete in Specimens P-3 to P-5 was calculated by subtracting the strains due to shrinkage to the total strain at the end of Stage 2. These experimental shrinkage and creep strains were compared to the ACI (1992) prediction models for plain concrete, adapted to account for the restraint provided by the steel shape. As seen in Figs. 3.10 and 3.11, the models predict well the shrinkage and creep behaviour of the specimens. The finite element models successfully reproduced the sequence of construction and the long-term effects.

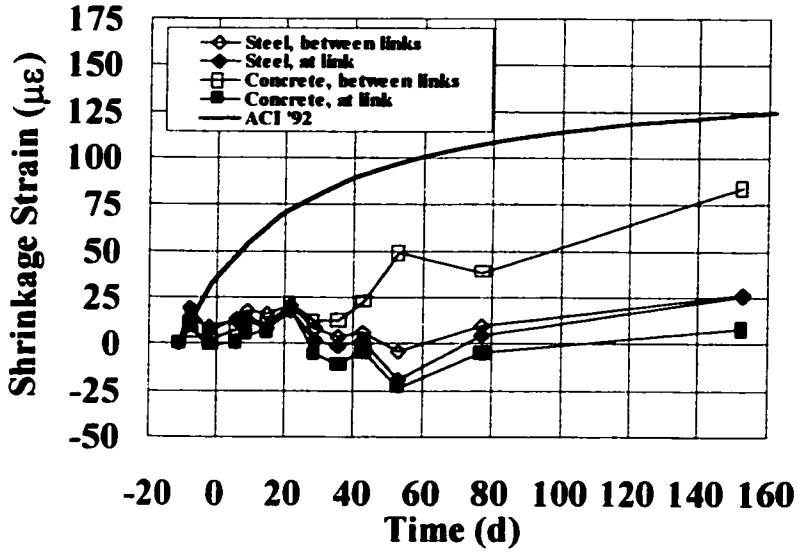

Figure 3.10. Average Shrinkage Axial Strain in Specimens P-1, P-2, and P-7

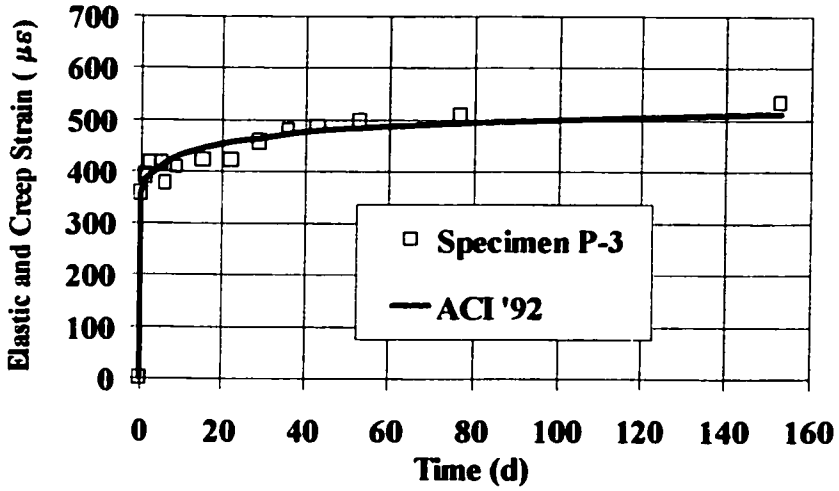

Figure. 3.11. Experimental and Predicted Elastic plus Creep Strain in Specimen P-3

3.3.2 Observations in tests at peak load

The failure in all specimens and finite element models occurred by crushing of the concrete together with local buckling at the same location (Fig. 3.12). The failure modes of Series 1 to 2 specimens are compared according to their link spacing, as this parameter was indicative of the failure mode. Test observations indicated that 450 mm and 600 mm specimens with s=d behaved in a similar manner near peak load, whereas the 300 mm had a more progressive and ductile failure.

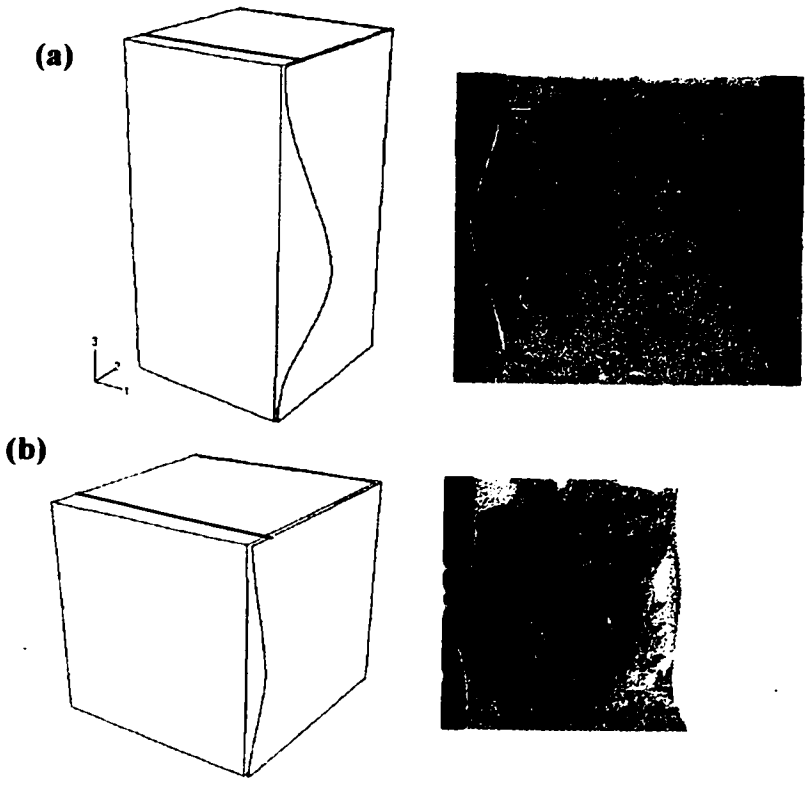

Figure 3.12 Predicted and experimental failure modes for specimens with: (a) s = d; (b) s = d/2

These results also showed that there is still no size effects near peak load between 450 mm and 600 mm specimens with s=d/2. For specimens in Series 3, local buckling of the steel flanges was observed only near peak load. The failure also occurred by crushing of the concrete between two consecutive transverse links, together with local buckling of the flanges at the same location. Concrete also crushed simultaneously or shortly after on the opposite side, but at different elevations. The failure was ductile and progressive, contrary to specimens with d=600 mm tested under load control.

3.3.3 Ultimate capacity and load-strain relation

As shown in Table 3.4, the finite element models gave a very good estimate of the ultimate capacity of the columns when using a concrete strength of $0.92\Psi f'_c$, giving a test-to-predicted ratio ($P_{u,exp}/P_{u,fem}$) ranging from 0.96 (C-10) to 1.06 (P-5) with an average of 1.00. The experimental peak loads for Specimens P-2 to P-4 with a load applied in Stages 1 and 2 are close to that of reference Specimens P-1, indicating that the sequence of loading and the long-term effects did not reduce the axial capacity of the columns. The load ratio for Specimen P-5 is high because of uncertainties about the quality of the concrete within. The table also shows that the models overestimated slightly the strain at peak load, with an experimental to FE model average ratio of 0.95. The strain in the model was localised to the failure zone while that of the specimens was measured over the full height of the column. Higher strength concrete was used over one

fifth of the height at the top and bottom of the columns to avoid end failure, therefore resulting in a smaller average strain.

TABLE 3.4 Results at Peak Load of Plastic Analyses of Composite Models with a Concrete Strength of f'_{ce}

Series	Spec.	P_0 (kN)	$P_{u,fem}$ (kN)	$P_{u,exp}$ (kN)	$P_{u,exp}$ / $P_{u,fem}$ (-)	$\varepsilon_{u,fem}$ (με)	$\varepsilon_{u,exp}$ (με)	$\varepsilon_{u,exp}$ / $\varepsilon_{u,fem}$ (-)
Series 1	C-2	9 938	9 889	10 100	1.02	2 500	2 306	0.92
	C-4	9 813	9 450	9 390	0.99	2 235	1 695	0.76
	C-5	10 189	10 189	10 000	0.98	2 380	2 330	0.98
	C-7	4 447	4 225	4 280	1.01	2 141	2 142	1.00
Series 2	C-8	17 623	16 742	16 470	0.98	2 050	1 845	0.90
	C-9	17 623	16 671	16 610	1.00	2 150	1 769	0.82
	C-10	17 557	16 995	16 240	0.96	2 285	2 256	0.99
	C-11	15 308	14 206	14 930	1.05	2 090	1 810	0.87
	C-12	18 009	17 540	17 450	0.99	2 310	2 580	1.12
Series 3	P-1	4 948	4 725	4 770	1.01	2 353	2 335	0.99
	P-2	4 948	4 716	4 670	0.99	2 717	2 730	1.01
	P-3	4 948	4 712	4 790	1.02	2 878	2 550	0.93
	P-4	4 948	4 708	4 975	1.06	3 020	2 910	1.01
	P-5	9 131	8 680	9 225	1.06	2 750	2 820	1.03
Mean[1]					1.00			0.95
SD[1]					0.03			0.09

Note: (1) Specimen P-5 not included

Figures 3.13 and 3.14 show the applied axial load versus the average axial strain, ε_a, of the Series 2 and 3 specimens, respectively. The average axial strain corresponds to the average shortening of the column as measured by the longitudinal LVDTs located at the four corners of each specimen, divided by the length between their attachment points on the column.

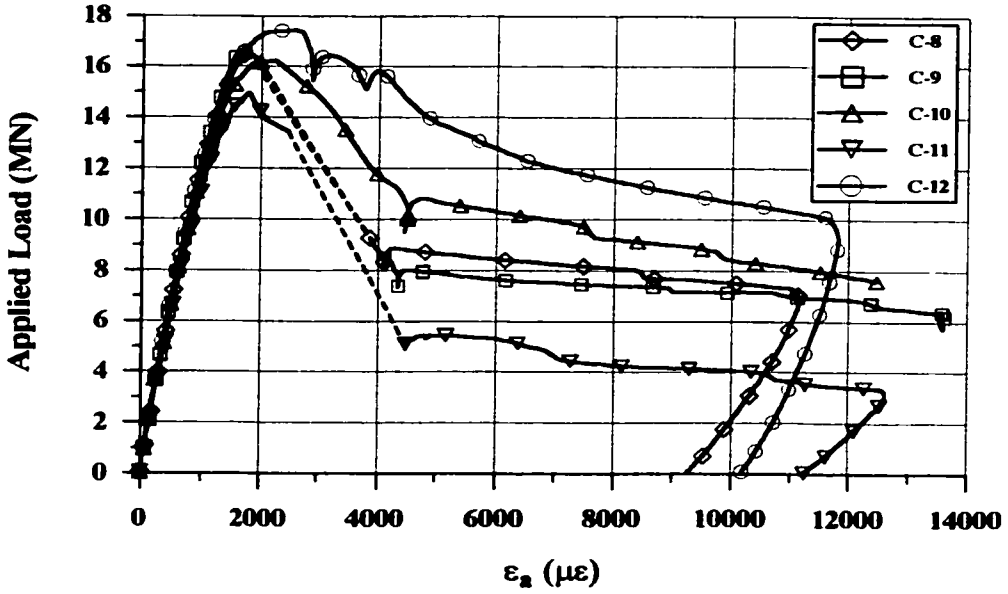

Figure 3.13. Load vs. Average Axial Strain Curves of Series 2 Specimens

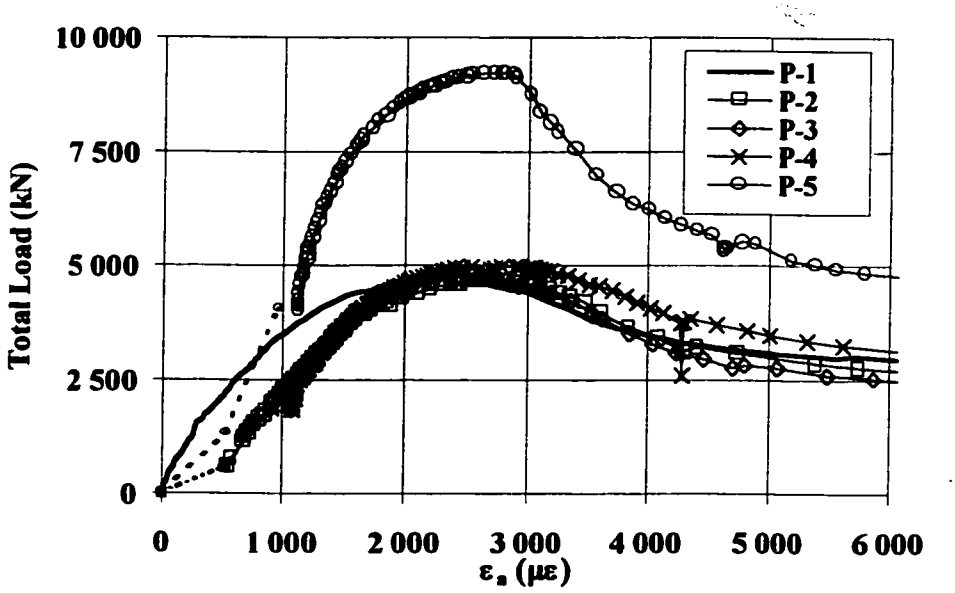

Figure 3.14. Load vs. Average Axial Strain Curves of Series 3 Specimens

In Fig.3.13, the behaviour of the specimens was linear up to approximately $0.6P_{u,exp}$. The strain at peak load for specimens with s=d were lower than the peak strain of the concrete cylinders but approximately corresponding to the yield strain of the steel. Larger strains were measured in specimens with s=d/2. The measurements clearly indicate that a link spacing of d/2 resulted in a more ductile response, with larger deformation near peak load, and a higher residual capacity after peak. Local buckling of the flanges was delayed and the failure of concrete was constrained to take place in a smaller volume. In addition, more numerous and closely spaced links provided a higher and more uniform confinement of the concrete near the face of the column. Furthermore, the b/t ratio, the link spacing, and the presence of additional reinforcements all influenced the ductility and post-peak response of this type of composite column.

In Fig. 3.14, the behaviour of Specimens P-1 to P-5 was linear up to about $0.6P_{u,exp}$. For all columns, the strains at peak load exceeds significantly the yield strain of the steel, clearly indicating that the steel had yielded when crushing of the concrete occurred at peak load, except near the web to flange welds where the residual stress had very high tension values. These large strains in the steel shape at peak load were possible because local buckling of the flange occurred only near peak load, as a result of having the local flange imperfections inwards. The figure shows that the increase in the steel stresses induced by the sequence of loading and the long-term effects were not detrimental to column ductility. These results for P-1 to P-5 are comparable with the behaviour observed on specimens of Series 1 with similar characteristics.

Figure 3.15 shows the experimental and FE model load-strain relation of some representative specimens. Overall, a very good agreement is obtained between the FE models with a concrete strength of $0.92\Psi f'_c$ and the experimental response for the elastic column stiffness, the peak load and the strain at peak load.

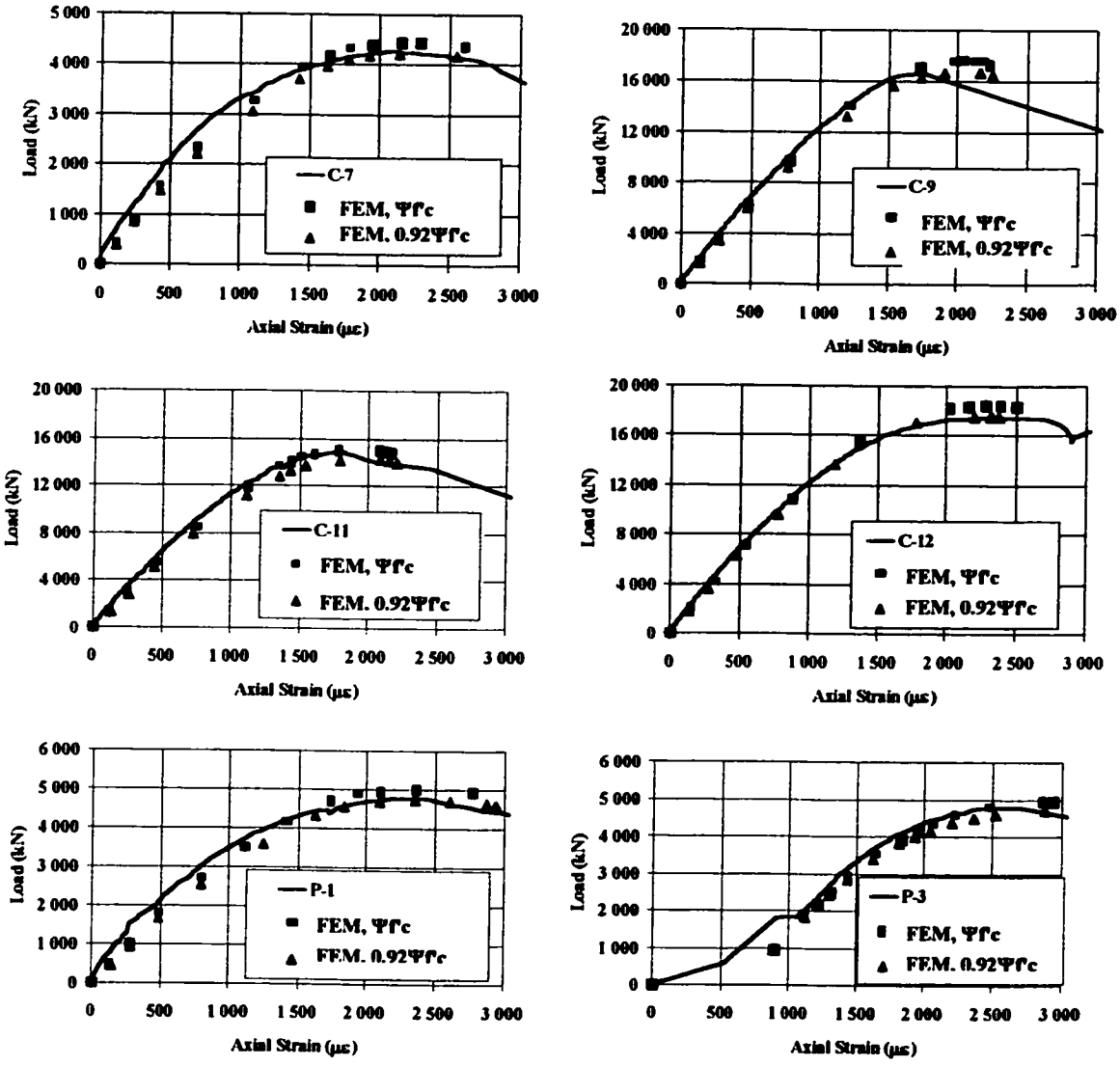

Figure 3.15 Load-strain behaviour of specimens and FE models

3.3.4 Stress efficiency ratios in the flange, the web, and the concrete in FE models

Table 3.5 gives the ultimate load normalised to P_0, the plastic capacity of the section, and the computed average stresses in the FE models at peak load in the flange, σ_{fl}, the web, σ_w, and the concrete, σ_c, normalised to F_y for the steel and f'_{ce} for the concrete to obtain stress efficiency ratios for all components.

TABLE 3.5 Normalized load and stresses at peak load for flange, web, and concrete

No.	$P_{u,fem}/P_0$ (-)	σ_{fl}/F_y (-)	σ_w/F_y (-)	σ_c/f'_{ce} (-)
C-2	1.00	0.97	0.96	1.02
C-4	0.96	0.88	0.95	1.02
C-5	1.00	0.97	0.96	1.03
C-7	0.95	0.87	0.87	1.02
C-8	0.95	0.86	0.94	1.01
C-9	0.95	0.85	0.95	1.00
C-10	0.97	0.92	0.94	1.01
C-11	0.93	0.75	0.94	1.00
C-12	0.97	0.92	0.94	1.01
P-1	0.96	0.88	0.88	1.02
P-2	0.95	0.87	0.91	1.01
P-3	0.95	0.87	0.93	1.00
P-4	0.95	0.85	0.94	1.01
P-5	0.95	0.86	0.97	1.00
Mean(1)	0.96	0.88	0.93	1.01
SD(1)	0.02	0.05	0.03	0.01

Note: (1) Specimen P-5 not included

Residual stresses and local imperfections both contribute to reduce the axial capacity of the flanges in the models. Table 3.4 shows that the stress efficiency ratio of the flange (σ_{fl}/F_y) is generally higher for specimens with s=d/2 than for specimens with

s=d (e.g. 0.97 for C-2 vs. 0.88 for C-4) and also for specimens with a lower b/t ratio (0.86 for C-8 vs. 0.75 for C-11). These results are typical for local buckling since the slenderness of the plate is determined with the parameters s/d and b/t (Salmon and Johnson, 1996). Table 3.4 also shows that the stress ratio for the flange ranges from 0.85 to 0.88 for all specimens with s=d and b/t=23, and higher for specimens with s=d/2, ranging from 0.92 to 0.97. No significant trend is observed for specimens of different sizes having the same s/d. The variation of the stress ratio with d is due to the way residual stresses were defined in the FE models. It was found that compressive and tensile residual stresses decrease the flange capacity by 5% on average. Local imperfections reduced the capacity of the flange by up to 6%.

Table 3.4 also shows that the web stress efficiency ratio (σ_w/F_y) for all specimens with b/t=23 ranges from 0.94 to 0.96. The stress ratios were lower for specimens C-7 and P-1 (0.88 and 0.87) because of the way residual stresses were modeled. It was found that the flange local imperfection had no effect on the stress ratio of the web. The detrimental effects of having tensile transverse stresses in the web reduced the capacity of the web up to 5%.

For the concrete, Table 3.4 shows that the stress efficiency ratio (σ_c/f'_{ce}) was close to one, indicating no significant gain in axial capacity due to possible confinement (maximum stress ratio of 1.03 for specimen C-5). Very localised confinement effects were observed in the vicinity of the weld and at the transverse links near the flange.

Slightly higher stress ratios were found in smaller specimens (1.02 f'_{ce} for 300 mm specimens vs. 1.00f'_{ce} for 600 mm specimens)

3.3.5 Transverse stresses in the steel shape

Strain readings on the steel shapes of the smaller test columns (Series 1) were available only for Specimens C-2 and C-7 and they were measured only on one side of the flange or web. Web measurements were used here to compare with larger specimens, as plate bending effects were less pronounced in the web. The ratios of longitudinal to yield stress, σ_l/σ_{vM}, were for C-2 and C-7 respectively 1.01 and 1.05, with compressive transverse stresses. These ratio are comparable to the values obtained for 600 mm columns: the average ratio σ_l/σ_{vM} near peak load for all Series 2 specimens were 1.00 for the flanges, and 0.99 for the web. In the FE models, the high tensile transverse stresses reduced the axial capacity of the web by only 3% to 5% at peak load. From these results, it can be concluded that the transverse stresses had a negligible influence on the longitudinal capacity of the steel shape of the test columns, and that no size effect was present.

3.3.6 Axial stresses in the transverse links

As mentioned in Paper 1, the link stresses in Series 2 specimens at peak load ranged from 90 to 151 MPa for specimens with s=d, and from 296 to 303 MPa for

specimens with s=d/2. The transverse links experienced much higher axial deformations than those observed on the steel shape in the transverse direction. The main reason for this difference is that both the steel shape and the concrete deformed transversely due to Poisson's effects whereas the transverse links behaved as a passive reinforcement, deforming at the same rate as the concrete. The measured Poisson's ratio of concrete test cylinders was equal to 0.18 up to about 1 000 με, after which it increased and exceeded that of steel (0.3) at 1 700 με. This explains the very low tensile transverse stresses observed in the steel shape and the higher rate of deformation for links in Specimens C-10 and C-12 at large longitudinal strains. On these two specimens, the closer link spacing also stiffened the flanges in bending, which then offered a higher restraint to the concrete expansion between the links. Hence, additional tensile forces were induced in the links acting as horizontal reactions for the flanges.

In Paper 2, the axial stresses in the transverse links of Specimens P-1 to P-5 at peak load ranged from 172 MPa to 298 MPa. At any given load during the test, the link stresses in Specimen P-1 were higher: for example, at 0.9 $P/P_{u,exp}$, the link stresses in the preloaded specimens were closely grouped and ranged from 25 MPa for Specimen P-5 to 75 MPa for Specimen P-4, while the one in Specimen P-1 was 100 MPa. This is explained by the fact that the stresses in the transverse link remain small when the steel section only is loaded (Stage 1) and increases with the transverse expansion of the concrete (Stages 2 and 3). The elastic unloading of the concrete due to relaxation and shrinkage around the link also reduced the axial stress to an average link stress of about

10 MPa in compression, at the end of Stage 2. The stress in the link of Specimen P-4 was higher because the column strain at peak load was higher. These results indicate that the stresses in the link at peak load are typically lower when the specimen has undergone a loading sequence and long-term deformations (P-2, P-3, P-5), but is also dependent on the magnitude of the volumetric expansion of the concrete near peak load, which is difficult to predict and may lead to high stresses (P-4).

For Series 2 and 3 specimens, the behaviour of the link was confirmed by transverse gauges readings on the concrete surface at link location giving values similar to those on the links. Very good agreement was generally obtained between the FE models and experimental results, indicating that the axial link stresses are only dependent on the transverse expansion of the concrete.

Based on the dimensions used in the experimental programme, the cross-section area of one transverse link should be equal to the greater of 0.025dt (or d.t/40) and 100 mm^2.

3.3.7 Discussion on predicting column behaviour with d greater than 600 mm

An important aspect of finite element modelling is the ability to expand the use of the model outside the range of the parameters covered in experimental programs. For example, it is likely that composite columns in actual buildings be larger than the

maximum size tested. It is believed that the models developed in this study will predict adequately the behaviour of larger columns because:

- The size effects on the ultimate concrete strength, f'_c, can be modelled adequately by modifying the input data to $f'_{ce} = 0.92\Psi f'_c$;
- The local flange imperfections were found to be comparable in the 300 mm, 450 mm, and 600 mm specimens;
- Compressive residual stresses were more important in specimens with d=300 mm, than in 450 mm and 600 mm columns, and are expected to remain as low than in the latter for larger columns. The width over which are distributed the tensile residual stresses is approximately constant in absolute terms, and becomes therefore relatively smaller as d increases. The heat-affected zone would decrease as the column size increases.

3.4 Prediction model for the axial capacity

The axial capacity of composite columns may be obtained by summing up the contribution of each component, i.e. the steel shape, the concrete, and the reinforcing steel, if any. Tremblay et al. (2000) proposed such an equation for PEC columns based only on experimental data. This equation has been modified based on the additional information generated by this FE study to obtain the following expressions, presented in Paper 3:

$$P_{u,pred} = A_{se} F_y + A_c f'_{ce} + A_r F_{yr} \qquad (3.5)$$

$$A_{se} = (d - 2t + 4\,b_e)\,t \tag{3.6}$$

$$\frac{b_e}{b} = (1 + \lambda_{fl}^{2n})^{(-1/n)} \tag{3.7}$$

$$\lambda_{fl} = \frac{b}{t}\sqrt{\frac{12(1-\nu^2)F_y}{\pi^2 E k_{fl}}} \tag{3.8}$$

$$k_{fl} = \frac{3.6}{(s/b)^2} + 0.05(s/b)^2 + 0.75, \quad 1 \le s/b \le 2 \tag{3.9}$$

The first term in Eq.(3.5) represents the contribution of the steel shape, based on the effective area for local buckling, A_{se}. The contribution of the concrete is based on the effective strength as defined in Eq.(3.2). The last term is the contribution of the reinforcing steel. In these equations, A_c and A_r are the cross section area of the concrete and the longitudinal rebars, respectively, and F_{yr} is the yield stress of the steel rebar.

The effective area of steel, A_{sc}, is given by Eq.(3.6). In this equation, the web is assumed to be fully effective although the FE analyses showed that the residual stresses and transverse stresses reduce its capacity by 5% on average. For simplification, this reduction in the web capacity has been assigned to the flange by including it in the calculation of the effective width of the flange, b_e. This simplification is deemed acceptable because the flange has twice the area of the web, which results in a small variation on b_e.

Equation (3.9) for the plate stiffness coefficient, k_{fl}, was derived empirically from elastic buckling analysis of FE models of steel column flanges, with fixed boundary conditions on three sides and free on one unloaded edge. These values for k_{fl} were close to the theoretical values (Salmon and Johnson, 1996) and typically smaller than those proposed by Tremblay et al. (2000).

Equation (3.7) is proposed to determine b_e/b for design. This equation is adapted from the column design curve expression proposed by Loov (1996) and implemented in the CSA-S16.1 Standard for the design of steel structures in Canada (1994b). Table 3.6 presents the experimental ($P_{u,exp}$) and predicted ($P_{u,pred}$) ultimate loads for Specimens of Series 1 to 3, with theoretical models presented in Papers 1 and 3. Both models predict well the experimental loads but the model presented in Paper 3 gives a more realistic distribution of the load carrying capacities of the steel shape and the concrete, and is therefore recommended for design, with a value of n in Eq.(3.6) equal to 1.5.

TABLE 3.6. Experimental and Predicted Ultimate Loads

Test Series	Design.	$P_{u,exp}$ (kN)	$P_{u,exp}/P_{u,pred.}$ Paper 1 (-)	$P_{u,exp}/P_{u,pred.}$ Paper 3[1] (-)
Series 1 (Small Specimens)	C-2	10 100	1.04	1.05
	C-3	9 690	1.02	1.03
	C-4	9 390	1.03	1.04
	C-5	10 000	1.00	1.01
	C-6	7 650	0.96	1.01
	C-7	4 280	1.03	1.04
Series 2 (Large Specimens)	C-8	16 470	0.99	1.01
	C-9	16 610	1.00	1.02
	C-10	16 240	0.94	0.95
	C-11	14 930	1.03	1.07
	C-12	17 450	0.98	0.99
Series 3 (Long-term Specimens)	P-1	4 770	1.02	1.04
	P-2	4 670	1.00	1.02
	P-3	4 790	1.02	1.05
	P-4	4 975	1.06	1.09
	P-5	9 225	1.12	1.09
Mean[2]			1.02	1.03
SD[2]			0.03	0.03

Notes: (1) With n=1.5
(2) Excluding P-5

CHAPTER IV

CONCLUSIONS and RECOMMENDATIONS

4.1 Conclusions for Paper 1

Five stub-column tests were performed on 600 x 600 mm partially encased composite (PEC) specimens made with slender steel I-shapes (Series 2). This test series supplemented previous tests (Series 1) performed on six smaller size specimens (300 mm and 450 mm) to assess possible size effects and to propose a design equation for the axial load capacity of this type of columns. The following observations can be drawn from the tests results presented:

- Modes of failure: All specimens failed by crushing of the concrete, in combination with local buckling of the steel shape flanges. The flanges on specimens with a link spacing equal to the depth started to buckle at around 75% of the test peak load and had a brittle and sudden failure. Specimens with a link spacing of half the depth and a flange width-to-thickness ratio of 23 experienced no buckling before peak load and showed a more ductile and progressive failure, and a higher post-peak residual capacity.

- Size effect: Comparison with previous tests revealed that 450 mm and 600 mm specimens failed in a similar manner. When compared to larger specimens with the same characteristics, a 300 mm specimen did not experience local buckling before peak load, had a more progressive failure, but exhibited the same post-peak response.

- Additional reinforcement: The additional longitudinal and transverse reinforcements, with the configuration used, improved the ductility and post-peak response of the column but no gain in the concrete strength due to confinement could be observed.

- Transverse stresses in the steel shape: Transverse stresses in the flanges and the web of the steel shape due to the expansion of concrete were found to have a negligible effect on the axial capacity of the columns, reducing its capacity by 1% on average.

- Axial stresses in the transverse links: High stresses developed in the transverse links, which acted as passive reinforcement to the transverse expansion of the concrete, resulting in stresses higher in the links than in the web. The stresses in the transverse links were typically doubled when the link spacing was halved, as a result of a better confinement of the concrete near the exposed face, a stiffening of the flanges which more effectively resisted the expansion of the concrete, and a higher axial strain at peak load.

4.2 Conclusions for Paper 2

Axial strains were measured in seven partially encased composite columns during a period of 150 days. Long-term loading was applied on four of the specimens. The nominal stress due to construction loads (Stage 1) was determined as 100 MPa in the steel shape, and the stresses after long-term service loads (Stage 2) were 170 MPa in the steel and 10 MPa in the concrete. This test series complemented previous tests performed

under short term loading (Series 1 and 2) to obtain data on the effects of creep and shrinkage of the concrete on the stresses in both materials, and to assess the possible effects of these parameters on the capacity of the columns. The following observations can be drawn from this study:

- Long-term column behaviour: At the end of the 150-day period, the compressive stress increase in the steel shape due to the shrinkage of the concrete was 7 MPa on average from the day of pouring. The ratio of creep to elastic strains for the concrete was 0.5 for specimens P-3 and P-4. Shrinkage and creep of the concrete produced respectively one-fifth and four-fifth of the long-term strains measured in the columns. The total average stress increase in the steel due to creep and shrinkage of the concrete under loading Stage 2, ranged from 37 MPa to 44 MPa in the steel shape, and with the values being slightly higher for the smaller specimens. The final stresses after 150 days, including the elastic stress, ranged from 215 MPa to 223 MPa in the steel shape, and from 6.5 MPa to 6.8 MPa in the concrete. The theoretical models presented in Paper 2 predicted adequately the long-term column strain due to shrinkage and creep of the concrete. The models were based on ACI (1992) equations for plain concrete and were adapted to PEC column to account for the restraint provided by the steel shape.
- Behaviour of column at failure: The failure mode of specimens which were subjected to long-term load was the same as that of identical specimens under short term loading: crushing of the concrete between two consecutive transverse links, together with local buckling of the flanges. Failure occurred on each concrete face nearly

simultaneously but at different elevations. The ultimate capacity of both type of specimens also very close, suggesting that the loading sequence and the creep of the concrete had negligible effects on the ultimate load of these columns. The model for the prediction of the ultimate load, presented in paper 1, and which did not include sequence of loading or long-term effects, still gave an accurate prediction for these specimens.

- Transverse stresses in the steel shape: The tensile transverse stresses in the web of the specimen not subjected to a long-term loading were high, but those in specimens with a long-term loading were significantly lower because the steel shape yielded before the concrete expanded rapidly near failure. It is therefore proposed not to reduce the axial capacity of the steel shape in the prediction model.
- Axial stresses in the transverse links: The tensile stresses in the transverse links at peak load ranged from 172 MPa to 298 MPa. The stress in the transverse link remains small when the steel section only is loaded (Stage 1) and increases with the transverse expansion of the concrete (Stages 2 and 3).

4.3 Conclusions for Paper 3

The conclusions regarding the key parameters that had to be reproduced by the FE models are presented herein:

- Capacity of the specimens: The numerical to experimental load ratio for Series 1, 2, and 3 composite specimens is equal to 1.00 if the concrete ultimate stress in the input

file is set to $f'_{ce}= 0.92\Psi f'_c$, a value that also represents better the experimental buckling load of the flange. The average numerical stresses carried by the flange, the web, and the concrete at peak load, were $0.88F_y$, $0.93\ F_y$, and $1.01\ f'_{ce}$, respectively, respectively. Slightly higher stress ratios were found in smaller specimens ($1.02\ f'_{ce}$ for 300 mm specimens vs. $1.00f'_{ce}$ for 600 mm specimens). High tensile residual stresses near the weld contributed to reduce the yield capacity in the web and the flange from zero to 8% when the column fails. The high tensile transverse stresses reduced the axial capacity of the web by 3% to 5% at peak load. Finally, the local imperfections reduce the axial capacity of the flange by approximately 2% for specimens with s=d/2 and 4% to 6% for specimens with s=d. Limited confinement increase by 1% to 3% the capacity of the concrete at peak load, for specimens with s=d/2. A new set of design equations were proposed to predict the axial capacity of this type of PEC columns of any size, which included the effects of local flange buckling, and strength variation with size of structural concrete.

- Strain at peak load: The FE models represented very well the load-strain behaviour of the test specimens, throughout the loading history. The numerical models overestimated the experimental strain at peak load by 8% on average, because the experimental strain was measured over the full height of the column, including zones with higher strength concrete, while the model strain was taken over the height of one link spacing only. The post-peak response was only partially obtained.
- Modes of failure: The failure modes in the FE analyses were identical to the experimental ones, with local buckling of the flange outwards. Furthermore, the

nonlinear analyses gave a better accuracy regarding failure modes and peak load when the local imperfections of the flange were initially set outwards instead of inwards, as measured experimentally. This is attributed to the incapacity of the FE model adopted to reproduce the volumetric expansion of concrete near peak load.

- Axial stresses in the transverse links: The stresses in the transverse links were very well represented by the numerical models and were found to be dependent on the transverse expansion of the concrete. At peak load, the models generally underestimated slightly the experimental link stresses. Based on the dimensions used in the experimental programme, the cross-section area of one transverse link should be at least equal to 0.025 d.t .
- Transverse stresses in the web of the steel shape: The FE model transverse stresses in the web were compressive at the beginning of the analysis, and tensile at peak load, because of the variation of the concrete Poisson's ratio, which confirmed most of the experimental observations.
- Loading sequence and long-term effects: The FE program used was capable of modelling satisfactorily the construction sequence, using the removal and addition of elements in the model. The effects of creep and shrinkage of the concrete on the steel shape were modelled by increasing the stresses in the steel only models, prior to composite action. These effects were found not to influence the axial capacity of the columns, as also observed in the tests.

4.4 Summary of conclusions

Based on the results from the experimental and finite element studies on PEC columns, it is concluded that:

- The failure mode occurs by buckling of the steel flanges between consecutive transverse links, together with concrete crushing.
- Behaviour of 300 mm specimens is more ductile larger specimens; specimens larger than 600 mm are expected to have behaviour similar to 600 mm specimens.
- More closely spaced links and additional reinforcements increase the column ductility but not significantly the axial capacity.
- The effects of the concrete confinement, the tensile transverse stresses in the steel shape, the sequence of construction, and the long-term loading may be neglected in computing the column axial capacity.
- High tensile stresses develop in the transverse links due to concrete expansion.
- The axial capacity of the column is well predicted using the design equations proposed in Paper 3, which include flange local buckling and structural concrete size effects.

4.5 Recommendations

Based on the experimental programme on stub-columns (Paper 1), it is recommended that:

- The transverse link spacing be equal to d/2 or less and that the b/t ratio be limited to 30 in order to avoid brittle column failure and ensure adequate post-peak behaviour. Based on the dimensions used in the experimental programme, the cross-section area of one transverse link should be equal to the greater of 0.025 d.t and 100 mm^2.
- Additional reinforcement (longitudinal rebars, U-stirrups) be omitted unless the column must retain a certain capacity at high strains after the peak load is reached, or to meet other ductility requirements (e.g. seismic response).
- Additional tests should be made with a small load eccentricity about the weak and strong axes to assess the importance of the axial capacity reduction when only one beam frames into the column.
- Additional test should be made on a PEC column without transverse links to define more precisely the role of these component on the axial capacity, the load redistribution between steel and concrete, and the global integrity of the column.
- Multiaxial strain gauges should be used to measure the effect of the concrete expansion on transverse stresses more accurately.
- The reduction in capacity of the steel web at column ultimate load should be investigated further.

- The longitudinal column shortening should be measured over a gauge length of 3d, excluding the zone of higher strength concrete.

Based on the long-term experimental programme on stub-columns (Paper 2), it is recommended that:

- Long-term measurements be performed with a system other them DEMEC points, which demand greater experience and care from the user due to its inherent variability. Strain gauges, vibrating wire gauges, string potentiometers or LVDTs may prove suitable alternatives.
- A better care should be given to strain measurements on standardised cylinders for evaluating the shrinkage and creep effects. Strain gauges are preferred over DEMEC points. More cylinders should also be made to measure the mechanical properties of each specimen. A total of 3 cylinders per specimens should be used to measure the compressive stress f'_c and the elastic modulus E_c, for each day that measurements are needed.
- Additional test could be performed in controlled atmospheric conditions on specimens similar to those already tested in ambient conditions, to assess the influence of environmental conditions on long-term behaviour.
- Additional testing could be done with using more usual concrete and also high-strength concrete.

Based on the finite element analyses on stub-columns (Paper 3), it is recommended that:

- The expansion of the concrete should be modelled so as to reflect more accurately the rapid increase of the Poisson's ratio near failure. A temperature variation applied to the concrete only may simulate adequately this phenomenon.
- Interaction between the concrete and the steel shape may be modelled more adequately by assigning more realistic values of adherence properties based on experimental and theoretical data (e.g. Mohr-Coulomb law).
- The numerical convergence problems preventing the analyses of the post-peak behaviour should be investigated. It is believed that the stiffness of the springs used to model the interface between steel and concrete are responsible for these problems since steel only and concrete only models exhibited adequate post-peak behaviour.
- The dimensions of the plate elements representing the steel shape could be reduced near the weld to model more accurately the residual strain.
- A finite element model similar to the one described in Paper 3 be used to perform any additional parametric analyses to broaden the scope of the experimental programme.
- Validated models could be used to model the behaviour of eccentrically loaded columns and slender columns.

Based on the conclusions of the two experimental programmes and the finite element model presented in this report, tests on 300 mm and 450 mm may be accurately extrapolated to represent adequately the behaviour of larger columns. The design equations proposed in Paper 3 be used to predict the axial capacity of PEC short columns (Height $\leq$ 5d) of any square cross-sectional dimensions, with the factor n set equal to 1.5.

REFERENCES

ABAQUS (2000) Documentation taken from *Abaqus.com* website.

ACI COMMITTEE 209 (1992) "Prediction of creep, shrinkage, and temperature effects in concrete structures." *ACI Manual of Concrete Practice*, Detroit, pp. 209R1-209R47.

BLOEM, D. (1968) "Concrete strength in structures." *ACI Journal*, 65-14, pp.176-187.

BODE, H. (1976) "Colonnes constituées de tubes en acier remplis de béton: dimensionnement et utilisation." *Acier-Stahl-Steel*, 11-12, pp.388-393.

BOUZAIENE, A., MASSICOTTE, B. (1997) "Programme MEF97 Manuel d'utilisation." *EPM/CS No. 1997-2*, Dept. of Civil, Geological and Mining Engineering, Ecole Polytechnique, Montreal, Canada. Draft version.

BRADFORD, M.A., GILBERT, R.I. (1990) "Time-dependent analysis and design of composite columns." *ASCE J. Struc. Div.*, **116**(12), pp. 3338-3357.

BRIDGE, R.Q. (1979) "Composite columns under sustained load." *ASCE J. Struc. Div.*, **104**(7), pp. 563-576.

BRIDGE, R.Q., O'SHEA, M.D. (1996) "Local buckling of square thin-walled steel tubes filled with concrete." *5th Intl. Coll. on Stability of Metal Structures*, Chicago, Il, pp.63-72.

BRIDGE, R.Q., RODERICK, J.W. (1978) "Behavior of built-up composite columns." *Journal of Structural Division*, ASCE, **104**(7), pp.1141-1155.

BRODERICK, B.M., ELNASHAI, A.S. (1994) " Seismic resistance of composite beam-columns in Multi-Storey structures. Part 2: analytical model and discussion of results." *J. Construct. Steel Research*, **30**, pp. 231-258.

CEN, AFNOR (1994) "Construction mixte acier et béton: Conception et dimensionnement des structures mixtes acier et béton. " *Eurocode 4* (in French).

CHICOINE, T., MASSICOTTE, B., TREMBLAY, R. (2000a) " Long-Term Behaviour and Strength of Partially Encased Composite Columns made with Built-Up Steel Shapes." *ASCE Journal of Structural Engineering*. In press.

CHICOINE, T., TREMBLAY, R., MASSICOTTE, B. (2000b) "Long-term test programme on partially encased built-up three-plate composite columns." *EPM/GCS No. 2000-20*, Dept. of Civil, Geological and Mining Engineering, École Polytechnique, Montreal, Canada.

CHICOINE, T., TREMBLAY, R., MASSICOTTE, B., M., RICLES, J., LU, L.-W. (2000c) "Behavior and strength of partially encased columns with built-up shape." *ASCE Journal of Structural Engineering*. In press.

CHICOINE, T., TREMBLAY, R., MASSICOTTE, B., YALCIN, M., RICLES, J., LU, L.-W. (2000d) "Test programme on large-scale partially-encased built-up three-plate composite columns." *Joint Report, EPM/GCS No. 00-06*, Dept. of Civil, Geological and Mining Engineering, École Polytechnique, Montreal, Canada – ATLSS Engineering Research Center, *No. 00-04*, Lehigh University, Bethlehem, Pennsylvania, USA.

CHICOINE, T., TREMBLAY, R., MASSICOTTE, B. (2001) " Finite element modelling of the experimental response of partially encased composite columns." *Steel and Composite Structures International Journal*. In press.

CHICOINE, T., TREMBLAY, R., MASSICOTTE, B. (2001a) " Finite element modelling of the experimental response of partially encased composite columns." *EPM/GCS No. 2001-06*, Dept. of Civil, Geological and Mining Engineering, Ecole Polytechnique, Montreal, Canada.

CSA (1994) *CAN/CSA-A23.3-94 Code for the design of concrete structures for buildings.* Canadian Standards Association, Rexdale, Ontario.

CSA (1994b) *CAN/CSA-S16.1-94 Limit States Design of Steel Structures.* Canadian Standards Association, Rexdale, Ontario.

CSA (2001) *CAN/CSA-S16.1-01 Limit States Design of Steel Structures.* Canadian Standards Association, Rexdale, Ontario. (Publication pending)

CUSSON, D., DE LARRARD, F., BOULAY, C., PAULTRE, P. (1996) "Strain localization in confined high-strength concrete columns." *Journal of Structural Engineering*, ASCE, **122**(9), pp.1055-1061.

DE LARRARD, F. (1999) *Concrete Mixture Proportioning – A scientific approach,* E & FN SPON, London, UK.

ELNASHAI, A.S., BRODERICK, B.M., DOWLING, P.J. (1995) "Earthquake-resistant composite steel/concrete structures." *Structural Engineer*, **73**(8), pp.121-132.

FAULKNER, D. (1977) "Compression tests on welded eccentrically stiffened plate panels." *Steel Plated Structures,* P.J. Dowling Ed, London, pp. 581-617.

FILION, I. (1998) "Étude expérimentale des poteaux mixtes avec section d'acier de classe 4", *Report n°. EPM/GCS-1998-06,* Dept. of Civil, Geological and Mining Engineering, Ecole Polytechnique, Montreal, Canada, 297 p.

FINTEL, M., GHOSN, S.K., IYENGAR, H. (1987) "Column shortening in tall structures – Prediction and compensation", *Report PCA EB108.01D*, Dept. Portland Cement Association, Skokie, Il., 35 p.

FUKUMOTO, Y., ITOH, Y. (1984) "Basic compressive strength of steel plates from test data" *Proc. JSCE*, No 344, April, pp.129-139.

FURLONG, R.W. (1967) "Strength of steel-encased concrete beam columns." *Journal Structural Division*, ASCE, **93**(5), pp.113-124.

GARDNER, N.J., JACOBSON, E.R. (1967) "Structural behavior of concrete-filled steel tubes." *ACI Journal*, **64**(7), pp.404-412.

GE, H., USAMI, T. (1992) "Strength of concrete filled thin walled steel box columns: Experiment." *Journal of Structural Engineering*, ASCE, **118**(11), pp.3036-3054.

HKS (2000) *Abaqus program version 5.8-19* Pawtucket, RI, USA.

HUNAITI, Y.M., ABDEL FATTAH, B. (1994) "Design considerations of partially encased composite columns." *Proc. Instn. Civ. Engrs Structs and Bldgs*, 106, pp.75-82.

JOHNSON, R.P., MAY, I.M. (1978) "Tests on restrained composite columns." *Structural Engineer*, **56b**(2), pp.21-28.

KATO, B. (1996) "Column curves of steel-concrete composite members." *Journal of Constructional Steel Research*, **39**(2), pp.121-135.

KNOWLES, R.B., PARK, R. (1970) "Axial load for concrete-filled steel tubes." *Journal Structural Division*, ASCE, **96**(10), pp.2125-2153.

KUPFER, H., HILSDORF, H.K. (1969) "Behavior of concrete under biaxial stresses" *ACI Journal*, Title no 66-52, pp.656-666.

LOOV, R. (1996) "A simple equation for axially loaded steel column design curve." *Can. J. Civ. Eng.*, 23, pp.272-276.

MARANDA, R. (1999) "Analyses par éléments finis de poteaux mixtes avec sections d'acier en I de classe 4" *Report n°. EPM/GCS-1998-11*, Dept. of Civil, Geological and Mining Engineering, École Polytechnique, Montreal, Canada, 139 p.

MORINO, S., KAWAGUCHI, J., CAO, Z.S. (1996) "Creep behaviour of concrete-filled steel tubular members." *Composite construction in steel and structures III*, Proceedings of an Engineering foundation conference, Irsee, pp.514-525.

NAKAI, H., KURITA, A., ICHINOSE, L.H. (1991) "An experimental study on creep of concrete filled steel pipes." *Proceedings of the 3rd international conference on steel and concrete composite structures*, pp.55-60.

NEVILLE, A.M. (1966) "A general relation for the strengths of concrete specimens of different shapes and sizes." *ACI Journal*, **63**, pp.1095-1108.

NEVILLE, A.M., DILGER, W.H., BROOKS, J.J. (1983) *Creep of plain and structural concrete.* Construction Press, London and New-York, 361p.

NEWMAN, K. (1987) "Labcrete, Realcrete, and Hypocrete. Where we can expect the next durability problems." *ACI SP-100 Concrete Durability, vol.2.*

O'SHEA, M.D., BRIDGE, R.Q. (2000) "Design of circular thin-walled concrete filled steel tubes." *ACI Journal of structural engineering*, **126**(11), pp.1295-1303.

PLUMIER, A., ABED, A., TILIOUNE, B. (1995) "Increase of buckling resistance and ductility of H-Sections by encased concrete." Behavior of Steel Structures in Seismic Areas, F.M. Mazzolani and V. Gioncu, Ed., E&FN SPON, London.

RICLES, J.M., PABOOJIAN, S.H. (1994) " Seismic Performance of Steel-Encased Composite Columns. " *Journal of Structural Engineering*, ASCE, **120**(8), pp.2474-2494.

ROIK, K., BERGMANN, R., AND MANGERIG, I. (1987) "The German design method for composite columns with regard to creep and shrinkage of concrete." *Composite construction in steel and concrete, Proceedings of Eng. Foundation Conf.*, ASCE, Henniker, New Hampshire, pp.561-565.

SALMON, C.G., JOHNSON, J.E. (1996) *Steel Structures: Design and Behavior*, HarperCollins, 4th Edition, New York, NY.

SAW, H.S., LIEW, J.Y.R. (2000) "Assessment of current methods for the design of composite columns in buildings." *Journal of Constructional Steel Research*, **53**, pp.121-147.

SIGIURA, K., ONO, K., OYAWA, W.O., WATANABE, E., YAMAGUCHI, T. (2000) "Interface interaction in filled steel tubular members as modeled by open sandwich beams." *Proc. Composite Construction IV*, Engineering Foundation, Banff, Canada.

SSRC, TASK GROUP 20 (1979) "A specification for the design of steel-concrete composite columns." *Engineering Journal*, vol.16, 4th quarter, AISC, pp.101-115.

SSRC (1998) *Guide to Stability Design Criteria for Metal Structures*, 5th ed., T.V. Galambos, Ed., John Wiley & Sons, New York, NY.

STEVENS, R.F. (1965) "Encased stanchions." *Structural Engineer*, **43**(2), pp.59-66.

TERREY, P.J., BRADFORD, M.A., GILBERT, R.I. (1994) "Creep and Shrinkage of concrete in concrete-filled circular steel tubes." *Proceedings of the 6th international symposium on tubular structures*, pp. 293-298.

TOMII, M., YOSHIMURA, K., MORISHITA, Y. (1977) "Experimental studies on concrete-filled steel tubular stub columns under concentric loading." *ASCE International Colloquium on Stability of Structures under Static and Dynamic Loads*, Washington, DC, pp.718-740.

TREMBLAY, R., MASSICOTTE, B., FILION, I., MARANDA, R. (1998) "Experimental study on the behavior of partially encased composite columns made with light welded H steel shapes under compressive axial loads." *1998 SSRC Annual Technical Meeting.*

TREMBLAY, R., CHICOINE, T., MASSICOTTE, B. (2000) "Design equation for the axial capacity of partially encased non-compact columns." *Proc. Composite Construction IV*, Engineering Foundation, Banff, Canada.

TSAI, W.T. (1988) "Uniaxial compression stress-strain relation of concrete." *ASCE J. Structural Engineering*, **114**(9), pp.2133-2136.

USAMI, T., FUKUMOTO,Y. (1982) "Local and overall buckling of welded box columns." *Journal of Structural Division*, ASCE, **108**(3), pp.525-542.

UY, B. (2000) "Strength of concrete filled steel box columns incorporating local buckling." *Journal of Structural Engineering*, ASCE, **126**(3), pp.341-352.

UY, B. (2001) "Static long-term effects in short concrete-filled steel box columns under sustained loading." *ACI Structural Journal*, **98**(1), pp.96-104.

VINCENT, R. (2000) "Design and application of partially encased non-compact composite columns for high-rise buildings." *Proc. Composite Construction IV*, Engineering Foundation, Banff, Canada.

WHEELER, A.T., BRIDGE, R.Q. BRIDGE (2000) "Thin walled steel tubes filled with high strength concrete in bending." *Proc. Composite Construction IV*, Engineering Foundation, Banff, Canada.

WINTER, G. (1968) "Thin-walled structures – Theoretical solutions and test results." *Proc. IABSE Congress*, pp.101-112.

WRIGHT, H.D. (1993) "Buckling of plates in contact with a rigid medium." *Structural Engineer*, **71**(12), pp.209-215.

APPENDIX A – PAPER 1

Behavior and Strength of Partially Encased Composite Columns with Built-Up Shapes

By Thierry Chicoine, Robert Tremblay, Bruno Massicotte,

James M. Ricles, and Le-Wu Lu

Submitted to : ASCE Journal of Structural Engineering, July 2000

Accepted for publication, September 2001

Behavior and Strength of Partially Encased Composite Columns with Built-Up Shapes

By Thierry Chicoine[1], Robert Tremblay[2], Bruno Massicotte[2], James M. Ricles[3], and Le-Wu Lu[3]

ABSTRACT: A comprehensive study has been conducted to investigate the behavior and strength of a new type of partially encased composite column made with thin-walled, welded I-section, stiffened with transverse links. Concrete is poured between the flanges of the steel section. The paper describes and presents the results of the testing of five large-size 600 x 600 mm short column specimens. Failure of all specimens was due to local buckling of the flange plates along with concrete crushing. Transverse stresses measured in the steel section were found to be small and did not impair the axial compressive strength of the steel section. High stresses, however, developed in the transverse links as a result of the lateral expansion of the concrete. The study also shows that a closer link spacing and the use of additional reinforcements can improve the post-ultimate load behavior.

A comparison is made with test results obtained in previous studies on smaller specimens and an improved formula for predicting the column axial load capacity

[1] Graduate Research Assistant, [2] Professor, Dept. Civil, Geological, and Mining Engineering, Ecole Polytechnique, Montreal, Canada H3C 3A7.
[3] Professor, Dept. of Civil and Environment Engineering and Center for Advanced Technology for Large Structural Systems (ATLSS), Lehigh University, Bethlehem, PA 18015.

accounting for local flange buckling and the variation of the concrete strength with column size is proposed for design application.

INTRODUCTION

A new type of steel and concrete composite column consisting of thin-walled, I-shaped steel section with concrete being poured between the flanges of the steel section has recently been developed and patented by the Canam Manac Group (Fig. 1a). The steel section features very slender plates exceeding the width to thickness ratio limits for non-compact sections. Transverse links between the flanges are spaced at regular intervals to enhance the resistance of the flanges to local buckling. The proposed composite column is intended to carry only axial loads in multi-storey buildings, the lateral loads being resisted by other structural systems such as shear walls.

Common types of composite column design include concrete filled tubes (CFT) and steel reinforced concrete columns (SRC), as respectively illustrated in Fig. 1b and 1c. However, these composite column concepts have limitations that may restrict their use in practice. For instance, the cross-section dimensions for small CFTs are limited to available standard steel tube shapes, and larger columns must be custom made. SRC columns require extensive formwork, especially at the beam-column connections. The new partially encased column studied in this paper aims at alleviating these restrictions, as the steel shape is made from plates flame-cut to the desired dimensions, and the beams connect directly to the flanges about the strong axis, or to a plate welded to the flange tips

about the weak axis (Vincent, 2000). The new system is also different from partially-encased composite column currently used in European practice (CEN-AFNOR, 1994) as the latter is made with hot-rolled standard W-shapes not prone to local buckling. By using thin steel plates in the new column design, the fraction of the load carried by the concrete is increased, leading to more cost-effective columns.

Extensive experimental studies have been performed on CFT (Furlong, 1967; Gardner and Jacobson, 1967; Knowles and Park, 1970; Tomii et al., 1977) and SRC columns (Stevens, 1965; Bridge and Roderick, 1978; Johnson and May, 1978; SSRC, 1979; Ricles and Paboojian, 1994) and design procedures have been developed for these systems (Saw and Liew, 2000). Research has also been carried out on partially-encased columns with W-shapes (e.g., Hunaiti and Abdel Fattah, 1994; Elnashai et al., 1995; Plumier et al., 1995) and local buckling in composite columns has also been studied and documented (e.g., Ge and Usami, 1992; Wright, 1993; Bridge and O'Shea, 1996; Uy, 2000).

Tremblay et al.(1998) reported on the first series of tests on the new column system and proposed a design equation accounting for local flange buckling. The specimens tested included six composite stub columns with a cross-section of 300 x 300 mm and 450 x 450 mm. This paper describes the test program performed on five 600 x 600 mm columns to evaluate possible size effects on the ultimate load and the failure mode of specimens with a larger cross-section. In addition, the need for additional

reinforcement such as longitudinal rebars and stirrups was examined and experimental data was obtained on the magnitude of transverse stresses in the steel shape and the links due to the lateral expansion of the concrete.

EXPERIMENTAL PROGRAM

Geometric Properties of Specimens

The characteristics of the specimens are listed in Table 1 and their geometry is illustrated in Fig. 2. In Table 1, series 1 refers to specimens C-2 through C-7 reported by Tremblay et al. (1998) and series 2 corresponds to tests C-8 through C-12 described in this paper. All five composite columns of series 2 had a cross-section of 600 x 600 mm and a height of 3 000 mm. The specimens met the SSRC (1998) requirements for stub columns: the column height being between three and five times the column depth (d) and less than 20 times the radius-of-gyration about the weak axis, r_y, ($20r_y \approx 20 \times 0.3d = 3\,600$ mm). For each specimen, the same plate thickness was used for the web and flanges. The nominal plate thicknesses were 9.53 mm for C-11 and 12.7 mm for the other columns. The measured thicknesses are presented in Table 1. The transverse links of the specimens were round bars with a diameter of 16 mm.

Specimen C-8 was identical to Specimen C-4 except that all dimensions were scaled up by a factor of 1.33 to examine possible size effects. In this specimen, a link spacing equal to the depth of the column was expected to provide only limited confinement of the concrete and to result in a reduced buckling strength for the steel

flanges. Specimen C-9 was a replica of Specimen C-8. It was included to assess the reproducibility of the results and obtain a more robust experimental database. Specimen C-10 was identical to Specimen C-2 except that all dimensions were also scaled up by a factor of 1.33. A closer link spacing was used in this column (s=d/2) to improve the local buckling capacity of the steel shape and the confinement of the concrete. Specimen C-11 had the same dimensions as C-8 except that thinner plates (9.53 mm) were used to investigate the influence of this parameter on local flange buckling behavior.

Specimen C-12 was identical to Specimen C-10 but included four additional longitudinal 20M rebars (ϕ=20mm), and two U-shaped 15M stirrups (ϕ=15mm). Holes were punched in the web of the steel shape to allow the legs of the stirrups to pass through and be anchored in the concrete on the opposite side of the web. The spacing of the stirrups was set the same as that of the transverse links and bar sizes were determined to meet the requirements of Clause 7.6.5.2 of the CSA-A23.3-94 Canadian Standard for the design of concrete structures (CSA, 1994): tie spacing equal to the lesser of 16 times the diameter of the smallest longitudinal bar or 48 tie diameters. This reinforcement was added to enhance the concrete confinement, hence improving the axial capacity and the post-peak load carrying capacity of the column.

Each specimen had extra transverse links and higher strength concrete over a height of d at each end to prevent local failure at these locations due to possible uneven loading (Fig. 2). End plates were also welded to each specimen to obtain a more uniform

load distribution in the column. All columns were cast and cured vertically to reproduce actual construction field conditions of placing and ageing of the concrete. All specimens were fabricated, instrumented and cast at the Canam Manac plant in Laval, Canada before being shipped for testing to the Fritz Engineering Laboratory of Lehigh University, Bethlehem, PA. More information on the test specimens and their preparation can be found in Chicoine et al. (2000).

Material Mechanical Properties

The nominal material properties were the same as for specimens C-2 to C-7: normal weight concrete of 30 MPa and steel plates with a nominal yield strength of 350 MPa. These were selected to reproduce common practice in structural design of columns, while accommodating the capacity of the testing equipment. The measured properties of the concrete in the middle 3/5 of Specimens C-8 through C-12 were: a strength of 34.2 MPa, a peak strain of 2 000 $\mu\varepsilon$, an elastic modulus of 27 300 MPa and a Poisson's ratio of 0.175. The concrete at the ends had a measured strength of 51 MPa. The actual static yield stress was 360 MPa for the 12.7 mm plates and 345 MPa for the 9.53 mm plates. The longitudinal rebars and the U-stirrups had a nominal yield strength of 400 MPa. The transverse links had a nominal yield strength of 300 MPa.

Geometric imperfections and residual stresses

Table 1 presents the mean (μ) and the standard deviation (σ) of the out-of-straightness of the column flanges, δ_0, as measured along the tip of each flange at mid-

distance between consecutive transverse links in the central 3/5 of the specimen height. For specimens with s=d/2, the mean amplitude was s/802 with a standard deviation of s/1980. The corresponding values were respectively s/433 and s/596 for specimens with s=d. Larger imperfections were measured on the smaller specimens, for which the mean and the standard deviation were, respectively, s/573 and s/1734 for s=d/2 and s/381 and s/1265 for s=d. For all column sizes the imperfections were also found to be generally larger for more widely spaced links, as more links better straightened the flanges.

In addition, inward imperfection measurements outnumbered the outward ones with a ratio of 18 to 1 on the 600 mm specimens, and no outward imperfections were found on the 300 mm and the 450 mm specimens. This tendency is due to the fabrication process used for the specimens. After welding the plates together, the flanges tended to bend inward due to uneven shrinkage during cooling. The flanges were then heated externally to regain some straightness, but not completely. The transverse links were thereafter forced between the slightly inward bent flanges, creating a concave surface between the links. The inward imperfections likely had a beneficial effect on the local buckling capacity of the flanges because the plates in contact with the concrete could not buckle outward until sufficient expansion of the concrete had overcome the imperfections.

Residual stresses were measured using the sectioning method (SSRC, 1998) on additional columns identical to the test specimens. Figure 3 presents the average residual

stresses (σ_r) on the flanges and web of Specimens C-8 to C-12 (continuous lines) together with the individual readings. As shown, the individual measurements were generally close to the average value. Since the specimens were to be tested under axial compression, the sign convention adopted in this paper refers to positive stresses as compression. As shown in Fig. 3, the values of σ_r in the flanges range from 64 MPa to –301 MPa for Specimen C-11, and from 66 MPa to –291 MPa for the other specimens. In the web, σ_r varies from 53 MPa to –86 MPa for Specimen C-11, and from 54 MPa to –32 MPa for the other specimens. The high tensile stresses at the junction of the flanges and web was the result of the welding operation and subsequent uneven cooling of the steel plates. Similar magnitude and distribution of σ_r were found in Specimens C-2 through C-6 (Tremblay et al.). On the smaller 300 mm Specimen C-7, however, σ_r were generally higher, ranging from 87 MPa to –374 MPa in the flanges and from 89 MPa to –59 MPa in the web.

Test setup and instrumentation

The tests were performed with a 5 million pound (22 250 kN) Universal-Testing Machine (Fig. 4) which provided essentially fixed end conditions to the specimens. Upon installation of the column in the machine, a thin layer (3 mm ±) of a high strength levelling grout (70 MPa) was placed between the platens and the specimen end plates to provide a uniform load distribution over the column cross section. During the test, the axial shortening of the column was measured using Linear Variable Displacement Transducers (LVDTs) installed at the four corners (Fig. 2). Longitudinal and transverse

strains were recorded with strain gauges located on the steel flanges and web in the mid-height region of the column. Strain gauges were also put on the transverse links and concrete at the same elevation as those on the steel. Typical instrumentation at link elevation is illustrated in Fig. 2.

Prior to testing, the alignment of the column was checked up to 20% of the predicted ultimate load using the longitudinal strain gauges and LVDTs. A specimen was considered properly aligned if the increment in strain measurements did not deviate by more than 10% from the average incremental strain readings. All specimens were properly aligned before testing except column C-12 for which the readings on two corners were offset by 27% and 32% with respect to the average strain. During that test, however, the difference diminished and the readings at the same corners were offset by only 7% and 9% at 0.95 P_u. After the alignment, the load was set back to zero, and the test was started. The stub column was gradually loaded at a rate of 220 kN per minute, in accordance with SSRC testing procedure (1998). This produced a strain rate which was approximately the same as that used in Series 1 testing. Near and after failure, the load was manually controlled to allow visual observations and capture post-peak behavior. The test was terminated after the specimen had shortened to three times the axial deformation at peak load.

EXPERIMENTAL OBSERVATIONS AND RESULTS

Experimental observations and failure modes

The experimental load ($P_{u,exp.}$) for the stub columns are presented in Table 1. In the following, the specimens are grouped according to their link spacing, as columns with the same s/d ratio exhibited a similar failure mode and post-peak behavior.

Specimens C-8, C-9, and C-11

Specimens C-8, C-9, and C-11 all had a link spacing equal to the depth d, but had different b/t ratios. The first sign of local buckling in Specimens C-8 and C-11 appeared at approximately 75% of the peak load. No buckling could be observed prior to ultimate load in Specimen C-9, probably because the inward imperfections of its flanges were larger, as shown in Table 1: 2.02 mm compared to 1.43 mm and 0.71 mm for C-8 and C-11, respectively.

The failure of these three specimens occurred by crushing of the concrete together with local buckling at the same location (Figs. 5 and 6a). The failure was brittle and sudden in all cases. Upon closer inspection of the main concrete crushing zone of these specimens, two failure planes could be identified. Transverse link welds failed at two locations on Specimen C-11 after the ultimate load was reached, as the concrete pushed against the link while the steel shape was buckling.

Specimens C-10 and C-12

Specimens C-10 and C-12 both had a link spacing equal to d/2 and no sign of local buckling could be seen on these columns before reaching the peak load. The failure occurred by crushing of the concrete together with local buckling of the steel shape and, for C-12, buckling of the longitudinal rebars at the same locations (Figs. 5 and 6b). Unlike the other specimens, the failure of columns C-10 and C-12 was ductile and progressive. Inspection of the concrete crushing zone revealed failure planes similar to the one observed for C-8, but over a height of 300 mm. In Specimen C-12, failure planes formed on both sides of the column, indicating that load redistribution from one side to the other took place during failure. A transverse link weld failed at one location on Specimen C-10 after the ultimate load was reached.

Load-deformation response

Figure 7 shows the applied axial load versus the average axial strain, ε_a, of the columns. The latter corresponds to the average shortening of the column as measured by the longitudinal LVDTs located at the four corners of each specimen, divided by the length between their attachment points on the column (2 600 mm).

The behavior of Specimen C-11 was linear up to approximately a load of 8 000 kN (0.53 P_u). The stiffness of all other specimens started to decrease at about 10 000 kN (0.57 to 0.62 P_u). The ratio of the secant stiffness at 0.4 P_u to the tangent stiffness at 0.85 P_u was 0.54, 0.53, and 0.53 for Specimens C-8, C-9, and C-11, and 0.46

and 0.48 for Specimens C-10 and C-12, respectively. The strain at peak load was 1 840, 1 770, and 1 810 με for Specimens C-8, C-9, and C-11, which had a link spacing of d. These strain values are lower than the peak strain of the concrete cylinders (2 000 με) but approximately correspond to the yield strain of the steel (C-8 and C-9: 1 800 με; C-11: 1 725 με). Larger strains were measured with a spacing of d/2: 2 250 and 2 580 με for specimens C-10 and C-12, respectively. The differences between the strains measured before and after peak load, at a load of 0.95 P_u, were : 538 με for C-11, 586 με for C-8, 1 031 με for C-10, and 1 134 με for C-12. These measurements clearly indicate that a link spacing of d/2 resulted in a more ductile response, with larger deformation near peak load. Local buckling of the flanges was delayed and the failure of concrete was constrained to take place in a smaller volume (see Fig. 5). In addition, more numerous and closely spaced links provided a higher and more uniform confinement of the concrete near the face of the column.

The ratio of the residual capacity to the peak load is equal to 0.56, 0.51, and 0.34 for specimens C-8, C-9, and C-11. A higher value of 0.66 is obtained for Specimen C-10 with s = d/2. The residual capacity is defined herein as the load where the post-peak response flattens, between 4 000 and 4 500 με. Specimen C-12 had additional reinforcement and behaved differently, exhibiting a softer post-peak response while maintaining a much higher capacity. At 5 000 με, its resistance reduced only to 0.79 P_u, which is 1.59 times the strength of Specimen C-8 at the same deformation. The load drop was so sudden for Specimens C-8, C-9, and C-11 that only a few readings could be taken

between the peak load and the residual load, as illustrated by the dotted lines on Fig. 7. Among all the specimens, C-11 developed the lowest residual capacity because it had thinner plates and a link spacing of d. Therefore, the b/t ratio, the link spacing, and the presence of additional reinforcement all influenced the ductility and post-peak response of this type of composite column.

Effect of transverse stresses on axial capacity of steel shape

The pressure exerted on the walls of the steel shape by the expansion of the concrete can induce transverse tensile (hoop) stresses in the steel shape, and such stresses can, in turn, reduce the yield strength of the steel in the longitudinal direction. The ratio σ_l/σ_{VM} near peak load was used to assess this possible detrimental effect on the capacity of the steel shape, where σ_l is the applied longitudinal stress and σ_{VM} is the von Mises stress. The value of σ_l is obtained from strain measurements in the longitudinal direction, ε_1, and the transverse direction, ε_2, assuming a biaxial stress state defined by:

$$\begin{bmatrix}\sigma_1\\ \sigma_2\end{bmatrix}=\frac{E}{1-\nu^2}\begin{bmatrix}1 & \nu\\ \nu & 1\end{bmatrix}\begin{bmatrix}\varepsilon_1+\varepsilon_r\\ \varepsilon_2-\nu\varepsilon_r\end{bmatrix} \qquad (1)$$

where σ_2 is the transverse stress, ε_r is the longitudinal residual strain corresponding to the value of the residual stresses at the gauge location, and E and ν are the elastic modulus (200 000 MPa) and the Poisson's ratio (0.3) of the steel, respectively. In the calculations, the residual stresses were assumed to occur only in the longitudinal direction of the column and $\nu\cdot\varepsilon_r$ was therefore subtracted from the transverse strain to obtain zero transverse stress induced by the longitudinal residual stresses. This assumption is realistic

because the flanges and web are free to deform transversely prior to placement of the concrete. The von Mises stress σ_{VM} is determined using the von Mises criterion for ductile material with a static yield strength F_{ys}:

$$\sigma_{VM}^2 = \sigma_1^2 - \sigma_1\sigma_2 + \sigma_2^2 \leq F_{ys}^2 \qquad (2)$$

Strains ε_1 and ε_2 were measured on one flange, at b/2 from the edge, and on the web, at mid-depth of the section (Fig. 2). At each measurement point, one longitudinal and one transverse strain gauge were installed on both sides of the steel plate (4 gauges total), to obtain an average stress value and eliminate plate bending effects due to local buckling and concrete expansion. In Specimens C-8, C-9, and C-11, the gauges were at elevations 1 200 mm (section with links) and 1 500 mm (section without links) from the base of the columns. Strain gauges in Specimens C-10 and C-12 were located at elevation 1 500 mm only (section with links).

Figure 8 presents the longitudinal stress (σ_1), the transverse stress (σ_2), and the von Mises stress (σ_{VM}) on the web of Specimen C-8. This behavior was typical of that observed in the flanges and webs of other specimens. As shown, transverse stresses are low (-8 MPa, in tension) compared to longitudinal stresses (+353 MPa) when yielding occurs, i.e., when σ_{VM} reaches F_{ys}. The von Mises and longitudinal stresses also remain close to each other up to yielding, at which point the ratio σ_1/σ_{VM} was equal to 0.99. In the figure, these two stresses at zero load correspond to the longitudinal residual stress measured at that location. When yielding occurred before peak load, it was assumed that all stresses remained constant until the peak load was reached. The mean and standard

deviation of the ratio σ_l/σ_{VM} near peak load for all specimens are 1.003 and 0.013 for the flanges, and 0.993 and 0.026 for the web. The ratio σ_l/σ_{VM} ranged from 0.957 for the web of C-10 to 1.037 for the web of C-12. From these results, it can be concluded that the transverse stresses had a negligible influence on the longitudinal capacity of the steel shape of the test columns.

Transverse link axial stress

Figure 9 illustrates the axial stress that developed in one link of Specimens C-8 through C-12, up to their respective peak strain. All results are for links located outside the concrete failure zone, where the strain gauges were functioning up to peak strains of the columns. As shown, the link stresses in specimens with s = d increased nearly linearly up to the peak strain whereas those in specimens with s = d/2 remained low up to about 1 300 $\mu\varepsilon$ (or 0.8 f'_c) after which they started to increase more rapidly. The tensile axial stresses present in the transverse links at peak load ranged from 90 to 151 MPa for specimens with s = d, and from 296 to 303 MPa for specimens with s = d/2.

The transverse links experienced much higher axial deformations than those observed on the steel shape in the transverse direction. The main reason for this difference is that both the steel shape and the concrete deformed transversely due to Poisson's effects whereas the transverse links behaved as a passive reinforcement, deforming at the same rate as the concrete. The behavior of the link was confirmed by transverse gauge readings on the concrete surface at the link location giving values

similar to those on the links. The measured Poisson's ratio of concrete test cylinders was equal to 0.18 up to about 1 000 με, after which it increased and exceeded that of steel (0.3) at 1 700 με. This explains the very low tensile transverse stresses observed in the steel shape and the higher rate of deformation for links in Specimens C-10 and C-12 at large longitudinal strains. On these two specimens, the closer link spacing also stiffened the flanges in bending, which then offered a higher restraint to concrete expansion between the links. Hence, additional tensile forces were induced in the links acting as horizontal reactions for the flanges. Based on the dimensions used in the experimental program, the cross sectional area of a transverse link should be equal to the greater of 0.025 d.t and 100 mm^2.

SIZE EFFECTS

One of the objectives of this test programme was to assess possible size effects through a comparison with previous tests on smaller specimens. Failure modes, post-peak behavior and transverse stresses are described first. The prediction of the axial capacity of columns of different sizes is discussed in a subsequent section.

Failure modes

The failure modes of the two series of test specimens are compared again according to their link spacing, as this parameter was indicative of the failure mode. Specimens C-4 (450 mm), C-7 (300 mm), C-8 (600 mm), and C-9 (600 mm) had a link spacing s = d and a b/t ratio of 23. Specimens C-4 and C-8 both experienced first local

buckling at 0.75 P_u. For Specimen C-7, local buckling did not develop until the load reached 0.96 P_u. The peak strain for this column was also higher (2 140 με) than that of Specimen C-4 (1 710 με), the latter being comparable to C-8 and C-9. The 600 mm specimens were tested under load control and failed in a brittle manner by concrete crushing and local buckling of the steel shape. The smaller specimens were tested under displacement control and the failure was more progressive. The strain difference at 0.95 P_u before and after peak load was similar for specimens C-4 (776 με) and C-8, whereas a higher value was obtained for C-7 (1 145 με). These observations indicate that 450 mm and 600 mm specimens behaved in a similar manner near peak load, while the failure was more progressive for the 300 mm columns.

Specimens C-10 and C-12 (600 mm) are compared to their smaller counterparts, C-2 and C-5 (450 mm), with a link spacing of d/2 and a b/t ratio of 23. The link diameter was 12.7 mm for C-2 and 22.2 mm for C-5. No 300 mm column with s = d/2 was tested. None of the specimens experienced local buckling before peak load. Failure of all the columns was due to concrete crushing and local buckling of the steel shape. The peak strains for Specimens C-2 (2 860 με) and C-5 (2 330 με) were similar to those of C-10 and C-12. As described previously, the smaller specimens were tested under displacement control while the largest were tested under load control. Even so, the failure for both the 450 mm and 600 mm specimens was more progressive than for specimens with s = d. The strain difference at 0.95 P_u before and after peak load for Specimens C-2 (1 400 με) and C-5 (1 290 με) were similar to those observed for C-10 and C-12. These

results show that there are no size effects near peak load between 450 mm and 600 mm specimens, as observed for specimens with s = d.

Post-peak behavior

Size effects on the post-peak response of these specimens were also examined. Because of strain localisation effects (Cusson et al., 1996), the post-peak plastic displacement was used instead of the axial strain as the latter cannot directly be compared between columns of different lengths. The post-peak plastic displacement is illustrated in Fig. 10 for Specimen C-5; it corresponds to the deformation measured from a straight line having a slope equal to the elastic stiffness of the column and which intersects the load deformation curve at peak load. The column elastic stiffness was taken as the secant stiffness computed at 0.4 P_u.

Figure 11 presents the computed post-peak plastic displacements of Specimens C-2, C-4, C-5, and C-7 of Series 1 tests and Specimens C-8, C-9, C-10, and C-12 of Series 2 tests. The curves are grouped into three categories according to their post-peak behavior. The first category includes specimens with the steepest load degradation and the lowest residual capacities. These specimens all had a link spacing of d (C-4, C-7, C-8, and C-9), assuming the real behavior of Specimens C-8 and C-9 is below the dotted lines joining the few available experimental data points. For Specimens C-8 and C-9, the load at a displacement of 12 mm was approximately 0.5 P_u. The second category includes Specimens C-2 and C-10, with a link spacing of d/2, which exhibit a better post-peak

behavior, with a load of 0.6 P_u at 12 mm. Specimens C-5 and C-12, with a larger link diameter and additional reinforcements, respectively, form the third category having the least post-peak capacity reduction: 0.7 P_u at 12 mm. These observations indicate that the size of the specimens had no effects on their post-peak behavior. In addition, it appears that more closely spaced links, additional reinforcements, and a larger link diameter can improve the post-peak response of this type of column.

Transverse stresses in the steel shape

Strain readings on the steel shapes of the smaller test columns were available only for Specimens C-2 and C-7 and they were measured only on one side of the flanges or web. Web measurements were used here to compare with larger specimens, as plate bending effects were less pronounced in the web. The values of σ_l/σ_{vM} for C-2 and C-7 were respectively 1.01 and 1.05, with compressive transverse stresses. These ratio are comparable to the values obtained for 600 mm columns. Hence, considering the available data, no size effect was observed regarding the reduction in axial capacity of the steel shape due to transverse stresses.

PREDICTION OF COLUMN AXIAL CAPACITY

Equations have recently been proposed to predict the axial capacity of this new type of composite column. These equations are reviewed in this section and modifications are proposed to account for the variation of the concrete strength with the column size. Tremblay et al. (1998) proposed a first set of equations to predict the ultimate load of the column, $P_{u,pred.}$. These equations were based on the results of tests on

Specimens C-2 to C-7 and they account for local buckling of the flanges by the use of an effective width which is a function of b/t and the link spacing:

$$P_{u,pred.} = 0.85A_c f'_c + A_{se} F_y + A_r f_{yr} \quad (3)$$

$$A_{se} = (d - 2t + 4b_e)t \quad (4)$$

$$\frac{b_e}{b} = \frac{0.6}{\lambda_p} \leq 1.0 \quad (5)$$

$$\lambda_p = \frac{b}{t}\sqrt{\frac{12(1-\nu^2)F_y}{\pi^2 Ek}} \quad (6)$$

$$k = \frac{4}{(s/b)^2} + \frac{15}{\pi^4}(s/b)^2 + \frac{20}{3\pi^2}(2-3\nu) \quad (7)$$

In Eqs. (3) to (7), A_c is the concrete area, A_{se} is the steel effective area accounting for local buckling, A_r and f_{yr} are the area and the yield strength of the longitudinal reinforcement, b_e is the total effective width of one flange, λ_p is the slenderness ratio for the flanges, and k is the plate buckling coefficient dependant on the s/b ratio. Using Eqs. (3) to (7), the test-to-predicted ratio for Specimens C-2 to C-7 was 0.99 with a standard deviation of 0.022. For the large columns C-8 to C-12, however, these equations give a test-to-predicted ratio of 0.95 and a standard deviation of 0.037 (Table 2).

Tremblay et al. (2000) proposed to replace Eq. (5) by:

$$\frac{b_e}{b} = (1 + \lambda_p^{2n})^{(-1/n)} \quad (8)$$

with n = 1.0, as an attempt to better fit to the experimental results, including those from the 600 mm specimens. Equation (8) was adapted from the equation proposed by Loov

(1996) for axially loaded steel columns. The axial capacities computed with Eq. (3) using Eq. (8) instead of Eq. (5) result in a mean experimental-to-predicted load ratio of 1.04 with a standard deviation of 0.04 for all specimens (C-2 to C-12). The computed ratio for each specimen is given in Table 2 and plotted as a function of flange slenderness (λ_p) in Fig. 12 (hollow symbols). The figure shows that the ratio generally decreases as the specimen size increases, with a mean of: 1.09 for 300 mm specimens, 1.05 for 450 mm specimens, and 1.01 for 600 mm specimens.

Such a variation can be explained by the reduction in the strength of concrete when the size of the column is increased. Neville (1966) examined several test results on cylinders and prisms of different sizes and shapes and found a correlation between the concrete strength and the parameter z/A, where z is the maximum cross section dimension, and A is the cross sectional area. Kupfer et al. (1969) also reported that 50 x 50 mm and 50 x 200 mm cross-section specimens (height of 200 mm) had the same compressive strength. This observation is an indication that the concrete strength is not dependent on the largest cross-section dimension. Figure 13 shows the data points reported by Neville for cylinders and prisms with a height, h, to z ratio of two or three. Specimens with h/z less than two were omitted because of the rigid platen effect that artificially increased the measured strength of the concrete. The parameter z in the selected specimens ranged from 152 mm to 914 mm and a linear regression performed on this data gives:

$$\frac{P}{P_{152cu}} = 0.676 + 0.104\left(\frac{152z}{A}\right) \tag{9}$$

where P is the concrete strength of a given specimen (MPa) and P_{152cu} is the strength of a 152 mm reference cube. Since Eq. (9) was established with prisms and cylinders with h/z greater than two and that h is not included as a parameter, it is normal that P/P_{152cu} is lower than 1.0 for a cube with h/z = 1, which would benefit from the rigid platen effect. Also from Eq. (9), the ratio P/P_{152cu} for a 152 mm cylinder (with h/z = 2) is 0.808, which is in agreement with other results reported by Neville (1996) comparing the strength of 152 mm cubes to that of 152 mm cylinders made of normal strength concrete. Equation (9) can be divided by 0.808 to relate the strength of a given concrete volume to that of a standard 152 mm cylinder, P_{152c} :

$$\frac{P}{P_{152c}} = 0.837 + 0.129\left(\frac{152z}{A}\right) \tag{10}$$

Figure 13 illustrates Eqs. (9) and (10), together with the experimental data normalised with respect to P_{152cu}. For the composite columns studied, A is equal to b x d, and z corresponds to d (see Fig. 1). Equation (3) already includes a reduction factor of 0.85 on f'_c to account for the difference between the strength of a 152 mm cylinder and that of larger structural elements. Based on the above evidence, a new factor ψ is proposed to replace 0.85 to account for the size of the concrete volume in accordance with Eq. (10):

$$\psi = 0.85\left(0.96 + \frac{22}{b}\right) \quad \begin{cases} \geq 0.85 \\ \leq 0.97 \end{cases} \tag{11}$$

Equation (10) gives P/P_{152c} = 0.864 for 914 mm cylinders, the largest test specimen reported by Neville. Equation (11) was slightly adjusted to give ψ equal to 0.85 for that same specimen, because it is proposed to keep 0.85 as the lower limit for ψ. The upper limit of ψ = 0.97 corresponds to the smallest specimens used by Neville. The values of b corresponding to the lower and upper limits of Eq. (11) are 550 mm and 120 mm, respectively.

Table 2 gives the test-to-predicted load ratio for each specimen when using its value of ψ instead of 0.85 in Eq. (3). These ratios are also illustrated in Fig.12 (solid symbols) and the computed mean value and standard deviation improve to 1.00 and 0.03, respectively. The variation with the size of the specimens also reduces as the mean test-to-predicted ratios are equal to 1.03, 1.01 and 0.99 for the 300 mm, 450 mm, and 600 mm specimens. For the design of this column system, it is therefore proposed to use Eq. (3) with the factor 0.85 being replaced by ψ from Eq. (11), together with Eqs. (4), (6), (7), and (8). Alternatively, the value of n in Eq. (8) can be reduced to give a more conservative prediction. For instance, a value of n = 0.8 instead of 1.0 gives a mean ratio of 1.03 and a standard deviation of 0.03.

CONCLUSIONS AND RECOMMENDATIONS

Five stub-column tests were performed on 600 x 600 mm partially encased composite specimens made with slender built-up steel I-shapes. This test series supplemented previous tests performed on six smaller size specimens (300 mm and 450

mm) and was used to assess possible size effects and to propose a design equation for the axial load capacity of this type of columns. The following observations can be drawn from the test results presented:

- All specimens failed by crushing of the concrete, in combination with local buckling of the steel shape flanges. The flanges on specimens with a link spacing equal to the depth started to buckle at around 75% of the test peak load and had a brittle and sudden failure. Specimens with a link spacing of half the depth experienced no local buckling before peak load and exhibited a more ductile and progressive failure as well as a higher post-peak residual capacity.
- The additional longitudinal and transverse reinforcements, with the configuration used, improved the ductility and post-peak response of the column, but no gain in the concrete strength due to confinement could be observed.
- Transverse stresses in the flanges and the web of the steel shape due to the expansion of concrete were found to have a negligible effect on the axial capacity of the columns. High stresses developed, however, in the transverse links, which acted as passive reinforcement to the transverse expansion of the concrete, resulting in higher stresses than in the steel shape. The stresses in the transverse links typically doubled when the link spacing was halved, as a result of a better confinement of the concrete near the exposed face and a stiffening of the flanges which more effectively resisted the expansion of the concrete. Based on the dimensions used in the experimental program, the cross sectional area of a transverse link should be equal to the greater of 0.025 d.t and 100 mm^2.

Comparison with previous tests revealed that 450 mm and 600 mm specimens behaved in a similar manner. When compared to larger specimens with the same characteristics, a 300 mm specimen did not experience local buckling before peak load, had a more progressive failure, but exhibited the same post-peak response. Design equations for the axial capacity proposed in earlier studies were improved by considering the variation of the concrete strength with column size.

Based on the results of the research programme, the following recommendations are given:

- The link spacing should be equal to d/2 or less and the b/t ratio should be limited to 30 in order to avoid brittle column failure and ensure adequate post-peak behavior.
- Additional reinforcement (longitudinal rebars, U-stirrups) is not required unless the column must retain a certain capacity at high strains after the peak load is reached or meet other ductility requirements (e.g., seismic response).
- The design equations proposed in this paper can be used to predict the axial capacity of columns having characteristics limited to those considered in the test programs described in this paper. A validated finite element model could be used to expand the range of these parameters.
- The welds connecting the transverse links to the flanges must be designed to develop the full yielding capacity of the transverse links. A rational method needs to be developed for the design of the links. Finite element modeling can be used to identify the parameters and assess their influence on the link stresses.

- Additional testing should be carried out to examine the possible effects of bending moments induced by load eccentricity such as in the case when beams frame into the column from one side only.

ACKNOWLEDGEMENTS

The authors wish to thank the technical personnel at Ecole Polytechnique of Montreal and Lehigh University, and Mr. Mehmet Yalcin who assisted in some of the tests. Funding was provided by Canam Steel Inc. and the Natural Science and Engineering Research Council of Canada.

APPENDIX I. REFERENCES

Bridge, R.Q., O'Shea, M.D. (1996) "Local buckling of square thin-walled steel tubes filled with concrete." *5th Intl. Coll. on Stability of Metal Structures*, Chicago, Il, 63-72.

Bridge, R.Q., Roderick, J.W. (1978) "Behavior of built-up composite columns." *Journal of Structural Division*, ASCE, 104(7), 1141-1155.

CEN, AFNOR (1994) "Construction mixte acier et béton: Conception et dimensionnement des structures mixtes acier et béton. " *Eurocode 4* (in French).

Chicoine, T., Tremblay, R., Massicotte, B., Yalcin, M., Ricles, J., Lu, L.-W. (2000) "Test programme on large-scale partially-encased built-up three-plate composite columns." *Joint Report, EPM/GCS No. 00-06*, Dept. Of Civil, Geological and Mining Engineering, Ecole Polytechnique, Montreal, Canada – ATLSS Engineering Research Center, *No. 00-04*, Lehigh University, Bethlehem, Pennsylvania, USA.

CSA (1994) *CAN/CSA-A23.3-94 Code for the design of concrete structures for buildings*. Canadian Standards Association, Rexdale, Ontario.

Cusson, D., de Larrard, F., Boulay, C., Paultre, P. (1996) "Strain localization in confined high-strength concrete columns." *Journal of Structural Engineering*, ASCE, 122(9), 1055-1061.

Elnashai, A.S., Broderick, B.M., Dowling, P.J. (1995) "Earthquake-resistant composite steel/concrete structures." *Structural Engineer*, 73(8), 121-132.

Furlong, R.W. (1967) "Strength of steel-encased concrete beam columns." *Journal Structural Division*, ASCE, 93(5), 113-124.

Gardner, N.J., Jacobson, E.R. (1967) "Structural behavior of concrete-filled steel tubes." *ACI Journal*, 64(7), 404-412.

Ge, H., Usami, T. (1992) "Strength of concrete-filled thin-walled steel box columns : experiment." *Journal of Structural Engineering*, ASCE, 118(11), 3036-3054.

Hunaiti, Y.M., Abdel Fattah, B. (1994) "Design considerations of partially encased composite columns." *Proc. Instn. Civ. Engrs Structs and Bldgs*, 106, 75-82.

Johnson, R.P., May, I.M. (1978) "Tests on restrained composite columns." *Structural Engineer*, 56b(2), 21-28.

Kato, B. (1996) "Column curves of steel-concrete composite members." *Journal of Constructional Steel Research,* 39(2), 121-135.

Knowles, R.B., Park, R. (1970) "Axial load for concrete-filled steel tubes." *Journal Structural Division*, ASCE, 96(10), 2125-2153.

Kupfer, H., Hilsdorf, H.K., Rusch, H. (1969) "Behavior of concrete under biaxial stresses." *ACI Journal*, 656-666.

Loov, R. (1996) "A simple equation for axially loaded steel column design curve." *Can. J. Civ. Eng.*, 23, 272-276.

Neville, A.M. (1966) "A general relation for the strengths of concrete specimens of different shapes and sizes." *ACI Journal*, 63, 1095-1108.

Neville, A.M. (1996) *Properties of Concrete*. 4th edition, John Wiley & Sons, New York, NY.

Plumier, A., Abed, A., Tilioune, B. (1995) "Increase of buckling resistance and ductility of H-Sections by encased concrete." Behavior of Steel Structures in Seismic Areas, F.M. Mazzolani and V. Gioncu, Ed., E&FN SPON, London.

Ricles, J.M., Paboojian, S.H. (1994) " Seismic Performance of Steel-Encased Composite Columns. " *Journal of Structural Engineering*, ASCE, 120(8), 2474-2494.

Saw, H.S., Liew, J.Y.R. (2000) "Assessment of current methods for the design of composite columns in buildings." *Journal of Constructional Steel Research*, 53, 121-147.

SSRC, Task Group 20 (1979) "A specification for the design of steel-concrete composite columns." *Engineering Journal*, vol.16, 4th quarter, AISC, 101-115.

SSRC (1998) *Guide to Stability Design Criteria for Metal Structures*, 5th ed., T.V. Galambos, Ed., John Wiley & Sons, New York, NY.

Stevens, R.F. (1965) "Encased stanchions." *Structural Engineer*, 43(2), 59-66.

Tomii, M., Yoshimura, K., Morishita, Y. (1977) "Experimental studies on concrete-filled steel tubular stub columns under concentric loading." *ASCE International Colloquium on Stability of Structures under Static and Dynamic Loads*, Washington, DC, 718-740.

Tremblay, R., Massicotte, B., Filion, I., Maranda, R. (1998) "Experimental study on the behavior of partially encased composite columns made with light welded H steel shapes under compressive axial loads." *1998 SSRC Annual Technical Meeting.*

Tremblay, R., Chicoine, T., Massicotte, B. (2000) "Design equation for the axial capacity of partially-encased non-compact columns." *Proc. Composite construction IV*, Engineering Foundation, Banff, Canada.

Uy, B. (2000) "Strength of concrete filled steel box columns incorporating local buckling." *Journal of Structural Engineering*, ASCE, 126(3), 341-352.

Vincent, R. (2000) "Design and application of partially encased non-compact composite columns for high-rise buildings." *Proc. Composite Construction IV*, Engineering Foundation, Banff, Canada.

Wright, H.D. (1993) "Buckling of plates in contact with a rigid medium." *Structural Engineer*, 71(12), 209-215.

APPENDIX II. NOTATION

The following symbols are used in this paper :

A = cross sectional area (mm^2);

A_c = concrete area (mm^2);

A_r = longitudinal reinforcement area (mm^2);

A_s = steel flange area (mm^2);

A_{se} = steel flange effective area (mm^2);

b = flange half-width (mm);

b_e = flange effective width (mm);

b_f = flange width (mm);

d = column depth (mm);

E = elastic modulus (MPa);

f'_c = concrete strength (MPa);

F_y = steel yield strength (MPa);

f_{yr} = longitudinal reinforcement yield strength (MPa);

F_{ys} = steel static yield strength (MPa);

k = plate buckling coefficient;

h = height of concrete specimens (mm);

L = column length (mm);

$P_{u,pred.}$ = predicted ultimate load (kN);

$P_{u,exp.}$ = experimental ultimate load (kN);

r_y = radius of gyration about the weak-axis (mm);

s = transverse link spacing (mm);

t = plate thickness (mm);

z = cross-section maximum dimension (mm);

δ_0 = local flange out-of-straightness (mm);

ε_1 = longitudinal strain (mm/mm);

ε_2 = transverse strain (mm/mm);

ε_a = average longitudinal strain (mm/mm);

ε_r = measured longitudinal residual strain (mm/mm);

λ_p = plate slenderness ratio;

μ = mean of local flange out-of-straightness (mm);

ν = Poisson's ratio;

σ = standard deviation of local flange out-of-straightness (mm);

σ_1 = longitudinal stress (MPa);

σ_2 = transverse stress (MPa);

σ_r = longitudinal residual stress (MPa);

σ_{VM} = stress satisfying the von Mises criteria (MPa); and

ψ = concrete strength modification factor.

TABLE 1. Properties of Test Specimens

Test Series	Spec. Design.	Plate Width by Depth b_f x d (mm)	Plate Thickness t (mm)	Width-to-Thickness ratio b / t	Link Spacing s (mm)	Initial flange Out-of-straight. δ_0 (mm)		Yield Stress of Plates F_y (MPa)	Comp. Strength of Concrete f'_c (MPa)	Exp. Ult. Load $P_{u,exp.}$ (kN)
						Mean μ	St. Dev. σ			
(1)	(2)	(3)	(4)	(5)	(6)	(7)	(8)	(9)	(10)	(11)
Series 1 (small spec.)	C-2	450 x 450	9.7	23.2	225	NA	NA	370	32.7	10 100
	C-3	450 x 450	9.7	23.2	337.5	0.83	0.52	370	32.4	9 690
	C-4	450 x 450	9.7	23.2	450	1.42	0.23	370	31.9	9 390
	C-5	450 x 450	9.7	23.2	225	0.39	0.13	370	34.3	10 000
	C-6	450 x 450	6.35	35.4	337.5	0.56	0.27	374	32.7	7 650
	C-7	300 x 300	6.35	23.6	300	0.63	0.20	374	31.9	4 280
Series 2 (large spec.)	C-8	600 x 600	12.88	23.3	600	1.43	1.38	360	34.2	16 470
	C-9	600 x 600	12.91	23.2	600	2.02	0.36	360	34.2	16 610
	C-10	600 x 600	12.81	23.4	300	0.38	0.15	360	34.2	16 240
	C-11	600 x 600	9.71	30.9	600	0.71	0.46	345	34.2	14 930
	C-12*	600 x 600	12.86	23.3	300	0.37	0.15	360	34.2	17 450

* With 4-20M (ϕ=20mm) longitudinal rebars and pairs of U-stirrups 15M (ϕ=15mm) @300 mm.

TABLE 2. Test-to-Predicted Load Ratios of Test Columns Using Different Models

Test Series (1)	Spec. Design. (2)	$P_{u,exp.}/P_{u,pred.}$ Tremblay(1998) (3)	Tremblay(2000) n=1 (4)	This study n=1 (5)
Series 1 (small spec.)	C-2	1.01	1.07	1.04
	C-3	0.97	1.07	1.02
	C-4	0.99	1.06	1.03
	C-5	0.97	1.03	1.00
	C-6	0.97	1.02	0.96
	C-7	1.02	1.09	1.03
Series 2 (large spec.)	C-8	0.95	1.01	0.99
	C-9	0.95	1.02	1.00
	C-10	0.90	0.96	0.94
	C-11	1.02	1.06	1.03
	C-12	0.94	1.00	0.98
Mean :		0.97	1.04	1.00
Standard deviation :		0.03	0.04	0.03

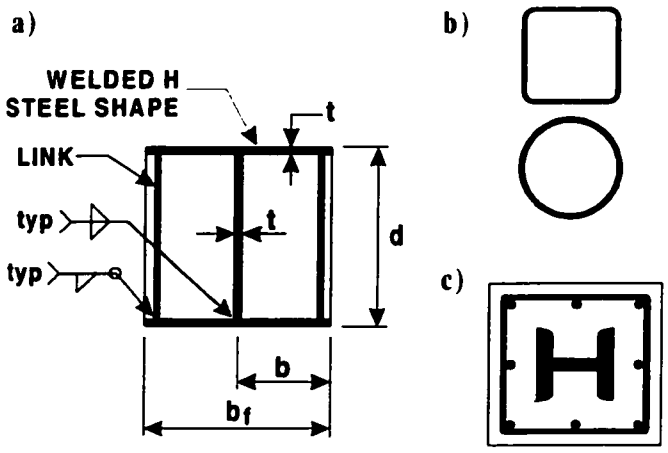

FIG. 1. Composite Columns : (a) Proposed New System; (b) CFT; (c) SRC.

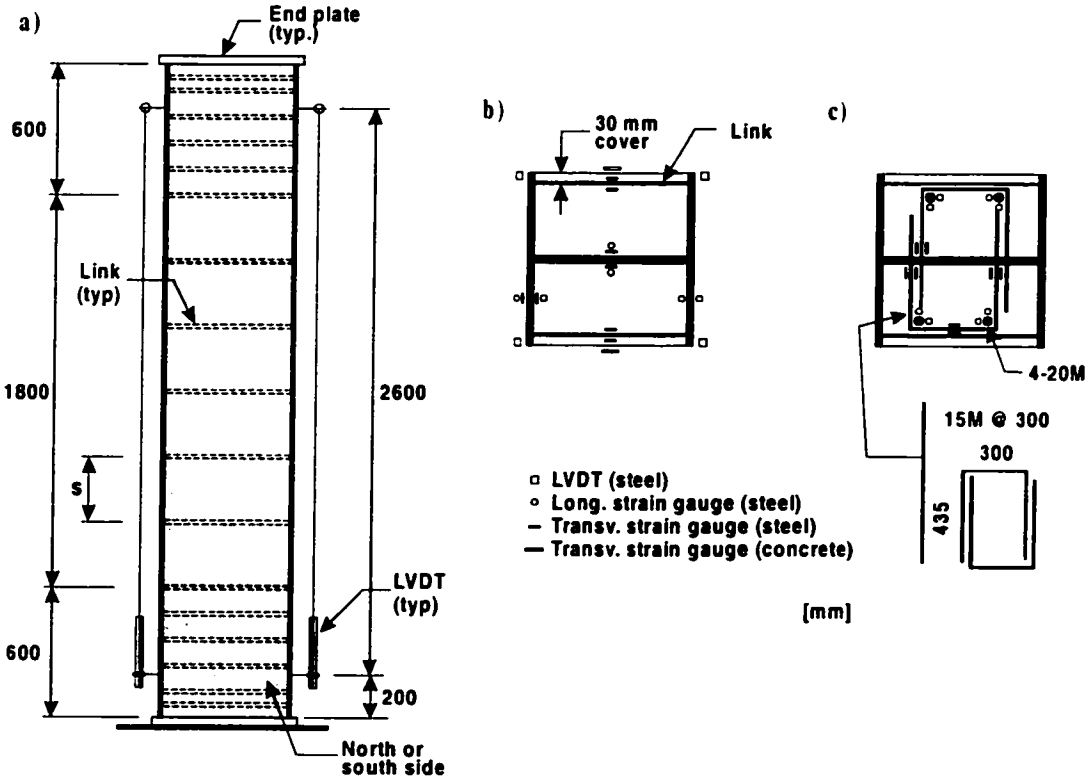

FIG. 2. Geometry and Instrumentation of Test Specimens: (a) Elevation; (b) Typical Cross-Section at Link Elevation; (c) Cross-Section at Link Elevation with Additional Reinforcement and Instrumentation for Specimen C-12

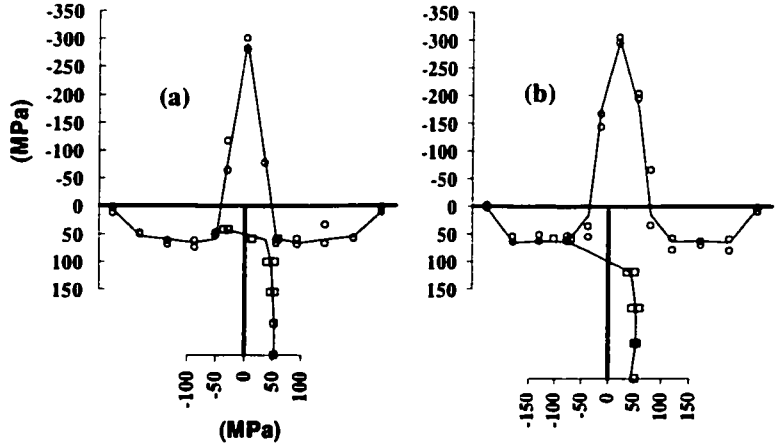

FIG. 3. Measured Residual Stresses: (a) C-8, C-9, C-10, C-12; (b) C-11

FIG. 4. Stub Column Test Setup

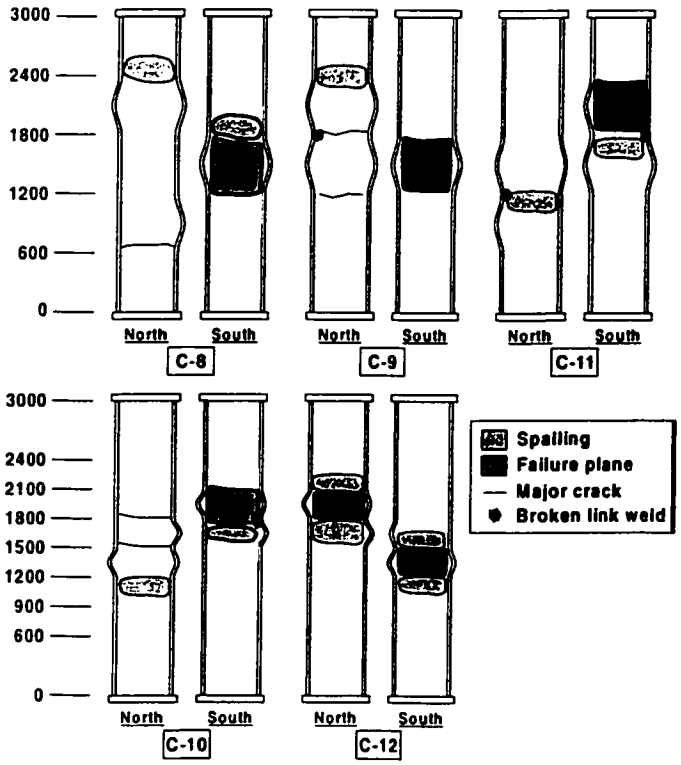

FIG. 5. Observations on Specimens C-8 to C-12 after Failure

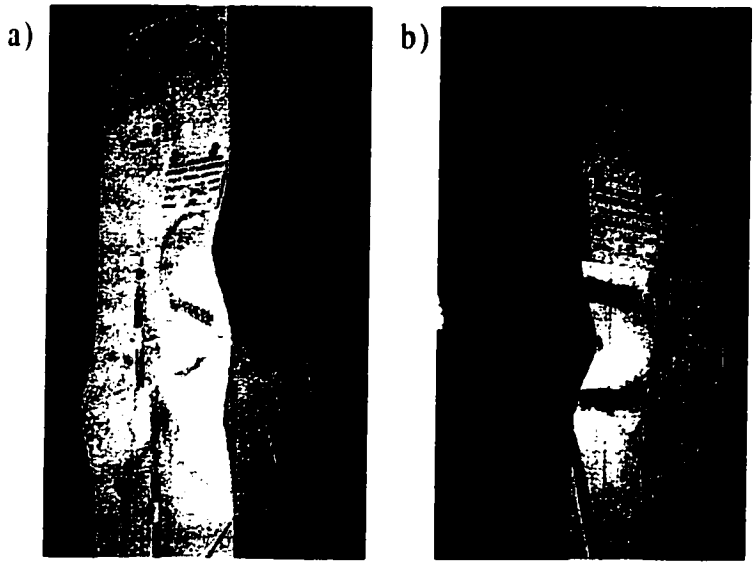

FIG. 6. Specimens after Failure: (a) SW Corner of Specimen C-11; (b) SE Corner of Specimen C-10

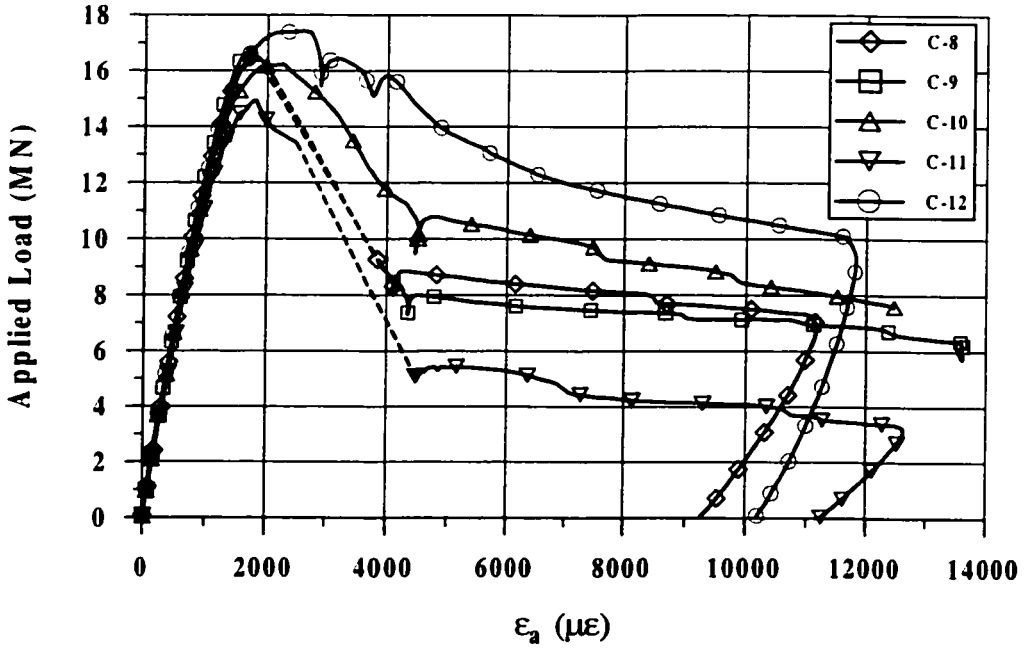

FIG. 7. Load vs. Average Axial Strain Curves of Test Specimens

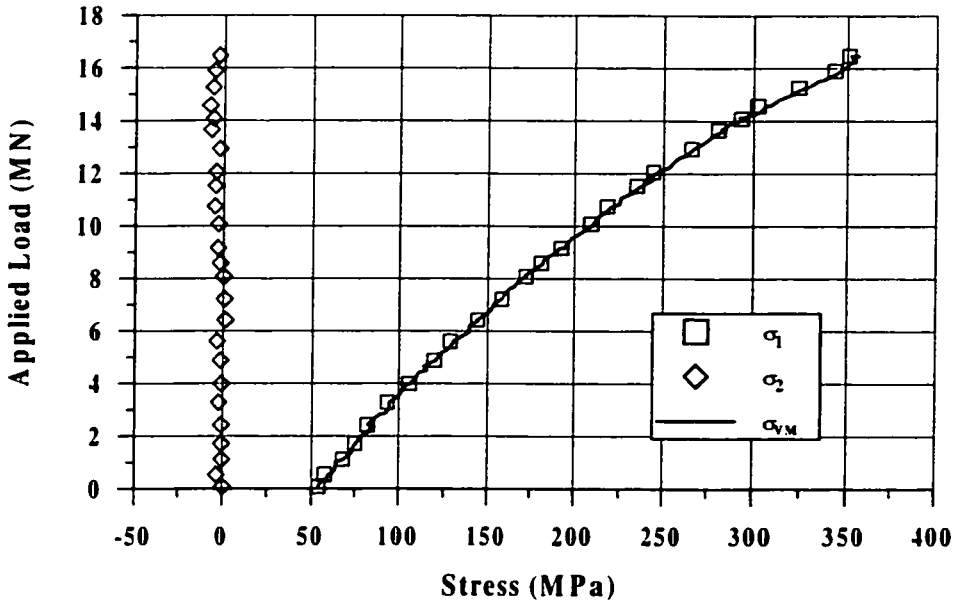

FIG. 8. Web Stresses in Specimen C-8

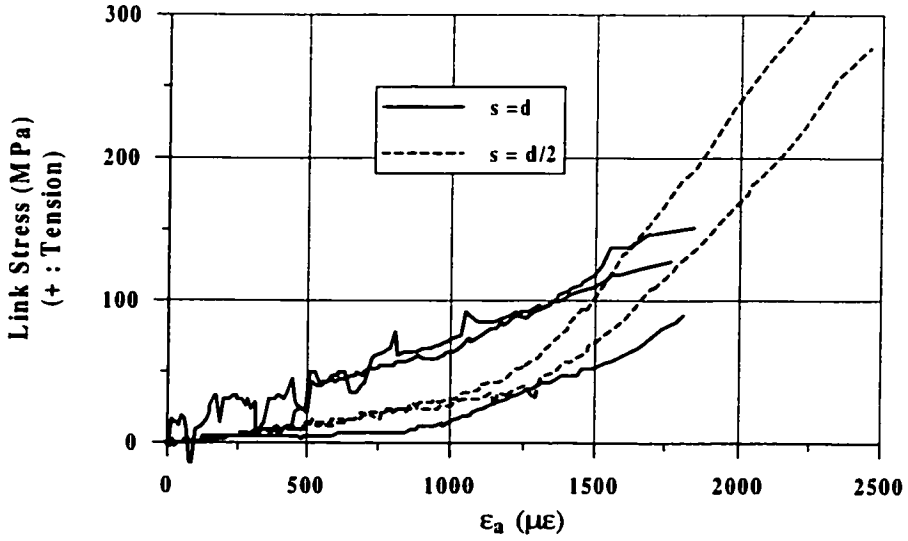

FIG. 9. Link Axial Stresses in Large Specimens Outside Concrete Failure Zone

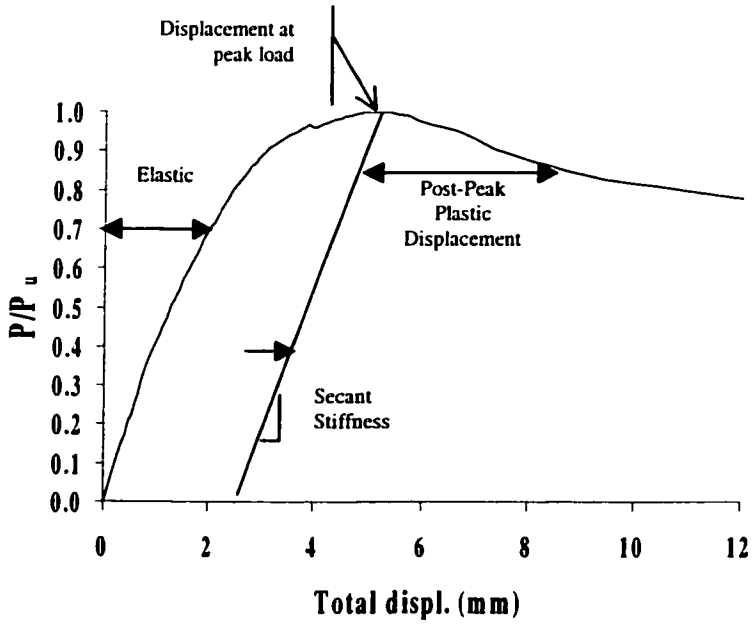

FIG. 10. Calculation of Post-Peak Plastic Displacement for Column C-5

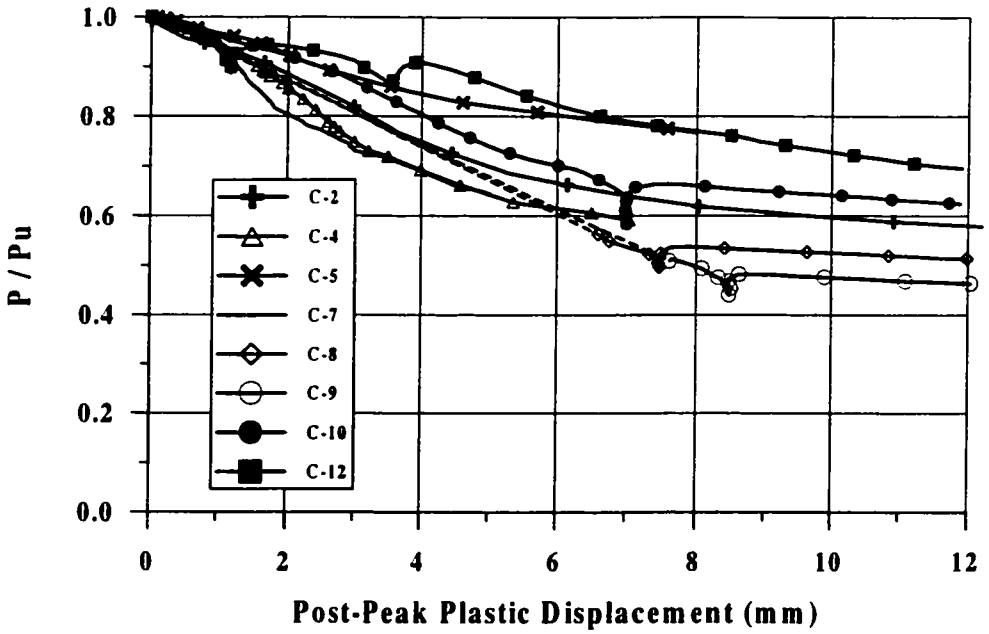

FIG. 11. Normalised Load vs. Post-Peak Plastic Displacement

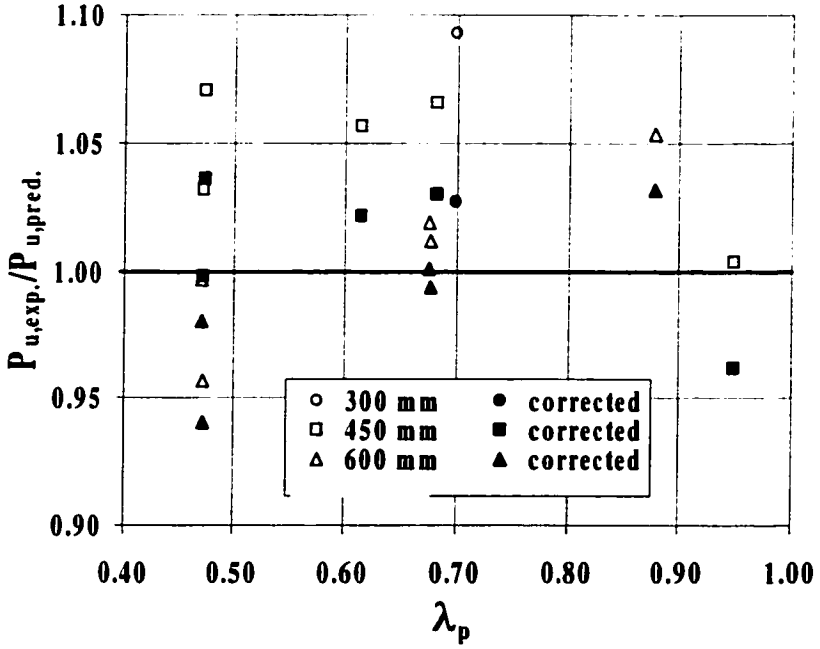

FIG. 12. Experimental-to-Predicted Load Ratio for Specimens C-2 to C-12

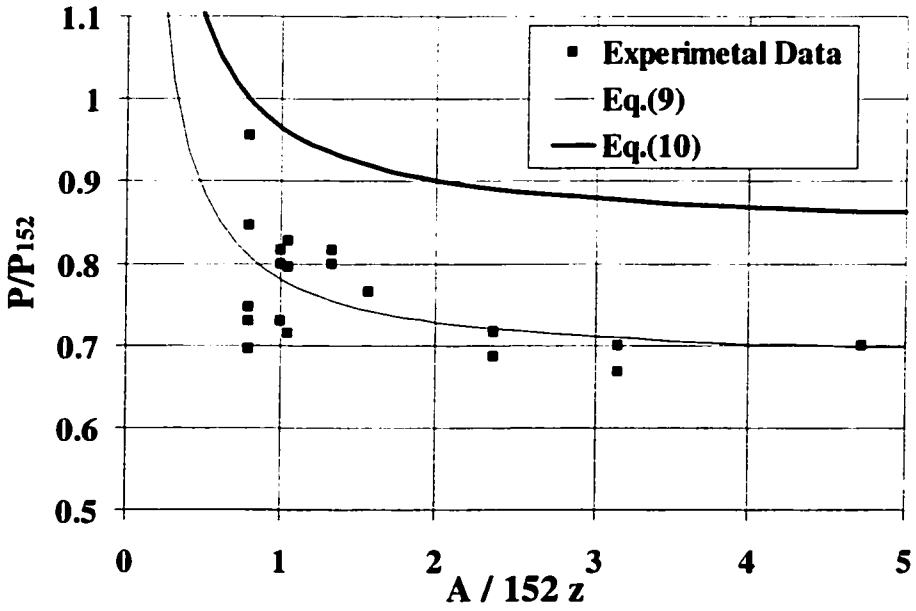

FIG. 13. Size Effect on Concrete Strength

APPENDIX B – PAPER 2

Long-Term Behaviour and Strength of Partially Encased Composite Columns made with Built-Up Steel Shapes

By Thierry Chicoine, Bruno Massicotte, and Robert Tremblay

Submitted to : ASCE Journal of Structural Engineering, February 2001

Long-Term Behaviour and Strength of Partially Encased Composite Columns made with Built-Up Steel Shapes

By Thierry Chicoine[1], Bruno Massicotte[2], and Robert Tremblay[2]

ABSTRACT: A comprehensive study has been conducted to investigate the long-term behaviour and strength of partially encased composite (PEC) columns made with thin-walled welded I-sections stiffened with transverse links. The paper presents the strain measurement history and load deformation response of five 300 x 300 mm and two 450 x 450 mm stub-column specimens. Four specimens were loaded for 150 days, following typical construction sequence, and five columns were tested up to failure. Long-term axial deformations due to shrinkage and creep of the concrete were recorded and are compared to prediction models. The tests showed that the relatively higher stresses in the steel shape due to the sequence of loading and shrinkage and creep of the concrete had no significant effect on the failure mode and ultimate capacity for this type of column. The transverse stresses in the web of the steel shape were lower in specimens subjected to long-term loading. The axial stresses in the transverse links at peak load, caused by the transverse expansion of the concrete, were found not to depend on the loading sequence.

[1] Former Graduate Research Assistant, [2]Professor, Department. Civil, Geological, and Mining Engineering, Ecole Polytechnique, Montreal, Canada H3C 3A7.

INTRODUCTION

A new type of partially encased composite (PEC) column consisting of a thin-walled, I-shaped steel section with concrete being poured between the flanges of the steel section has recently been developed and patented by the Canam Manac Group (Fig. 1). The steel section features very slender plates exceeding the width-to-thickness ratio limits for non compact sections. Transverse links between the flanges are spaced at regular intervals to enhance the resistance of the flanges to local buckling. The proposed PEC column is intended to carry only axial loads in multi-storey buildings, the lateral loads being resisted by other structural systems such as shear walls. The main advantages of this system over traditional composite column design have been presented elsewhere (Vincent et al., 2000), along with a series of tests on PEC columns and a proposed design equation accounting for local flange buckling (Tremblay et al, 1998; Tremblay et al., 2000; Chicoine et al., 2001).

Figure 2 shows the column system at three different stages during construction. The formwork for the columns only consists in plywood sheeting closing the space between the column flange tips. Normal strength concrete (20-40 MPa) is poured in the columns one level at a time, while pouring the slab at the level above. For simplicity, the same concrete mix is used for the columns and the slab. According to typical construction sequence, the steel shape alone must be able to carry, without the contribution of the concrete, dead load and construction live loads for up to a maximum of 12 floors, including three floors where the slab is poured. Any additional load on the columns is resisted by the composite section.

This construction sequence results in relatively higher stresses in the steel. In addition, shrinkage and creep of the concrete induce additional axial stresses in the steel shape. These stresses do not reduce the axial capacity of the column if the full steel section is capable of yielding without local buckling. If local buckling is a possibility, as in the column system studied herein, long-term loading induced deformations and the sequence of construction may reduce the overall capacity of the composite column.

Relatively few references document the long-term behaviour of composite columns. Bode (1976) suggested that the concrete in concrete-filled tubes (CFT) is subjected to shrinkage and creep, but to a lesser extent than in conventional reinforced concrete columns because the steel shape offers more restraint to the axial deformations and the exchange of humidity with the exterior environment is mostly prevented. Uy (2001) conducted an experimental programme to assess the shrinkage and creep effects in short concrete-filled steel box columns under sustained loading. High-strength concrete was used in the experiments and the maximum shrinkage strain after 140 days was 160 με. This is higher than the value of 30 με at 130 days obtained in CFT columns with normal strength concrete by Nakai et al. (1991) and Terrey et al. (1994). De Larrard (1999) noted that the shrinkage strain of plain concrete may be divided into two categories: drying and autogenous shrinkage. The first type of shrinkage is negligible in CFT columns because the encased concrete is not exposed to ambient environment. The latter type results from the chemical reaction of the cement paste with water, and is typically higher for high-strength concrete, which explains the higher shrinkage strain

obtained by Uy (2001). The ratio of creep strain to elastic strain for CFT columns was found to vary between 0.5 and 1.5 (Uy 2000, Nakai et al. 1991, Terrey et al. 1994, and Morino et al. 1996). That ratio reached 2.7-2.8 for plain concrete reference columns (Nakai et al., 1991). Experimental studies have also been carried out to investigate the long-term behaviour of the concrete on the buckling load of slender columns (Bridge, 1979; Roik et al., 1987; Bradford and Gilbert, 1990). The findings of these studies have been implemented in several standards for the design of axially loaded composite columns (CSA, 1994; SSRC, 1979; CEN, 1994). The experimental results on CFT columns, however, cannot apply directly to the new PEC columns as shrinkage and creep strains are dependent upon the type of concrete used and the ratio of the volume to the exposed surface of the concrete. The PEC columns are made of normal strength concrete and, unlike CFT columns, they have two concrete faces exposed to the ambient environment. The ACI (1992) shrinkage and creep models for plain concrete take into account these parameters and these models can be adapted to PEC columns.

The objectives of this project are: i) to evaluate experimentally the behaviour of the proposed column system under typical construction loading sequence and long-term loading, and obtain data on the effects of creep and shrinkage on the deformations and stresses in the steel and the concrete, ii) to check the applicability to predict the long-term deformations in both materials with existing analytical models developed for plain concrete, and iii) to evaluate the influence of creep and shrinkage of the concrete on the ultimate axial capacity of the columns and on its behaviour near peak load, including the

failure mode of the column, the ultimate strain, the steel shape transverse stresses, and the transverse link stresses. A test programme was developed which included a total of seven composite stub-columns: five 300 x 300 mm specimens and two 450 x 450 mm columns. Strain readings were taken on each specimen over a measurement period of approximately 150 days to determine long-term axial deformations. Four of the specimens were loaded according to anticipated construction sequence, and five columns were tested up to their ultimate capacity.

EXPERIMENTAL PROGRAMME

Geometric properties of specimens

The characteristics of the specimens are listed in Table 1 and their geometry is illustrated in Fig. 1. Five of the seven composite columns had a cross-section of 300 x 300 mm (P-1 to P-4, and P-7), while the other two had a cross-section of 450 x 450 mm (P-5 and P-6). All specimens except P-6 had a height of 5d and met the SSRC (1998) requirements for stub columns. The transverse links in these columns were uniformly distributed over the central 3d segment, and additional links were provided at both ends, over a distance d, to force failure in the middle 3/5 of the columns. Specimen P-6 was only 900 mm (2d) in height with closely spaced links over 230 mm at each end. End plates were welded to each specimen to obtain a more uniform load distribution in the columns. For each specimen, the same plate thickness was used for the web and flanges. Measured thicknesses are presented in Table 1. Nominal thicknesses were 6.35 mm (P-1 to P-4, and P-7), and 9.53 mm (P-5 and P-6). The transverse links consisted of round bars with a nominal diameter of 12 mm.

Loading sequence and choice of specimens

The range of stresses that can be expected in the steel shape and the concrete of PEC columns has been determined for a variety of typical structures (Chicoine et al. 2000). Figure 3 shows an example of the stress distribution in both materials for a 36-storey office building. In the design, three-storey column tiers were used and regular steel columns were selected when the required PEC column size was less than 300 mm (top 6 storeys in Fig. 3). Loading Stage 1 corresponds to the load carried by the steel shape, before concreting. An additional load is applied at loading Stage 2 to reach a loading level corresponding to the total long-term service load. For the latter, up to 50% of the live load was included to obtain a conservative estimate of creep effects. Based on these results, a loading sequence that included a total of three stages was developed for the experimental program. At Stage 1, an axial load P_1 was applied to the steel shape to induce a nominal compressive stress of 100 MPa. At Stage 2, 14 days after pouring the concrete, the applied load was increased to reach the anticipated axial load due to the long-term service load, $P_1 + P_2$. This load increased the stress in the steel up to approximately 170 MPa and produced a stress of 10 MPa in the concrete. The day when Stage 2 loading was applied is referred to as "Day 0" herein. The load at this stage, $P_1 + P_2$, was maintained until approximately "Day 150". At loading Stage 3, the applied load on the composite column was increased further up to failure.

As illustrated in Fig.4, the setup for preloading the specimens included heavy W-shaped cross-beams and high-strength steel tension bars (F_y=700MPa). High-strength

steel was used to minimize the cross-section area and axial stiffness of the tension bars and, thereby, the loss of applied load when concrete shrinkage and creep are taking place during loading Stage 2. For loading Stage 3, the specimens together with the preloading setup, were placed into a 11 MN Universal Testing Machine and the load was applied to the specimens through the cross-beams.

The load applied at each stage and the actual elastic stresses in the materials, as computed from strain readings upon loading, are presented in Table 2 for each specimen. Specimen P-1 was used to measure the partially restrained shrinkage strains for 300 mm specimens over a period of six months, and no load was applied on this column at stages 1 and 2. The ultimate capacity of Specimen P-1 at Stage 3 was used as a reference for comparison with other columns subjected to loading Stages 1 and 2. Specimen P-2 was identical to Specimen P-1, but loads were applied at Stages 1 and 3. This specimen was used to assess the effect of shrinkage on the level of prestress in the steel shape. No effort was made to maintain constant the applied load up to Stage 3 on this specimen in order to avoid loading the concrete upon readjustment. Specimens P-3 and P-4 were identical to Specimen P-1 except that they were loaded in sequence to Stage 1 and then Stage 2. These two specimens were used to assess the redistribution of strain between the two materials due to shrinkage and creep of the concrete. For these two specimens, the long-term load was continually adjusted to compensate for the loss in axial load due to long-term shortening. These specimens were also used to assess the effect of construction sequence and long-term loading on the ultimate load (Stage 3). Specimen P-5 was a

scaled model of Specimens P-3 and P-4, with the cross-section dimensions being scaled up by 1.5 to assess any size effects. Specimen P-6 had the same cross-section as Specimen P-5 and was used to isolate shrinkage strains. Finally, Specimen P-7 was used as a replica of Specimen P-1 to obtain robust experimental data on shrinkage strains. All columns except Specimens P-6 and P-7 were tested to ultimate capacity (Stage 3).

Material mechanical properties

The nominal material properties were the same for all specimens: normal weight concrete with a nominal strength of 25 MPa and steel plates with a nominal yield strength of 350 MPa. These were selected to reproduce common practice in structural design of columns while accommodating the capacity of the testing equipment. Higher strength concrete was used over 1d at both ends of Specimens P-1 to P-5. The properties of the concrete in the middle 3/5 of the Specimens were measured from concrete cylinders at different dates, as illustrated in Table 1. The concrete of these cylinders had, at loading Stage 3 (180 days after pouring), a peak strain of 2,350 $\mu\varepsilon$, a peak stress of 36.8 MPa, an elastic modulus of 29,900 MPa, and a Poisson's ratio of 0.22. Specimens P-5 and P-6 were poured one day after the other specimens. The strength of the concrete for these two specimens was not be measured at loading Stage 3 and a strength of 30 MPa was estimated from extrapolation of cylinder tests at an earlier age. The actual measured static yield stress of the steel was 390 MPa for the 6.35 mm plates and 345 MPa for the 9.53 mm plates.

Geometric imperfections and residual stresses

Relative out-of-straightness of the column flanges, δ_0, was measured along the tip of each flange at mid-distance between consecutive transverse links in the central 3/5 of the specimen height. The average values are presented in Table 1. These imperfections ranged from 0.35 mm (P-3) to 0.74 mm (P-1), representing an average value of s/610 with a standard deviation of s/1,200 for Specimens P-1 to P-5. All imperfections were inwards due to the fabrication process (Chicoine et al., 2000).

Residual stresses were measured using the sectioning method (SSRC, 1998) on additional columns identical to the test specimens. Figure 5 presents the average residual stresses (σ_r) on the flanges and web of Specimens P-1 to P-5 (continuous lines) together with the individual readings. Because the specimens were to be loaded only in compression, compression stresses are taken as positive in this paper. Average values of σ_r in the flanges ranged from 106 MPa to –390 MPa for specimens with d = 300 mm, and from 83 MPa to –295 MPa for specimens with d = 450 mm. In the web, the measured σ_r ranged from 32 MPa to 71 MPa for specimen with d = 300 mm, and from 45 MPa to –96 MPa for specimens with d = 450 mm. The high tensile stresses at the junction of the flanges and the web resulted from the welding operation and subsequent uneven cooling of the steel plates. Similar magnitude and distribution of σ_r were found in similar specimens tested previously (Tremblay et al., 1998).

Instrumentation and loading procedure

Mechanical strain targets and a micrometer (Demec®) were used to measure the strains in both materials in the middle 3/5 of the specimens during loading Stages 1 and 2. The micrometer had a gauge length of 150 mm and an accuracy of 10.7 με. Readings were taken daily up to one week after loading of the concrete, then each week for the first month and once a month until Stage 3 loading.

At loading Stage 3, the load was applied hydraulically by a movable head mounted on four columns (Fig.6). The axial shortening of the columns was measured using Linear Variable Displacement Transducers (LVDTs) that were located at each corner of the specimens and had a gauge length of (5d – 300) mm. Longitudinal and transverse strains were recorded with strain gauges located on the flanges and web of the steel shape, in the mid-height region of the column. Strain gauges were also installed at mid-height of the columns on the transverse links and on the concrete surface. Prior to applying loading at Stage 3, the alignment of the column was checked and all specimens were considered properly aligned. The columns were loaded using load control up to about $0.75P_{u,pred}$, at which point the load control was switched to displacement control to obtain a better transition before and after the peak load.

LONG-TERM EXPERIMENTAL RESULTS

Shrinkage strain measurements in Specimens P-1, P-2, P-6, and P-7

The average strain measurements on Specimens P-1, P-2, and P-7 were used to represent the shrinkage behaviour of the 300 mm columns in laboratory conditions.

Temperature strains were taken out of all the measurements presented herein, and an axial shortening is represented as positive. During the measurement period, the load on Specimen P-2 decreased by only 20 kN, from 575 kN to 555 kN, inducing a negligible relief of 5 με on the composite section. Therefore, the long-term strain in Specimen P-2 can be attributed only to shrinkage and, hence, can be directly compared to that of P-1 and P-7 because no stresses were applied directly to the concrete in these specimens. Figure 7 presents the time history of the average shrinkage strain in these three specimens. Strain readings began at "Day –11", after the formwork was removed on the specimens. The restrained shrinkage strains were very low, ranging from 10 με to 85 με at "Day 150", with an average value of 35 με, corresponding to a compressive stress in the steel shape of 7 MPa. The strain variations in time arose from changes in ambient relative humidity and because the readings were in the order of magnitude of the micrometer used (11 με). Such low shrinkage strain was due in part to the low water content of the concrete at pouring, which had a slump of only 5 mm.

Figure 7 also shows the predicted axial strain in the column due to shrinkage, t days after the end of curing, and accounting for the presence of the steel shape. This restrained shrinkage strain, $\varepsilon'_{sh}(t)$, is calculated using Eq. (1), and was obtained from static equilibrium, assuming a perfect bond between the two materials.

$$\varepsilon'_{sh}(t) = \varepsilon_{sh}(t) \frac{E_c A_c}{E_s A_s + E_c A_c} \qquad (1)$$

In Eq. (1), $\varepsilon_{sh}(t)$ is the unrestrained shrinkage strain of the concrete only, computed using the procedure outlined in ACI (1992), assuming a 3-day wet cure, a relative humidity of 40 %, a volume to exposed surface ratio (V/S) of d/2, a slump of the plastic concrete of 5 mm, as measured after mixing, a cement weight of 350 kg/m^3, a fine-to-coarse aggregate ratio of 46%, based on concrete mix composition, and an air content of 1.8% as measured in the plastic concrete after mixing. The elastic modulus of the steel, E_s, was taken as 200,000 MPa, and the elastic modulus of the concrete at 28 days, E_c, was 29,200 MPa. Parameters A_c and A_s are respectively the area of concrete and steel.

In the ACI model, the basic ultimate shrinkage strain was adjusted from 780 με to 420 με in order to match the shrinkage strain measured in companion ϕ150 mm cylinders, at t = 160 days: 300 με. After this calibration, the unrestrained shrinkage strain, ε_{sh}, for the concrete in Specimens P-1, P-2, and P-7 was calculated as 180 με at t = 160 days after the end of the cure ("Day 150" in Fig. 7), with the ultimate shrinkage strain equal to 220 με. According to Eq.(1), the restrained shrinkage strain, ε'_{sh}, in Specimen P-1 is equal to 68% of the unrestrained shrinkage strain, resulting in a strain of 125 με at "Day 150", and an ultimate strain value of 150 με. Therefore, the predicted shrinkage strain conservatively estimates the average experimental shrinkage strain at "Day 150": 35 με.

The experimental average shrinkage strain values obtained from Specimens P-1, P-2, and P-7 were subtracted from the total strains measured in Specimens P-3 and P-4 to

determine the strains due to creep in these two columns. The shrinkage strains measured in Specimen P-6 were not retained due to experimental difficulties, and the shrinkage strains in Specimens P-1, P-2, and P-7 were used to compute the creep strain in Specimen P-5.

Strain measurements in specimens P-3, P-4, and P-5

The time history of the total strain measurements for Specimen P-3 is illustrated in Fig.8. Specimens P-4 and P-5 exhibited a similar response. These measurements include the elastic, shrinkage, and creep strains. The load on the bare steel section (load P_1) is shown to be applied at "Day –15", just before the concrete was poured in the column. The stresses in the steel shape from Stage 1 loading are given in Table 2. All stresses in the steel are obtained by multiplying the measured strain by the elastic modulus of steel, E_s. Between pouring of the concrete at "Day –14" to "Day 0", the axial strains in the steel and the concrete varied only slightly due to shrinkage of the concrete (less than 20 $\mu\varepsilon$).

At "Day 0", load P_2 was applied to the composite section of Specimens P-3 to P-5. Table 2 gives the average strain and stress increase in the steel shape and the concrete upon application of this load. Stresses in the concrete were obtained using a representative value of the elastic modulus at a concrete age of 14 days ("Day 0"), $E_{c,14}$, given by:

$$E_{c,14} = \frac{P_2 - E_s A_s \Delta\varepsilon}{A_c \Delta\varepsilon} \qquad (2)$$

In this equation, $\Delta\varepsilon$ is the average elastic strain increase at Stage 2 (Table 2) measured in both materials under load P_2. The values of $E_{c,14}$ are 27,400 MPa, 28,200 MPa, and 21,600 MPa for Specimens P-3 to P-5, respectively. These elastic modulus values were preferred over measurements on concrete cylinders because they represent more adequately the actual properties of the concrete in the specimens.

Strains in the steel and the concrete changed gradually with time due to creep and shrinkage and the total measured strain increments, from "Day –14" to "Day 150" are given in Table 2. The shrinkage strain of 35 $\mu\varepsilon$, as obtained from Specimens P-1, P-2, and P-7 during that period of time represents 14% to 19% of the total strain increase recorded in Specimens P-3 to P-5. As shown in Table 2, the total stress increases in the steel shape of Specimens P-3 to P-5, at the end of loading Stage 2, are respectively: 41 MPa, 44 MPa, and 37 MPa, giving total stresses of 215 MPa, 219 MPa, and 223 MPa, respectively. From equilibrium, the stresses in the concrete were calculated as 6.8 MPa, 6.5 MPa, and 6.5 MPa, respectively. Total strains at "Day 150", including elastic and long-term effects, are also given in Table 2 for Specimens P-3 to P-5. Based on these results, Specimens P-3, P-4, and P-5 had a similar stress distribution at the end of the measurement time period.

Creep strain calculations for Specimens P-3, P-4 and P-5

The column axial strain due to creep of the concrete in Specimens P-3 to P-5 was calculated by subtracting the strains due to shrinkage, measured in the load free Specimens P-1, P-2, and P-7, from the total strains at the end of Stage 2. These

experimental creep strains were thereafter compared to the ACI (1992) prediction model based on the effective time dependent long-term elastic modulus of the concrete, $E'_c(t)$. The model assumes that the stresses in the steel and the concrete remain in the elastic range during the long-term loading period and that the axial strain variation in both materials are the same. The first assumption is verified by the experimental results as the elastic stresses in the concrete of Specimens P-3 to P-5 during Stage 2 (between 9 and 10 MPa) were lower than 40% of the concrete strength at "Day 0" (≈25 MPa). Strain variation in both materials was approximately the same and the computed average strain was used in the stress calculations. The time-dependent strain in the steel and the concrete due to creep of the concrete, including the elastic strain from Stage 2, $\varepsilon_{el+cr}(t)$, can be predicted using:

$$\varepsilon_{el+cr}(t)=\frac{P_2}{E_s A_s + E_c'(t) A_c} \tag{3}$$

where

$$E_c'(t)=\frac{E_{c,14}}{1+\phi(t,t_0)} \tag{4}$$

In these equations, P_2 is the additional load at Stage 2 (see Table 2), and $E'_c(t)$ is the time-dependent effective concrete elastic modulus, t is the number of days after pouring the concrete, $E_{c,14}$ is the elastic modulus of the concrete computed using Eq.(2), $\phi(t,t_0)$ is the creep coefficient proposed by ACI (1992), and "t_0" is the age of the concrete at loading (14 days). The $\phi(t,t_0)$ factor was computed assuming the same parameters as for the calculations of the shrinkage strain.

Figure 9 compares the experimental strains due to elastic and creep deformations (hollow symbols) in Specimen P-3 to the predicted $\varepsilon_{el+cr}(t)$ given by Eq.(3). As shown, the model predicts very well the creep behaviour of this Specimen. Similar correlation was obtained for Specimens P-4 and P-5. The elastic plus creep predicted strain values in Specimens P-3 to P-5 were 512 με, 504 με, and 570 με respectively, which compare very well to the average measured values of 532 με, 518 με, and 568 με. For Specimens P-3 and P-4, the experimental and predicted ratios of creep-to-elastic strains were respectively 0.50 and 0.45 at "Day 150", while the predicted ultimate ratio was estimated as 0.6.

EXPERIMENTAL OBSERVATIONS AND RESULTS OF TESTING TO CAPACITY

Experimental observations and failure modes

Specimens P-1 to P-5 were tested to ultimate capacity (loading Stage 3). For all of these specimens, initiation of local buckling of the steel flanges was observed just before or after peak load. The failure occurred by crushing of the concrete between two consecutive transverse links, together with local buckling of the flanges at the same location (Figs. 10 and 11). Concrete also crushed simultaneously or shortly after on the opposite side but at a different elevation. The failure was ductile and progressive, contrary to specimens with d=600 mm tested under load control in previous programme (Chicoine et al., 2001). One transverse link weld failed after peak load on Specimen P-5 at a load of 5,000 kN, corresponding to an axial strain of 5,200 με.

Load–deformation response

The measured ultimate load at Stage 3, $P_{u,exp}$, is presented in Table 2. These values were computed as the sum of the load applied by the testing machine and the tension bars. The very flexible tension bar and bolt assembly typically deformed at half the rate of the specimen, and it was still in tension at peak load, contributing for 1%, 22%, 19%, and 23% of the total peak load for Specimens P-2 to P-5, respectively. The experimental loads for Specimens P-1 to P-4 were close to each other, all being within 4% of the average value for these four specimens (4,800 kN). The small differences between P-1 to P-4 suggest that the loading sequence and the creep of the concrete had little effects on the capacity of these columns. Chicoine et al. (2001) proposed a model to predict the ultimate load, $P_{u,pred}$, of this type of column under short tem loading. The predicted loads in Table 2 for Specimens P-1 to P-4 (4,675 kN) are in good agreement with the experimental values, confirming the negligible influence of the long-term effects on the capacity of the columns. The same conclusion can be drawn for Specimen P-5, except that caution should be exercised with this result because uncertainty exists on its concrete strength.

Figure 12 presents the applied load with respect to the average column axial strain, ε_a, for all tested specimens. The strain ε_a corresponds to the sum of the average strain at Stages 1 and 2 plus the average strain in the columns computed from the LVDT reading. The response under loading Stages 1 and 2 are indicated by the dotted lines. The figure shows that the plots for Specimens P-2 to P-4 are offset relative to P-1 due to the

sequence of loading and followed each other closely until about 4,000 kN (85% $P_{u,exp}$). The strain at peak load was 2 340 με for Specimen P-1 and ranged from 2,550 με to 2,910 με for the other specimens. For all columns, these strains exceed significantly the yield strain of the steel (1,950 με for P-1 to P-4, and 1,725 με for P-5). This clearly indicates that the steel had yielded when crushing of the concrete occurred at peak load except near the web to flange welds where very high tensile residual stress were computed. Figure 13 illustrates the axial stresses in the steel and the concrete of Specimen P-4with respect to the axial strain. These stresses are normalized to F_y and $\Psi f'_c$, respectively, where Ψ is a size effect factor defined in Chicoine et al. (2001) and they include the loading sequence and the long-term deformations. For clarity, the stress in the steel shape was represented by a straight line at yielding, and the strain in the concrete was offset by a value equal to the elastic strain after loading Stage 1, for direct comparison with the steel at any strain level. The figure shows that when the steel yields, at 1,950 με, the stress in the concrete is only $0.8\Psi f'_c$. It is believed that the steel could undergo such large strains because the concrete could carry the additional load applied to the specimen until crushing failure occurred. These large strains in the steel shape at peak load were also possible because initial imperfections of the flange were inwards. The peak strains for Specimens P-2 to P-4 were greater than that of Specimen P-1 by 400 με, 220 με, and 570 με, because of the strain induced in the steel shape after Stage 1 loading and the long-term average strain increase after Stage 2.

The ductility of the column may be assessed by examining the differences in strains at $0.95P_u$ before and after the peak load, as well as by the post-peak residual capacity. The strain differences at $0.95P_u$ were equal to 960 με, 960 με, 915 με, 1,270 με, and 930 με for Specimens P-1 to P-5, respectively. After peak, the residual loads and corresponding strains for Specimens P-1 to P-5 were, approximately 65% to 75% $P_{u,exp}$ at about 4,000 με. The similitude between Specimen P-1 and the other specimens, together with the fact that these results are comparable with the behaviour observed on similar specimens by Chicoine et al. (2001), indicate that the relatively higher stresses in the steel shape induced by the sequence of loading and the long-term effects are not detrimental to column ductility.

Confinement effects

Transverse expansion of the concrete is smaller than that of the steel until approximately 70% of the concrete strength. Beyond that point, the Poisson's ratio of the concrete becomes larger than that of the steel. Near peak load, this concrete expansion can induce tensile transverse stresses in the web of the steel shape, reducing its longitudinal yield capacity. The method for evaluating these confinement effects on the steel capacity is presented by Chicoine et al. (2001).

The first signs of yielding in the web of all columns occurred at approximately $0.9\ P_{u,exp}$. At, yielding, the transverse stresses at different locations in the web of Specimen P-1, ranged from -25 MPa to -91 MPa in tension. In Specimen P-2, the

transverse stresses in the web ranged from -32 MPa to -137 MPa. Lower transverse stresses were obtained for Specimens P-3 to P-5, ranging from -43 MPa (P-4) to +44 MPa (P-3). In these specimens, the longitudinal stresses at the beginning of Stage 3 were relatively higher due to long-term effects and yielding occurred earlier during the tests, before the concrete started to expand more rapidly than the steel. Long-term loading of the composite section resulted in a significant decrease in transverse stresses and therefore is not considered detrimental to the axial capacity of the steel shape.

Axial stresses in the transverse links

Contrary to the steel shape, the axial tensile stresses in the transverse links are only due to the expansion of the concrete and transverse strain gauges on both the link and the concrete face adjacent to the links gave similar readings. At peak load, the axial stresses obtained on two transverse links at an elevation of 2d in Specimens P-1 to P-5 are 260 MPa, 186 MPa, 172 MPa, 298 MPa, and 213 MPa, respectively. As expected, these results are similar because the concrete in all specimens reached comparable level of axial deformation in all specimens, regardless of the applied loading sequence. The variation in the results may be attributed to the relative position of the concrete failure zone with respect to the position of the instrumented links.

CONCLUSIONS

Axial strains were measured in seven partially encased composite columns during a period of 150 days. Long-term loading was applied to four of the specimens. The nominal stress due to construction loads (Stage 1) was determined as 100 MPa in the

steel shape, and the initial stresses due to long-term service loads (Stage 2) were 170 MPa in the steel and 10 MPa in the concrete. This test series complemented previous tests performed under short term loading to obtain data on the effects of creep and shrinkage of the concrete on the stresses in both materials, and assess these effects on the capacity of the columns. The following observations can be drawn from this study:

- At the end of the 150 day long-term measurement period, the average compressive stress increase in the steel shape due to the shrinkage of the concrete was 7 MPa, corresponding to a strain of 35 $\mu\varepsilon$. Such low shrinkage deformation is attributed to the high volume to surface ratio of the columns and to the low water content of the concrete used for the specimens, with a slump of only 5 mm. The total average stress increase in the steel due to creep and shrinkage of the concrete under loading Stage 2, ranged from 37 MPa to 44 MPa in the steel shape. The final stresses after 150 days, including the elastic stress, ranged from 215 MPa to 223 MPa in the steel shape, and from 6.5 MPa to 6.8 MPa in the concrete. The ratio of creep-to-elastic strains for the concrete was 0.5 for Specimens P-3 and P-4. Theoretical models conservatively predicted the long-term column strain due to shrinkage and creep of the concrete.
- The failure mode of the specimens which were subjected to long-term loading was the same as that observed for identical specimens under short-term loading: crushing of the concrete between two consecutive transverse links, together with local buckling of the flanges. Failure occurred on both concrete faces nearly simultaneously but at different elevations. The ultimate capacity of both types of comparable specimens were also very close to each other, suggesting that neither the loading sequence used

in this programme nor the creep and shrinkage of the concrete had a significant effect on the ultimate load of these columns. An existing model for the computation of the ultimate load under short-term loading gave an accurate prediction for these specimens, confirming the small influence of long-term effects and sequence of construction.

- Near peak load, the concrete expansion can induce tensile transverse stresses in the web of the steel shape, reducing its longitudinal yield capacity. Long-term loading of the composite section resulted in a significant decrease in transverse stresses and therefore is not considered detrimental to the axial capacity of the steel shape.
- The tensile stresses in the transverse links at peak load ranged from 172 MPa to 298 MPa. The axial tensile stresses in the transverse links were found to be dependant only upon the expansion of the concrete.

These conclusions suggest that long-term axial strains due to restrained shrinkage and creep of the concrete in PEC columns may be conservatively predicted based on equations (1) to (4) presented herein. It is also recommended that the design equations proposed by Chicoine et al. (2001), based on short-term loading tests, be used without modifications to compute the long-term axial capacity of this type of columns, provided that the stress in the steel shape under long-term service loads does not exceed 230 MPa, including the effects of construction sequence, and shrinkage and creep of the concrete.

ACKNOWLEDGMENTS

The authors wish to thank the technical personnel at Ecole Polytechnique of Montreal and McGill University. Funding was provided by Canam Steel Inc. and the Natural Science and Engineering Research Council of Canada (NSERC).

APPENDIX I. REFERENCES

ACI Committee 209 (1992) "Prediction of creep, shrinkage, and temperature effects in concrete structures." *ACI Manual of Concrete Practice*, Detroit, 209R1-209R47.

Bode, H. (1976) "Colonnes constituées de tubes en acier remplis de béton: dimensionnement et utilisation." *Acier-Stahl-Steel*, 11-12, 388-393.

Bradford, M.A., Gilbert, R.I. (1990) "Time-dependent analysis and design of composite columns." *J. Struct. Division*, ASCE, **116**(12), 3338-3357.

Bridge, R.Q. (1979) "Composite columns under sustained load." *J. Struct. Division*, ASCE, **104**(7), 563-576.

CEN, AFNOR (1994) "Construction mixte acier et béton: Conception et dimensionnement des structures mixtes acier et béton. " *Eurocode 4* (in French).

Chicoine, T., Tremblay, R., Massicotte, B. (2000) "Long-term test programme on partially encased built-up three-plate composite columns." *EPM/GCS No. 2000-20*, Department of Civil, Geological and Mining Engineering, Ecole Polytechnique, Montreal, Canada.

Chicoine, T., Tremblay, R., Massicotte, B., Yalcin, M., Ricles, J., Lu, L.-W. (2001) "Behavior and strength of partially encased columns with built-up shape." *J. Struct. Engrg.*, ASCE, In press.

CSA (1994) *CAN/CSA-S16.1-94 Limit States Design of Steel Structures.* Canadian Standards Association, Rexdale, Ontario.

De Larrard, F. (1999) *Concrete Mixture Proportioning – A scientific approach,* E & FN SPON, London, UK.

Morino, S., Kawaguchi, J., Cao, Z.S. (1996) "Creep behaviour of concrete-filled steel tubular members." *Composite construction in steel and structures III,* Proceedings of an Engineering foundation conference, 514-525.

Nakai, H., Kurita, A., Ichinose, L.H. (1991) "An experimental study on creep of concrete filled steel pipes." *Proceedings of the 3rd international conference on steel and concrete composite structures*, 55-60.

Neville, A.M., Dilger, W.H., Brooks, J.J. (1983) *Creep of plain and structural concrete.* Construction Press, London and New-York.

Roik, K., Bergmann, R., and Mangerig, I. (1987) "The German design method for composite columns with regard to creep and shrinkage of concrete." *Composite construction in steel and concrete,* Proceedings of an Engineering foundation conference, ASCE, Henniker, New Hampshire, 561-565.

SSRC, Task Group 20 (1979) "A specification for the design of steel-concrete composite columns." *Engineering Journal*, vol.16, 4th quarter, AISC, 101-115.

SSRC (1998) *Guide to Stability Design Criteria for Metal Structures*, 5th ed., T.V. Galambos, Ed., John Wiley & Sons, New York, NY.

Terrey, P.J., Bradford, M.A., Gilbert, R.I. (1994) "Creep and Shrinkage of concrete in concrete-filled circular steel tubes." *Proceedings of the 6th international symposium on tubular structures*, 293-298.

Tremblay, R., Massicotte, B., Filion, I., Maranda, R. (1998) "Experimental study on the behavior of partially encased composite columns made with light welded H steel shapes under compressive axial loads." *1998 SSRC Annual Technical Meeting.*

Tremblay, R., Chicoine, T., Massicotte, B. (2000) "Design equation for the axial capacity of partially encased non-compact columns." *Proc. Composite Construction IV*, Engineering Foundation, Banff, Canada.

Uy, B. (2001) "Static long-term effects in short concrete-filled steel box columns under sustained loading." *ACI Structural Journal*, **98**(1), 96-104.

Vincent, R. (2000) "Design and application of partially encased non-compact composite columns for high-rise buildings." *Proc. Composite Construction IV*, Engineering Foundation, Banff, Canada.

APPENDIX II. NOTATION

The following symbols are used in this paper :

A_c = concrete area (mm^2);

A_s = steel flange area (mm^2);

b = flange half-width (mm);

b_f = flange width (mm);

d = column depth (mm);

$E'_c(t)$ = time-dependant concrete elastic modulus (MPa);

f'_c = concrete strength (MPa);

F_y = steel yield strength (MPa);

L = column length (mm);

P_1 = load applied at Stage 1 (kN);

P_2 = additional load applied at Stage 2 (kN);

$P_{u,pred.}$ = predicted ultimate load (kN);

$P_{u,exp.}$ = experimental ultimate load (kN);

s = transverse link spacing (mm);

t = plate thickness (mm);

δ_0 = local flange out-of-straightness (mm);

$\Delta\varepsilon$ = average strain increase from the steel and the concrete (mm/mm)

ε_a = average longitudinal strain (mm/mm);

ε_{el+cr} = Elastic and creep strain of the column under Stage 2 load (mm/mm)

ε'_{sh} = restrained shrinkage strain of the column (mm/mm)

ε_{sh} = unrestrained shrinkage strain of the concrete (mm/mm)

$\phi(t,t_0)$ = creep coefficient (-);

σ_r = longitudinal residual stress (MPa);

TABLE 1. Properties of Long-Term Test Specimens

Specimen no. (1)	b_f x d x t (mm) (2)	b/t (-) (3)	L (mm) (4)	S (mm) (5)	Link ϕ (mm) (6)	Materials Strength at Testing		Average Flange Out-of-Straightness[a] δ_0 (mm) (9)
						F_y (MPa) (7)	f'_c (MPa) (8)	
P-1	300x300x6.5	23.6	1,500	300	12.7	390	36.8	0.74
P-2	300x300x6.5	23.6	1,500	300	12.7	390	36.8	0.58
P-3	300x300x6.5	23.6	1,500	300	12.7	390	36.8	0.35
P-4	300x300x6.5	23.6	1,500	300	12.7	390	36.8	0.44
P-5	450x450x9.6	23.2	2,350	450	12.7	345	30.0	0.52
P-6	450x450x9.7	23.2	900	440	12.7	345	30.0	N/A
P-7	300x300x6.5	23.6	1,500	300	12.7	390	36.8	N/A

Note: (a) Positive inward

TABLE 2. Long-Term Load and Stress History for Specimens P-1 to P-7

Stage	Material	P-1		P-2		P-3		P-4		P-5	
		Strain (με)	Stress[a] (MPa)	Strain (με)	Stress[a] (MPa)	Strain (με)	Stress[a] (MPa)	Strain (με)	Stress[a] (MPa)	Strain (με)	Stress[a] (MPa)
(1)	(2)	(3)	(4)	(5)	(6)	(7)	(8)	(9)	(10)	(11)	(12)
Stage 1	Elastic	P_1 = 0 kN		P_1 = 575 kN		P_1 = 585 kN		P_1 = 585 kN		P_1 = 1 315 kN	
	Steel	-	-	500	100	515	103	525	105	515	103
Stage 2	Elastic	P_2 = 0 kN		P_2 = 0 kN		P_2 = 1 225 kN		P_2 = 1 225 kN		P_2 = 2 755 kN	
	Steel	-	-	-	-	365	71	357	70	394	83
	Concrete	-	-	-	-	349	9.7	344	9.8	435	9.0
	Average	-	-	-	-	357	-	350	-	414	-
	Long-term Increase[c]	P_1, P_2 = 0 kN		P_1, P_2 = 560 kN		P_1, P_2=1 810 kN		P_1, P_2=1 810 kN		P_1, P_2=4 070 kN	
	Steel	-	-	-	+7	+200	+41	+222	+44	+211	+37
	Concrete	-	-	-	-0.1	+217	-2.9	+241	-3.3	+171	-2.5
	Average	-	-	+35[b]	-	+209	-	+232	-	+185	-
	Total	P_1, P_2 = 0 kN		P_1, P_2 = 560 kN		P_1, P_2=1 810 kN		P_1, P_2=1 810 kN		P_1, P_2=4 070 kN	
	Steel	-	-	535	107	1 080	215	1 104	219	1 120	223
	Concrete	-	-	35	-0.1	566	6.8	585	6.5	606	6.5
	Average[d]	-	-	535	-	1 076	-	1 097	-	1 114	-
Stage 3		Load (kN)		Load (kN)		Load (kN)		Load (kN)		Load (kN)	
	$P_{u,exp}$	4 770		4 670		4 790		4 975		9 225	
	$P_{u,pred}$	4 675		4 675		4 675		4 675		8 610	
	$P_{u,exp}/P_{u,pred}$	1.02		1.00		1.02		1.06		1.07	

Notes: (a) Stresses in steel and concrete computed from average strain, positive in compression
(b) Average shrinkage strain from Specimens P-1, P-2, and P-7
(c) From day of concrete pouring
(d) Average total strain in the steel computed from summation of Stage 1 elastic strain and Stage 2 average elastic and long-term strains

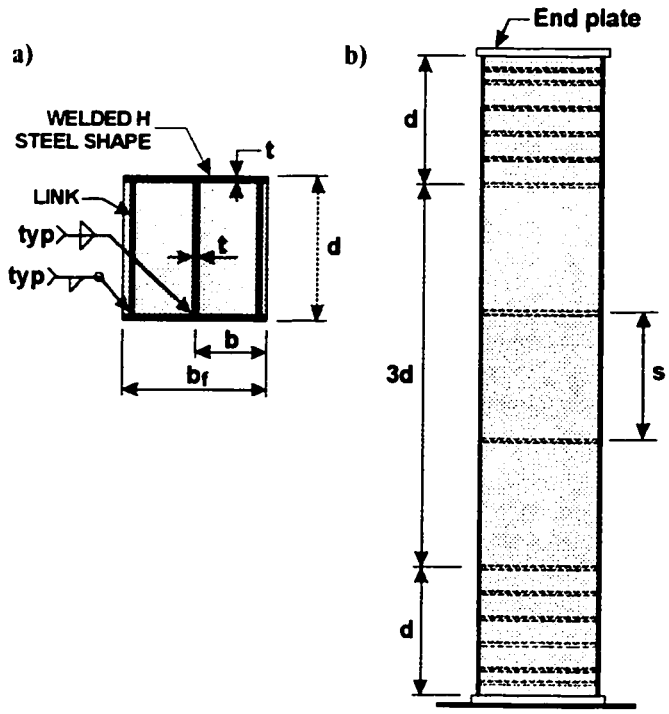

FIG. 1. Geometry of Stub Columns:
(a) Cross-Section; (b) Elevation View

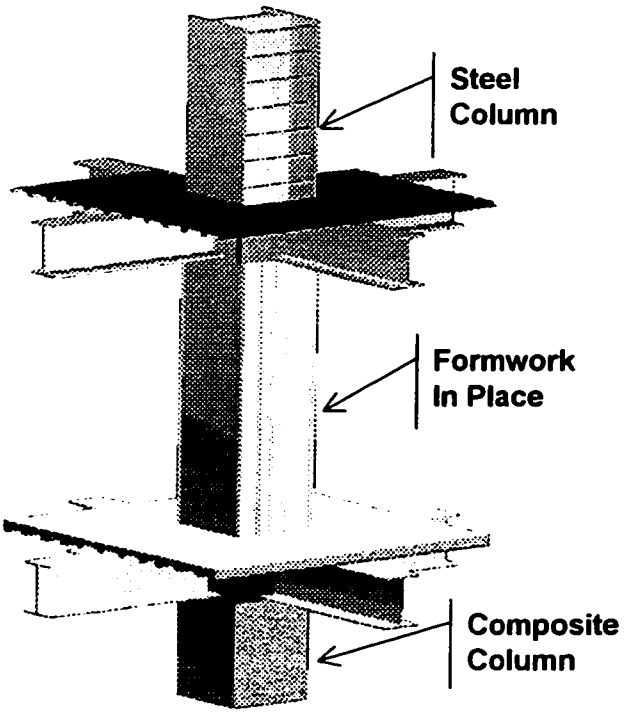

FIG. 2. Construction Stages for Partially Encased Composite Column

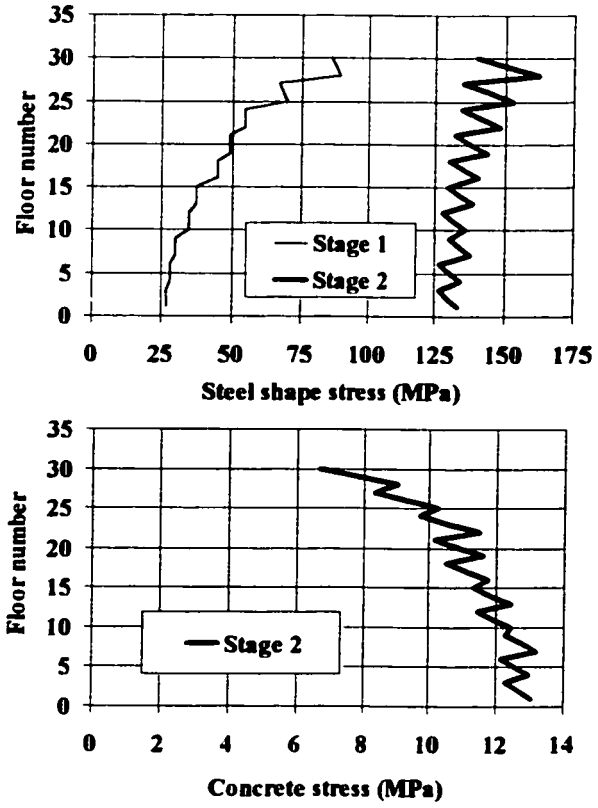

FIG. 3. Anticipated Stresses in Steel and Concrete of Columns in a 36-Storey Office Building

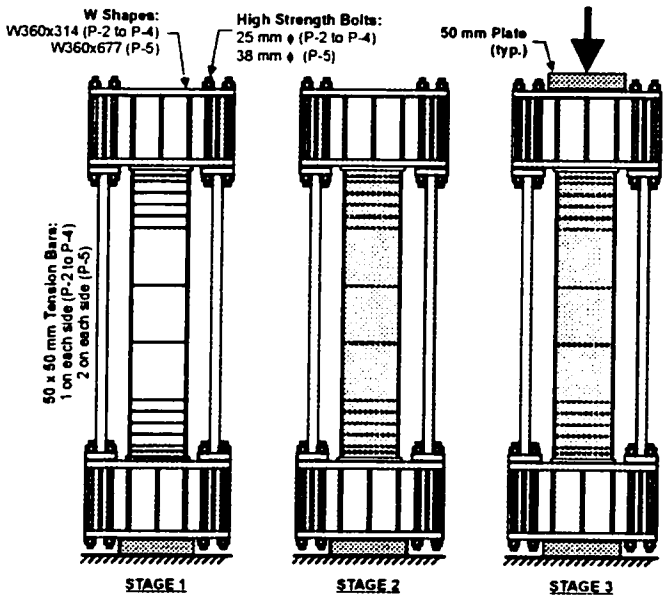

FIG. 4. Loading Stages 1 to 3

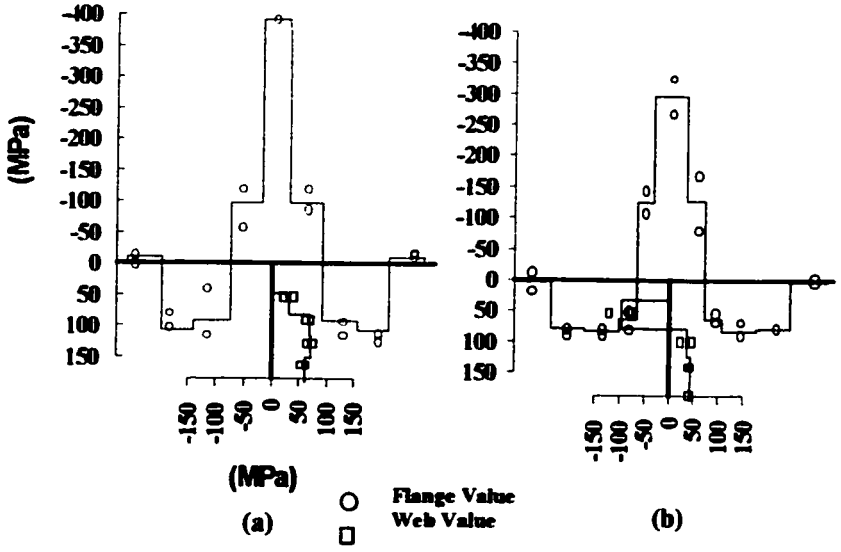

FIG. 5. Measured Residual Stresses:

(a) P-1 to P-4; (b) P-5

FIG. 6. Specimen in the MTS Testing Machine

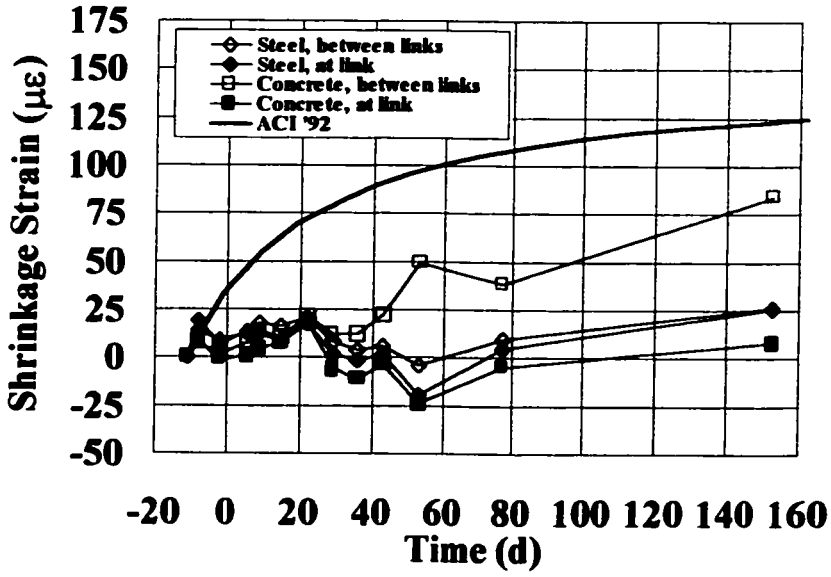

FIG. 7. Average Shrinkage Axial Strain in Specimens P-1, P-2, and P-7

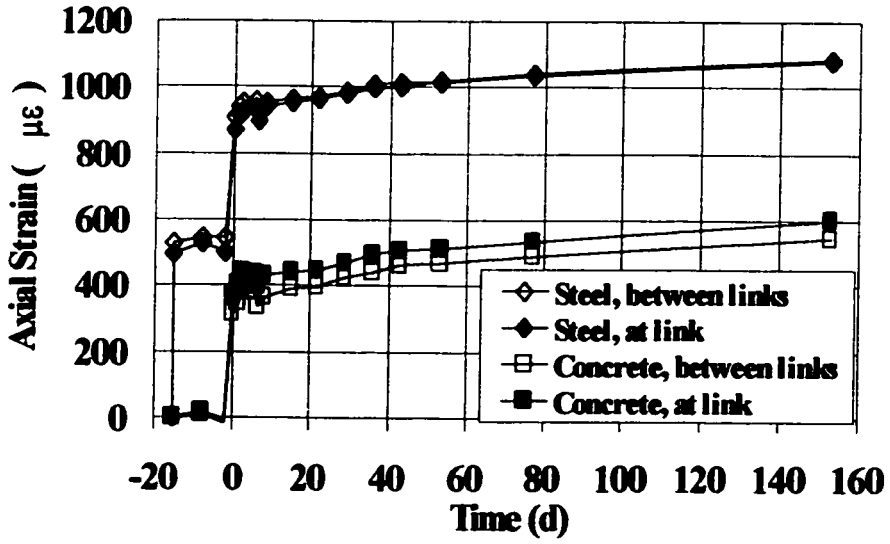

FIG. 8. Total Strain History for Specimen P-3

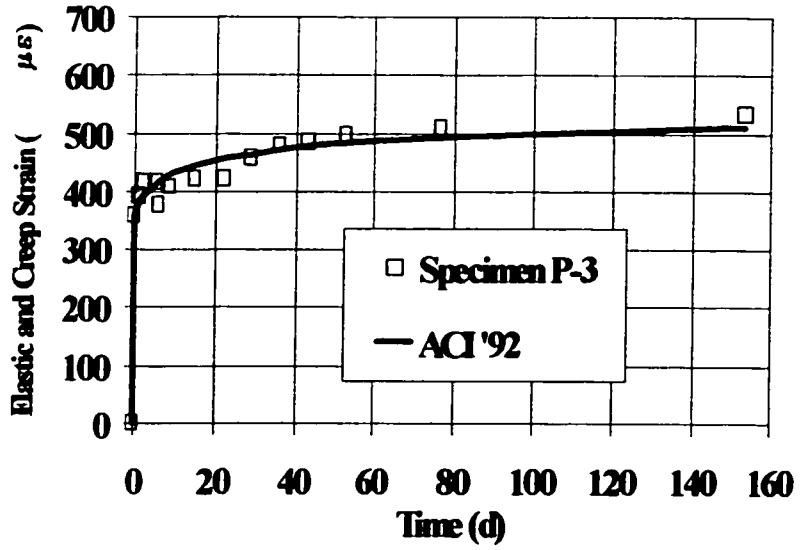

FIG. 9. Experimental and Predicted Elastic plus Creep Strain in Specimen P-3

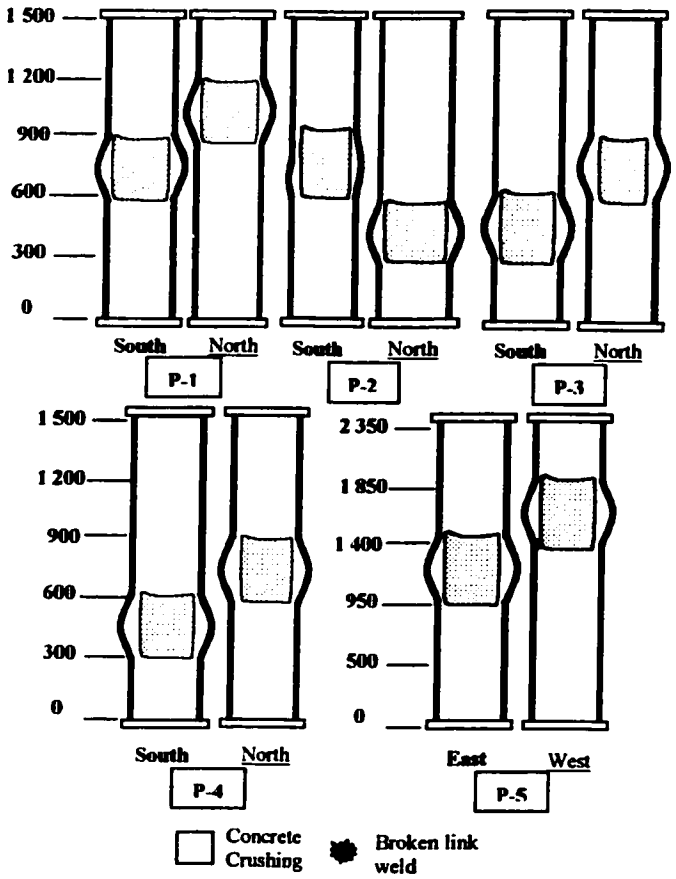

FIG. 10. Visual Observations on Specimens P-1 to P-5, after Failure

FIG. 11. Specimen P-3 After Failure:
(a) SW Corner; (b) North Face.

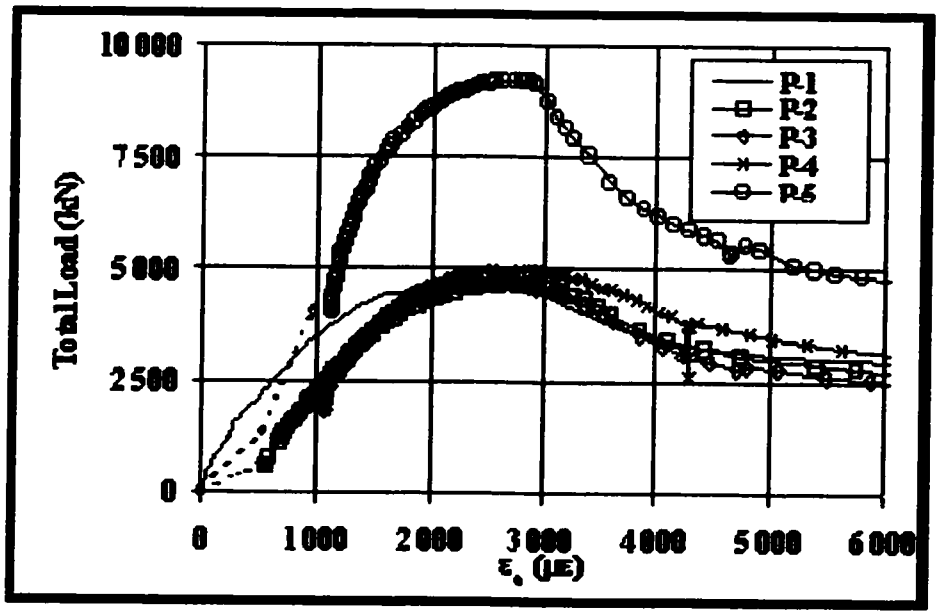

FIG. 12. Axial Load-Deformation Response of Specimens P-1 to P-5

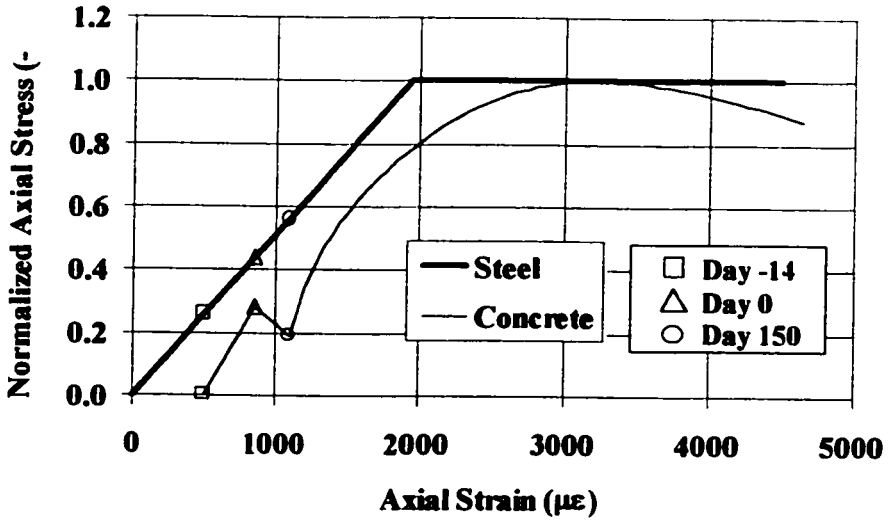

FIG. 13. Stress-Strain Response in Steel and Concrete of Specimen P-4

APPENDIX C – PAPER 3

Finite element modelling of the experimental response of partially encased composite columns

By Thierry Chicoine, Bruno Massicotte, and Robert Tremblay

Submitted to : Steel and composite structures international Journal, May 2001

Finite element modelling of the experimental response of partially encased composite columns

Thierry Chicoine†, Bruno Massicotte‡, and Robert Tremblay‡

Department of Civil, Geological, and Mining Engineering, Ecole Polytechnique, Montreal, H3C 3A7, Canada

Abstract. In this paper, the behaviour of axially loaded partially encased composite columns made with light welded H steel shapes is examined using ABAQUS finite element modelling. The results of the numerical simulations are compared to the response observed in previous experimental studies on that column system. The steel shape of the specimens has transverse links attached to the flanges to improve its local buckling capacity and concrete is poured between the flanges only. The test specimens included 14 stub-columns with a square cross section ranging from 300 mm to 600 mm in depth. The transverse link spacing varied from 0.5 to 1 times the depth and the width-to-thickness ratio of the flanges ranged from 23 to 35. The numerical model accounted for nonlinear stress-strain behaviour of materials, residual stresses in the steel shape, initial local imperfections of the flanges, and allowed for large rotations in the solution. A Riks displacement controlled strategy was used to carry out the analysis. Plastic analyses on the composite models reproduced accurately the capacity of the specimens, the failure mode, the axial strain at peak load, the transverse stresses in the web, and the axial stresses in the transverse links. The influence of applying a typical construction loading sequence could also be reproduced numerically. A design equation is proposed to determine the axial capacity of this type of column.

---

† Graduate research assistant
‡ Professor

1. Introduction

A new type of partially encased composite (PEC) column consisting of thin-walled, I-shaped steel section with concrete being poured between the flanges of the steel section has recently been developed and patented by the Canam Manac Group (Figs.1 and 2). The steel section features very slender plates exceeding the width to thickness ratio limits for non-compact sections. Transverse links between the flanges are spaced at regular intervals to enhance the resistance of the flanges to local buckling. The proposed PEC column is intended to carry only axial loads in multi-storey buildings, the lateral loads being resisted by other structural systems such as shear walls.

The advantages of this system over traditional composite column design have been presented by Vincent (2000) and several series of axially loading tests have been performed on large-scale columns (Tremblay et al., 1998; Chicoine et al., 2000c). Failure of test columns occurred by crushing of the concrete with yielding and local buckling of the steel shapes. In specimens with larger b/t and s/d ratios, local buckling of the flanges occurred before the peak load was reached. A series of tests (Chicoine et al., 2000a) was also performed to investigate the influence of construction loading sequence and examine the long-term behaviour of these columns. Design equations accounting for local flange buckling have been proposed by Tremblay et al. (1998, 2000), and Chicoine et al. (2000c).

Finite element models of partially encased composite columns were initiated by Maranda (1999) using the computer program MEF (Bouzaiene and Massicotte, 1997). By taking advantage of the double symmetry of the column, only a quarter of the cross section was modelled, including the local imperfections of the steel flange and the residual stresses. The model by Maranda reproduced adequately the experimental axial capacity of test specimens, with an average ratio of experimental to numerical peak loads of 0.95, and a standard deviation of 0.03. In most of the analyses, however, the post-peak response could not be obtained. Broderick and Elnashai (1994) studied the seismic behaviour of partially encased composite columns having a compact steel section and transverse links when subjected to inelastic earthquake loading. The reference test specimens had various axial load levels and were tested under dynamic and pseudo-dynamic protocols. The authors proposed a numerical model using the computer program ADAPTIC. This program featured three types of concrete confinement: unconfined concrete between the exposed face and the transverse links, fully-confined concrete near the web of the steel shape, and partial confinement for the concrete located between these two regions. The authors did not specify the residual stresses nor the local imperfections in the steel shape. Good agreement with the experimental results was obtained for predicting the displacement and rotation ductility, the ultimate moment, and the seismic efficiency for this type of composite system could be demonstrated. The finite element program ABAQUS was used by Sugiura et al. (2000) in modelling a composite sandwich beam that had been tested in flexure. The interface between the concrete and the reinforcing material on the tension side of the cross-section was modelled using a set of

non-linear springs in the three principal directions of the coordinate system. The concrete part was modelled using 20-node quadratic brick elements with reduced integration (C3D20R).

2. Objectives and scope of the research

The objectives and scope of this study were to examine several aspects of the behaviour of PEC columns using finite element (FE) techniques to recommend design equations for the axial capacity of the columns. A model was first developed with the computer program ABAQUS (HKS, 2000) to reproduce the experimental behaviour of 14 full-scale stub-column tests: strain at peak load, transverse stresses in the web of the steel shape, tensile force in transverse links, local buckling behaviour of the steel plates, loading sequence and long term effects. The model allowed for large displacements in the solution and included the following features: non-linear stress-strain behaviour of materials, residual stresses in the steel shape, initial local imperfections of the flanges, and contact elements between the concrete and the steel web. The model was then used to examine the influence of residual stresses, initial local imperfections, and sequence of loading. The results permitted to develop a design equation that predicts accurately the axial load capacity of the PEC columns.

3. Reference test database

Tests on 14 partially encased composite column specimens were selected from the experimental programs performed by Tremblay et al. (1998) and Chicoine et al. (2000a,

2000c) for the purpose of verifying the FE models developed in this study. Table 1 gives the characteristics of these columns (see also Fig. 2), including the yield stress of the steel, F_y, as well as the ultimate strength, f'_c, the elastic modulus, E_c, and the strain at peak load, ε'_c, of the concrete, as measured from tests on cylinders. The selection covers the full range of the main geometric parameters of the columns, i.e., the column depth, d, the width-to-thickness ratio of the flanges, b/t, and the relative spacing of the transverse links, s/d. Test series 1 and 2 were short-term axial tests on partially encased composite columns with a cross section ranging from 300 mm x 300 mm to 600 mm x 600 mm. The sequence of construction and long-term behaviour of the column system was examined on 300 mm x 300 mm and 450 mm x 450 mm columns in Test Series 3. Specimens C-3 and C-6 in Series 1, which had a link spacing of 3d/4, were not modelled but the results from these tests are used later to validate the proposed design equations.

The loading sequence for specimens of Series 3 included a total of three stages, as illustrated in Fig.3. At Stage 1, an axial load was applied to the steel shape only by tensioning the high strength bolts to induce a nominal compressive stress of 100 MPa before concreting. This stress corresponds to the maximum anticipated effects of typical construction loading carried by the steel shape alone. At Stage 2, 14 days after pouring the concrete, the applied load was increased to reach the anticipated axial load due to the long-term service load: 100%Dead load + 50%Live load. This load was maintained for a period of approximately 6 months and produced a total stress of 170 MPa in the steel and

10 MPa in the concrete. At Stage 3, the load on the composite column was increased further up to failure.

4. Characteristics of the finite element models

4.1. Geometric properties

By making use of the symmetry of the cross section and of the failure mode observed in the tests, the finite element models only included a quarter of the cross section, over a height of one transverse link spacing (Fig.4a). The complete models are presented in Figs.4b and 4c for link spacing of s = d/2 and s = d, respectively. Eight-node shell elements (S8R) were used to model both the flange and the web. This element type was preferred over a four-node shell element because it provides a better prediction of the buckling capacity of the steel shape for the same number of elements. In the model with s = d/2, the mesh for the flange and the web each had 7 elements over the width and 6 elements over the height (84 elements total). The size of 72 shell elements matched that of the adjacent concrete elements and each had a length-to-width ratio close to the optimal value of one. Near the connection between the flange and the web in the specimens, narrower plate elements extended both the flange and the web over a width equal to half the plate thickness to connect to the centreline of each plate. Using such narrow elements did not downgrade the quality of the solution since they were away from the buckling zone and were expected to carry axial load only. A mesh of 6 x 6 x 6 type C3D20R solid elements (216 elements total) was used to model the concrete. This 3D

solid element type has a total of 20 nodes, with 8 nodes on each face. This permitted a perfect node-by-node match with the S8R shell elements, enabling to capture well the interaction between the steel and the concrete. The transverse links at the top and bottom ends of the models were made up of 7 type B32 beam type elements (14 elements total). This beam element type has three nodes and the length of each of these elements matched the width of the adjacent concrete elements, except between the steel flange and the concrete where the length of the link was equal to half the flange thickness. The same configuration was used for the model with s = d except that the number of elements was doubled in the longitudinal direction, effectively doubling the total number of 168 shell and 432 solid elements.

Two-node spring elements of type Spring2 were introduced at every nodal point between the steel flange and the opposing concrete face. These elements were given a very high stiffness in compression to prevent inward buckling of the flange due to the presence of the concrete, and a very low tensile stiffness to allow the flange to buckle freely in the outward direction. The displacements of the nodes in the web shell elements and the adjacent concrete face were coupled in directions 1 and 3 by means of stiff Spring2 elements to simulate perfect contact between the concrete and the steel web. All nodes of the transverse links were coupled to the adjacent concrete nodes in the axial direction of the links, to simulate the perfect bond between the links and the concrete transverse expansion and permit the development of tensile stresses in the links.

4.2. Material mechanical properties

A bilinear strain-stress behaviour was assumed for steel, with an elastic modulus of 200 GPa, a yield stress, F_y, as given in Table 1, and a strain hardening slope of 800 MPa, based on typical stress-strain curves obtained from tensile tests on steel coupons. The mechanical properties assigned to the concrete elements are presented in Table 2. The analyses were made with an effective concrete strength, f'_{ce}, and an effective elastic modulus, E_{ce}, given by:

$$f'_{ce} = 0.92\Psi f'_c \tag{1}$$

$$E_{ce} = \sqrt{0.92\Psi}\, E_c \tag{2}$$

where f'_c and E_c are respectively the concrete strength and elastic modulus measured from cylinders at the day of column testing. The parameter Ψ was proposed by Chicoine et al. (2000c), based on experimental data reported by Neville (1966), to account for the size effect on the concrete strength in PEC columns:

$$\psi = 0.85\left(0.96 + \frac{22}{b}\right) \quad \begin{cases} \geq 0.85 \\ \leq 0.97 \end{cases} \tag{3}$$

The additional reduction factor of 0.92 mainly accounts for the lower quality of the concrete used in structural elements when compared to the concrete in test cylinders.

Such difference arises from variation in compaction, handling, workmanship, and curing methods (Newman, 1987). As discussed later, the value of 0.92 was obtained through an iterative process until a test-to-predicted ratio of 1.0 was obtained, in average, for all test specimens. This value confirms the finding by Maranda that material strength has to be reduced in the numerical model to match more precisely the test results. This reduction factor is also in line with the value of 0.9 proposed by Bloem (1968) and with the provisions included in modern standards for the design of concrete structures. For instance, in CSA-A23.3 Standard (1994), a factor of 0.9 has been included in the design equation for reinforced concrete columns to account for this difference between cylinder and structure concrete.

The stress-strain relationship of the concrete in uniaxial compression was defined in 100 με increments by adjusting the parameters in the formulation proposed by Tsai (1988) to match the measured peak strain (Table 1) and the effective elastic modulus and strength (Table 2). The tensile strength of the concrete was set to 9% of the compressive strength in the model. The Poisson's ratio of steel was taken as 0.3. For concrete, that ratio was set equal to 0.18 in the elastic range (up to 40%f'_{ce}), and thereafter increased linearly up to 0.45 at peak stress. The value of 0.18 was obtained from measurements on cylinders in test Series 1 to 3, while the final value is the maximum value that can be obtained from the program built-in concrete model, based on solid mechanics. Figure 5 compares the Poisson's ratios obtained from concrete cylinders of Series 3 and the FE concrete model. The figure shows that the Poisson's ratio in the cylinders starts

increasing at about 500 με, and exceeds that of the steel for strains greater than 1 000 με. Good agreement is obtained between the concrete prediction model and the experimental values up to about 1 000 με. Near peak strain, the model underestimates the lateral expansion of the cylinders because the concrete no longer is a homogeneous material in the cylinders after extensive cracking.

No cylinders were tested at the day of testing for Specimen P-5. The concrete strength was extrapolated from measurements at an earlier age (Chicoine et al., 2000a) and the elastic modulus was taken equal to 4 $500\sqrt{f_c'}$. Therefore, the mechanical properties of the concrete for this specimen represent only estimates and caution must be exercised when using these values.

4.3. Initial out-of-straightness and residual stresses in the steel shape

Measured out-of-straightness of the flanges of the specimen steel shape, δ_{0m}, varied from 0.35 mm (P-3) to 2.02 mm (C-9), which corresponds to s/875 and s/297, respectively. On specimens with a link spacing of d/2, the mean imperfection was s/670 (standard deviation, SD, of s/1870), a value smaller than for specimens with a spacing of d: δ_{0m} = s/500 with SD of s/1200. When considering all link spacings, however, the similar mean imperfections were found in small and large specimens (s/550 vs. s/530). Due to the fabrication process, the imperfections were typically inwards, resulting in a favourable condition for resistance to local buckling. In the FE models, these initial

deformations of the steel flanges were included by applying a deformed shape corresponding to the first buckling mode obtained from eigenvalue analysis performed on models that included only the steel shape. The deformed shape was then scaled to match the value of δ_{0m} measured for each specimen, as given in Table 2. Preliminary analyses indicated that setting the imperfection inwards resulted in a buckling mode of the flange that was different from that observed experimentally. Near failure, lateral expansion of the concrete in the test columns exceeded that in the model (see Fig.5) and likely forced the flanges to buckle outwards. The imperfections were therefore set outwards in the FE models to reproduce the observed behaviour. This assumption is conservative and is justified later by the analysis results.

Typical residual stresses measured on the specimen steel shapes are shown in Fig. 6. Also given in the figure are the amplitude and distribution of the residual stresses that were adopted in the analytical models. The residual stresses are characterised by high tensile values at the welds connecting the flanges to the web and compressive values away from the welds. The residual stresses were introduced in the numerical models as uniform initial axial stresses in each of the shell element of the flange and web. As shown, the compression residual stresses could be reproduced accurately in the model but some error was introduced for the tensile stresses because the sharp gradient exhibited by the experimental stresses could not be captured adequately due to the size of the elements. In addition, equilibrium between tension and compression residual stresses in the models was obtained by adjusting only the tensile stresses, as the compression values

were considered more reliable. For some columns, this contributed in increasing further the difference between experimental and numerical tensile residual stresses.

4.4. Sequence of loading and analysis strategy

For reproducing the various loading stages in the long-term test series (specimens P-2 to P-5), the model was first entirely defined with the concrete and the steel elements. The concrete elements were then removed and the steel shape was first loaded to match the long-term stresses. The concrete elements were put back in place and the load was increased further on the composite section in Stages 2 and 3. The long-term effects on the concrete were not modelled directly using the program built-in creep models. Instead, the long-term deformations were taken into account by adding the stress increase in the steel in loading Stage 2 to the stresses applied at Stage 1. So doing, the stresses in both materials at the end of Stage 2 corresponded to the stresses obtained experimentally, as shown in Table 3 In loading Stage 3, the load was increased up to failure.

The solution strategy in the analysis was a Riks displacement control scheme, with an initial arc length increment corresponding to 10% of the ultimate load. This method is best suited for nonlinear or unstable problems, such as the inelastic buckling of a plate, and generally permits to determine the post-peak response of a structural model.

5. Plastic analysis of the composite sections

5.1. Prediction of failure modes and ultimate capacity

Typical failure modes for specimens with s=d (Specimen C-8) and s=d/2 (Specimen C-10) are given in Fig. 7. As shown, failure occurred in both cases by crushing of the concrete with local buckling of the flanges that developed between two adjacent transverse links. Table 4 presents the results of the plastic analysis of the composite models. In the table, the squash load of the column, neglecting local buckling effects, P_0, corresponds to:

$$P_0 = A_s F_y + A_c f'_{ce} \tag{4}$$

The table also gives the peak load obtained from the FE model analyses on the full-cross section, $P_{u,fem}$, the experimental load, $P_{u,exp}$, the test-to-predicted ratio for the ultimate load, the longitudinal strain in the web at peak load as obtained from the analysis, $\varepsilon_{u,fem}$, and from the experiments, $\varepsilon_{u,,exp}$, and the test-to-predicted ratio for the longitudinal strain. The FE models give a very good estimate of the ultimate capacity of the columns when using a concrete strength of f'_{ce}, the test-to-predicted ratio ranging from 0.96 (C-10) to 1.06 (P-5) with a mean of 1.00. The load ratio for specimen P-5 is relatively high but this result can be attributed to the uncertainty in the concrete strength for that column and, therefore, was not included in the calculation of the statistical values.

Table 4 also shows that the FE models generally give higher strains at peak load, with an experimental to numerical average ratio of 0.95. The reason for this is that the FE strain represents the average strain over a column segment of height s in which failure takes place. In the test columns, the strains were obtained from LVDT measurements of the axial deformation of the specimens over nearly their total height. Failure in test columns typically occurred over 1/5 of the specimen height and hence, experimental strains near peak load include the strains due to inelastic unloading outside of the failed area. Moreover, in order to avoid end failure in the test columns, higher strength concrete was used at both ends of the column specimens, reducing further the experimental average strain.

5.2. Axial load–strain behaviour of composite models

Figure 8 compares the experimental and numerical load-strain responses of representative specimens obtained using a concrete strength of $\Psi f'_c$ and $0.92\Psi f'_c$. The results show the effects of the specimen size (C-7 vs. C-9), the link spacing and additional reinforcement (C9 vs. C-12), the plate slenderness (C-9 vs. C-11), and long-term effect (P-1 vs. P-3). Overall, a very good agreement on the elastic column stiffness, the peak load and the strain at peak load was obtained between the experiments and FE models when an effective concrete strength of $f'_{ce} = 0.92\Psi f'_c$ was specified. For test Series 3 specimens subjected to long-term loading (P-2 to P-5), the prediction at the end of loading Stage 2 is represented by the hollow symbols in the figure. As shown, it compares well with the corresponding experimental data point.

For all specimens, the response could not be reproduced far beyond the peak load due to numerical convergence problems that occurred. However, a negative stiffness was obtained at the end of all analyses, indicating that the analysis had reached the post-peak domain.

5.3. Influence of residual stresses and initial imperfections on material efficiency

Table 5 gives the ultimate load normalised to P_0 and the computed average stresses at peak load in the flanges, σ_{fl}, the web, σ_w, and the concrete, σ_c. These stresses were obtained by dividing the total load acting on each component by its cross-section area. They were then normalised to F_y for the steel and f'_{ce} for the concrete to obtain stress efficiency ratios. Table 6 presents the results of a study on the sensitivity of representative specimens (different d, s/d, and b/t) to residual stresses and local imperfections. Case 1 in the table corresponds to the actual test conditions with $\delta_0=\delta_{0m}$ and $\sigma_r=\sigma_{rm}$. In Cases 2 and 3, the effects of having respectively the residual stresses and the initial imperfections set to zero were examined. Cases 4 and 5 were considered to study the influence of increasing the amplitude of initial imperfections (Case 4: $\delta_0=3\delta_{0m}$) and setting the imperfection inwards (Case 5: $\delta_0=-\delta_{0m}$).

5.3.1 Stress efficiency ratio for the flange under short-term loading

Table 5 shows that the stress efficiency ratio of the flange (σ_{fl}/F_y) varies from 0.75 to 0.97, with a mean value of 0.88. It is generally higher for specimens with s=d/2 than

for specimens with s=d (e.g., 0.97 for C-2 vs. 0.88 for C-4). It is also higher for specimens with a lower b/t ratio (0.86 for C-8 vs. 0.75 for C-11). These two observations are typical for local buckling behaviour as the flange slenderness increases with s/d and b/t.

Table 5 also shows that the stress ratio for the flanges does not vary much with the size of the columns when s/d and b/t are kept constant. For instance, σ_{fl}/F_y ranges from 0.85 to 0.88 for all specimens with s=d and b/t=23, and it varies from 0.92 to 0.97 for specimens with s=d/2. These slight variations in the stress ratio with d are attributed to the aforementioned differences in the modelling of the residual tensile stresses from one column to another. The steel in areas of the cross-section subjected to high tensile residual stresses does not reach the yield stress at peak load, when crushing of the concrete occurs. This contributes in reducing the efficiency of the steel shape and any variation in the modelling of the tensile residual stresses has an influence on the flange efficiency ratio. Therefore, variations with d may be induced by the limitations of the model.

The compressive residual stresses also contribute in reducing the efficiency of the steel flanges by promoting inelastic local buckling of the flanges. It is believed that such effect was adequately captured by the model, considering the good match between the experimental and analytical compression residual stresses. Nevertheless, in order to eliminate the dependency of the model to tensile residual stresses, cases 1 and 2 are

compared in Table 6 for columns with the same residual stress patterns (Fig. 6: C-2 vs. C-4 and C-8 vs. C-10) to assess the influence of these stresses on the behaviour of the columns. It can be seen that neglecting residual stresses in these specimens leads to a similar increase of the stress ratio for a same pattern: 1% for C-2 vs. 3% for C-4, and 7% for both C-8 and C-10. The increase in stress ratio is larger, however, for the 600 mm columns because relatively higher tensile residual stresses were included in the models for these columns. Overall, the influence of both the compressive and tensile residual stresses resulted in a decrease of the flange capacity of 1% (C-2) to 8% (C-11), with an average of 5%.

Comparing cases 1 to 3 in Table 6 shows that the flange capacity was also reduced by the presence of local initial imperfections. This reduction is more important for specimens with s=d than for specimens with s=d/2: 6% for C-42 vs. 2% for C-2, and 4% for C-8 vs. 1% for C-10. This can be explained by the fact that the measured flange imperfections were typically greater in specimens with s=d. In addition, the slenderness of the flanges in specimens with s=d/2 was lower, as indicated by a stress ratio closer to unity in Table 6, in which case local imperfections have limited effects. For specimen C-11, with a b/t ratio of 31, the local imperfection had negligible effects because the flange buckled nearly elastically. Overall, for the 6 specimens described in Table 6, local imperfections decrease the capacity of the flanges by as much as 6% with an average reduction of 3%.

Having initial flange imperfections three times larger than those measured on the test columns (Case 4) reduces further the flange capacity. Again, the reduction is greater for specimens with s=d than for specimens with s=d/2, as shown when comparing Cases 3 and 4 (5% for C-2 vs. 12% for C-4, 9% for C-8 vs. 2% for C-10). The average imperfections for the 4 specimens with s=d in Table 6 is s/500, which approximately corresponds to three times the limit of s/200 specified in CSA (2001). For these specimens, the flange capacity and the overall column strength decrease by up to 6% and 2%, respectively, when amplifying three times the imperfections. This result will be considered later when establishing the design equation. Table 6 also shows the effects of specifying inward flange imperfections, as measured experimentally (Case 5). No significant change in flange capacity was obtained for specimens with s=d/2 but important benefits were observed for the s=d specimens with σ_f/F_y increasing from 9% to 15%. In view of the limitation of the model in reproducing the very large concrete expansion near peak load, and its detrimental effects on flange stability, it is recommended that such increase be neglected until further studies with more realistic models are performed.

5.3.2 Stress efficiency ratio for the web under short-term loading

In Table 5, the stress efficiency ratio for the web (σ_w/F_y) for all 450 mm and 600 mm specimens ranges from 0.94 to 0.96, indicating negligible influence of the column size and link spacing on the web capacity. This was expected as the web is prevented

from buckling in the column. The web stress ratio is lower for 300 mm specimens C-7 and P-1 (0.87 and 0.88 for C-7 and P-1, respectively) but this can be attributed to the difficulty of modelling accurately the tensile residual stresses, as explained earlier. The effects of residual stresses on the web capacity can be assessed by comparing cases 1 and 2 in Table 6. Because web buckling is not possible, only the tensile residual stresses impact on the web efficiency and the results show that they result in a reduction varying from 0 to 3% for the 450 and 600 mm columns and reaching 7% for the 300 mm P-1 column.

In Case 2, it can be also noted that the efficiency ratio without residual stresses is still lower than 1.0. The missing capacity ranges from 3% for specimen C-10 to 5% in column P-1 and is due to the detrimental effects of transverse tensile stresses that develop in the web, as discussed in section 5.4. Table 6 also shows that, as expected, flange local imperfections had no effect on the stress ratio of the web.

5.3.3 Stress efficiency ratio for the concrete core under short-term loading

For the concrete, Table 5 shows that the stress efficiency ratio for the concrete (σ_c/f'_{ce}) was close to one, indicating no significant gain in axial capacity due to possible confinement (maximum stress ratio of 1.03 for specimen C-5). Very localised confinement effects were observed only in the vicinity of the welds and at the transverse links, near the flange. As shown in Fig.9, the axial stresses at peak load in the models ranged locally from 0.9 f'_{ce}, in regions where transverse tensile stresses were present, to

1.3 f'_{ce} in zones of maximum confinement. These findings suggest that concrete confinement should be ignored in the design of these columns.

5.4. Influence of concrete transverse expansion under short-term loading

The transverse expansion of the concrete upon axial loading induces tensile axial stresses in the transverse links and transverse tensile stresses in the web of the steel shape.

5.4.1 Tensile axial stresses in the transverse links

Figure 10 compares the variation of the experimental and numerical transverse link axial stresses up to peak load as a function of the average longitudinal strain of the column. The experimental results are from Chicoine et al. (2000a; 2000c). Tension stresses are shown as positive. Very good agreement is generally obtained between the numerical and experimental results, indicating that the axial link stresses are only dependent on the transverse expansion of the concrete. The experimental link stresses near peak load are higher in some specimens (e.g., column C-10 in the figure), indicating that the actual Poisson's ratio of the concrete in the columns was probably greater than 0.45 when, when the concrete expanded significantly upon crushing.

5.4.2 Transverse stresses in the web

Figure 11 compares the variation of the experimental and FE model transverse stresses in the web with the average longitudinal column strain. The stresses are

examined at the intersection of the two axes of symmetry of the cross-section and at two different heights: at the links and halfway between two consecutive links. The model results are from the analyses with a concrete strength of f'_{ce} and transverse stresses are positive in tension. The numerical and experimental transverse stresses in the web are plotted up to the peak load but the experimental transverse stresses were considered to remain constant after the von Mises yield criteria was met in the web.

A similar behaviour was observed in all FE models for the web transverse stresses, reflecting the effects of the variable concrete Poisson's ratio. Transverse expansion of concrete is smaller than that of steel until approximately 70% of the concrete strength, after which point the Poisson's ratio of concrete becomes larger than that of steel. Near peak load, concrete expansion induces tensile transverse stresses in the web of the steel shape, reducing the web longitudinal yield capacity. The effect of the transverse stresses in the web was estimated as varying between 3 and 5% from Table 6, by taking the difference between 1.0 and the web stress efficiency ratio for Case 2. The experimental transverse stresses in the web near peak load are higher in some specimens, likely because the actual Poisson's ratio of the concrete in the columns was greater than 0.45 near peak load, which could not be reproduced by the numerical model. Furthermore, it is possible that the contact between the strain gauges on the web and the concrete in the test specimens be damaged near peak load, resulting in less accurate experimental data.

5.5. *Effects of construction sequence and long-term loading*

Figure 11 shows that the transverse stresses in the web at peak load were approximately equal to 20 MPa under both long-term loading (specimen P-4) and short-term loading ones (specimen C-8). In Table 5, however, the efficiency ratio of the web increases for long-term loading compared to short-term loading (0.94 for P-4 vs. 0.88 for P-1). The additional compression axial stresses at peak load in the steel shape due to the sequence of loading and the long-term effects contributed in diminishing the detrimental effects of the tensile residual stresses on the efficiency ratio of the web. This beneficial effect had, however, a small impact on the overall column capacity, as the load ratio $P_{u,fem}/P_0$ was nearly the same ($\cong 0.95$) for all Series 3 specimens.

The global capacity of a column exposed to extreme creep and shrinkage conditions was also investigated with the numerical model. Under such conditions, a long-term increase in the steel stress of 69 MPa was first determined using available creep and shrinkage models. This exceeds the value of 45 MPa imposed on Specimens P-3 and P-4 in the experiments (Table 3). When specifying this higher value, the FE model gave an axial capacity reduction of only 1% of $P_{u,fem}$ compared to P-3, suggesting that the sequence of loading and long-term effects have no significant influence on the capacity of PEC columns and can be neglected in design. A similar behaviour is expected for specimens with different d, s/d, and b/t.

5.6. Discussion on predicting column behaviour with d greater than 600 mm

An important aspect of finite element modelling is the ability to expand the use of the model out of the range of the parameters covered in the reference experimental programs. For example, it is likely that composite columns in actual buildings be larger than the maximum size tested. It is believed that the models developed in this study will predict adequately the behaviour of larger columns because:

- The size effects on the concrete strength can be modelled adequately by using the effective concrete strength f'_{ce};
- The measured local flange imperfections were comparable in the 300 mm, 450 mm, and 600 mm specimens, suggesting that similar imperfections will be found in larger columns;
- The overall effect of the residual stresses on the column capacity are expected to generally decrease as the influence of the fabrication process (welding and cutting) on the residual stresses diminishes when the size of the column plates is increased.

6. Prediction model for the axial capacity

The axial capacity of composite columns may be obtained by summing up the contribution of each component, i.e. the steel shape, the concrete, and the reinforcing steel, if any. Tremblay et al. (2000) proposed such an equation for PEC columns. This equation was based only on experimental data and has been modified to reflect the additional information generated by this FE study to obtain the following expression:

$$P_{u.pred} = A_{se} F_y + A_c f'_{ce} + A_r F_{yr} \quad (5)$$

$$A_{se} = (d - 2t + 4\, b_e)\, t \quad (6)$$

$$\frac{b_e}{b} = (1 + \lambda_{fl}^{2n})^{(-1/n)} \quad (7)$$

$$\lambda_{fl} = \frac{b}{t}\sqrt{\frac{12(1-\nu^2)F_y}{\pi^2 E k_{fl}}} \quad (8)$$

$$k_{fl} = \frac{3.6}{(s/b)^2} + 0.05(s/b)^2 + 0.75, \quad 1 \le s/b \le 2 \quad (9)$$

In Eq.(5) the contribution of the steel shape is based on the effective steel area for local buckling, A_{se} and the contribution of the concrete is determined using the effective strength as defined in Eq.(1). In this equation, A_c and A_r are the cross section area of the concrete and the longitudinal rebars, respectively, and F_{yr} is the yield stress of the steel rebar.

The effective area of steel, A_{se}, is given by Eq.(6). In this equation, the web is assumed to be fully effective although the FE analyses showed that the residual stresses and transverse stresses could reduce its capacity by 5% in average (Table 6). For simplification, this reduction in the web capacity has been assigned to the flanges by including it in the calculation of the effective width of the flange, b_e. This simplification

is deemed acceptable because the flange has twice the area of the web, which results in a small variation on b_e. From the test results, values for b_e were computed with Eqs. (5) and (6), taking $P_{u,pred}$ equal to $P_{u,exp}$, and are presented in Fig. 12 as a function of the plate slenderness λ_{fl}, as given in Eq.(8). As shown, the experimental values of b_e are in close agreement with stress efficiency ratio of the flanges (b_e/b taken as σ_{fl}/F_y in Table 5) and with several empirical plate buckling models proposed in past research (Winter, 1968; Faulkner, 1977; Usami and Fukumoto, 1982; Fukumoto et al., 1984; Ge and Usami, 1992; and Uy, 2000). Obtaining such reasonable values of b_e assuming a fully effective web supports the use of this simplified approach in the design of PEC columns. The figure also shows that assuming a concrete strength of $\Psi f'_c$ gives unrealistic estimates of the buckling strength of the steel plates when compared to the other models and, hence, confirms again the relevance of using an effective concrete strength of $0.92\Psi f'_c$. In this figure, the model by Tremblay et al. (2000) is also presented and is shown to be too conservative.

Equation (9) for the plate stiffness coefficient, k_{fl}, was derived empirically from elastic buckling analysis of FE models of steel column flanges, with fixed boundary conditions on three sides and free on one unloaded edge. These values for k_{fl} were close to the theoretical values (Salmon and Johnson, 1996) and typically smaller than those proposed by Tremblay et al. (2000).

Equation (7) is proposed to determine b_e/b for design. This equation is adapted from the column design curve expression proposed by Loov (1996) and implemented in the CSA-S16.1 Standard for the design of steel structures in Canada (1994b). As shown in Table 7, using n equal 2.0 in Eq.(7) gives an average test-to-predicted ratio of 1.00, with a standard deviation of 0.03, for the ultimate axial capacity of all columns. Figure 13 shows that the prediction model with n=2.0 is in close agreement with the experimental and numerical values, throughout the range of plate slenderness, including the capacity reduction for relatively stockier plates.

In order to account for the possibility that flange imperfections in actual columns be closer to the fabrication tolerances specified in CSA (2001) rather than being similar to those measured in the reference test columns, a value of n=1.5 is recommended for the calculation of b_e in design. As shown in Table 7, the mean test-to-predicted load ratio is increased to 1.03, with a standard deviation of 0.03, when using n=1.5, which gives a sufficient margin to account for this more critical imperfection condition.

7. Conclusions

The conclusions regarding the parameters that were reproduced by the FE models are presented herein:

- Capacity of the specimens under short-term loading. The mean numerical to experimental peak load ratio for Series 1, 2, and 3 composite specimens is equal to

1.00 when an effective concrete strength $f'_{ce}= 0.92\Psi f'_c$ is specified in the numerical model, a value that also permits to reproduce closely the experimental local buckling capacity of the flanges. At peak load, the average stresses carried by the flange, the web, and the concrete were $0.88F_y$, $0.93\ F_y$, and $1.01\ f'_{ce}$, respectively. Buckling, together with compression residual stresses and initial imperfections, and high tensile residual stresses near the welds contributed in reducing the capacity of the flanges. The decrease in capacity due to residual stresses varied between 1 and 8% and the average reduction due to local imperfection was found to be 3%. In the web, the reduction in capacity is attributed to the combined effects of the tensile residual stresses near the welds (0 to 3% for the large columns) and of the tensile transverse stresses that develop due to the rapid expansion of the concrete near peak load (3-5%). The small increase in concrete strength ($1.01\ f'_{ce}$) is due to localised confinement effects that can be neglected in design.

- Strain at peak load. The FE models represented very well the load-strain behavior of the test specimens, throughout the loading history. The FE models gave values of the strain at peak load 5% higher, in average, than those measured in the experiments. This apparent discrepancy is due to the fact that the experimental strain was measured over the full height of the column, including zones with higher strength concrete, while the model strain was taken over the height of one link spacing only. The post-peak response of the columns could be obtained only over a short deformation range due to convergence problems in the numerical model.

- Failure modes. The failure modes in the FE analyses were identical to the experimental ones and good agreement in the ultimate load was obtained when local flange imperfections were modelled outwards instead of inwards, as measured on the reference test columns. Different buckling modes and higher capacity were obtained when setting the imperfections inwards. This is attributed to the incapacity of the FE model adopted to reproduce the rapid volumetric expansion of concrete near peak load.
- Axial stresses in the transverse links. The stresses in the transverse links were very well represented by the numerical models and were found to be dependent on the transverse expansion of the concrete. At peak load, however, the numerical models generally underestimated the experimental link stresses, again because the expansion of the concrete was underestimated.
- Transverse stresses in the web of the steel shape. The FE model transverse stresses in the web were compressive at the beginning of the analysis, and tensile at peak load, because of the variation of the concrete Poisson's ratio, which confirmed the findings of the experimental programs.
- Loading sequence and long-term effects. The FE program was capable of modelling satisfactorily the construction sequence, using the removal and addition of elements in the model. The effects of creep and shrinkage of the concrete on the steel shape were modelled by increasing the stresses in the model that included the steel shape only, prior to composite action. These effects were found not to influence the axial capacity of the columns, as also observed in the tests.

Based on the findings of this study, a new expression was proposed to predict the axial capacity of PEC columns for design purposes. It is recommended that further study be pursued to better capture the effects of the rapid expansion of the concrete near peak load on the flange buckling capacity and the amplitude of transverse stresses in the web.

ACKNOWLEDGMENTS

Funding for this research was provided by the Natural Science and Engineering Research Council of Canada (NSERC), the Steel Structures Education Foundation, and the Canam Manac Group.

REFERENCES

Bloem, D. (1968) "Concrete strength in structures." *ACI Journal*, 65-14, 176-187.

Bouzaiene, A., Massicotte, B. (1997) "Programme MEF97 Manuel d'utilisation." *EPM/CS No. 1997-2*, Dept. of Civil, Geological and Mining Engineering, Ecole Polytechnique, Montreal, Canada. Draft version.

Broderick, B.M., Elnashai, A.S. (1994) " Seismic resistance of composite beam-columns in Multi-Storey structures. Part 2: analytical model and discussion of results." *J. Construct. Steel Research*, **30**, p. 231-258.

Chicoine, T., Tremblay, R., Massicotte, B. (2000a) " Long-term behaviour and strength of partially encased composite columns made with built-up steel shapes." *ASCE Journal of Structural Engineering*. Submitted for publication.

Chicoine, T., Tremblay, R., Massicotte, B. (2000b) "Long-term test programme on partially encased built-up three-plate composite columns." *EPM/GCS No. 2000-20*, Dept. of Civil, Geological and Mining Engineering, Ecole Polytechnique, Montreal, Canada.

Chicoine, T., Tremblay, R., Massicotte, B., Yalcin, M., Ricles, J., Lu, L.-W. (2000c) "Behavior and strength of partially encased columns with built-up shape." *ASCE Journal of Structural Engineering*. Submitted for publication.

Chicoine, T., Tremblay, R., Massicotte, B., Yalcin, M., Ricles, J., Lu, L.-W. (2000d) "Test programme on large-scale partially-encased built-up three-plate composite columns." *Joint Report, EPM/GCS No. 2000-06*, Dept. of Civil, Geological and Mining Engineering, Ecole Polytechnique, Montreal, Canada – ATLSS Engineering Research Center, *No. 00-04*, Lehigh University, Bethlehem, Pennsylvania, USA.

Chicoine, T., Massicotte, B., Tremblay, R. (2001) " Finite element modelling of the experimental response of partially encased composite columns." *EPM/GCS No. 2001-06*, Dept. of Civil, Geological and Mining Engineering, Ecole Polytechnique, Montreal, Canada.

CSA (1994) *CAN/CSA-A23.3-94 Code for the design of concrete structures for buildings.* Canadian Standards Association, Rexdale, Ontario.

CSA (1994b) *CAN/CSA-S16.1-94 Limit States Design of Steel Structures.* Canadian Standards Association, Rexdale, Ontario.

CSA (2001) *CAN/CSA-S16.1-01 Limit States Design of Steel Structures.* Canadian Standards Association, Rexdale, Ontario. (Publication pending)

Faulkner, D. (1977) "Compression tests on welded eccentrically stiffened plate panels." *Steel Plated Structures,* P.J. Dowling Ed, London, p. 581-617.

Fukumoto, Y., Itoh, Y. (1984) "Basic compressive strength of steel plates from test data" *Proc. JSCE,* No 344, April, p. 129-139.

Ge, H., Usami, T. (1992) "Strength of concrete filled thin walled steel box columns: Experiment." *Journal of Structural Engineering,* ASCE, **118**(11), 3036-3054.

HKS (2000) *Abaqus program version 5.8-19.*

Loov, R. (1996) "A simple equation for axially loaded steel column design curve." *Can. J. Civ. Eng.*, 23, p.272-276.

Maranda, R. (1999) "Analyses par éléments finis de poteaux mixtes avec sections d'acier en I de classe 4" *Report n°. EPM/GCS-1998-11*, Dept. of Civil, Geological and Mining Engineering, Ecole Polytechnique, Montreal, Canada, 139 p.

Neville, A.M. (1966) "A general relation for the strengths of concrete specimens of different shapes and sizes." *ACI Journal*, 63, 1095-1108.

Newman, K. (1987) "Labcrete, Realcrete, and Hypocrete. Where we can expect the next durability problems." *ACI SP-100 Concrete Durability, vol.2.*

Salmon, C.G., Johnson, J.E. (1996) *Steel Structures: Design and Behavior*, HarperCollins, 4th Edition, New York, NY.

Sigiura, K., Ono, K., Oyawa, W.O., Watanabe, E., Yamaguchi, T. (2000) "Interface interaction in filled steel tubular members as modeled by open sandwich beams." *Proc. Composite Construction IV*, Engineering Foundation, Banff, Canada.

Tremblay, R., Massicotte, B., Filion, I., Maranda, R. (1998) "Experimental study on the behavior of partially encased composite columns made with light welded H steel shapes under compressive axial loads." *1998 SSRC Annual Technical Meeting.*

Tremblay, R., Chicoine, T., Massicotte, B. (2000) "Design equation for the axial capacity of partially encased non-compact columns." *Proc. Composite Construction IV*, Engineering Foundation, Banff, Canada.

Tsai, W.T. (1988) "Uniaxial compression stress-strain relation of concrete." *ASCE J. Structural Engineering*, **114**(9), p.2133-2136.

Usami, T., Fukumoto,Y. (1982) "Local and overall buckling of welded box columns." *Journal of Structural Division*, ASCE, **108**(3), 525-542.

Uy, B. (2000) "Strength of concrete filled steel box columns incorporating local buckling." *Journal of Structural Engineering*, ASCE, **126**(3), 341-352.

Vincent, R. (2000) "Design and application of partially encased non-compact composite columns for high-rise buildings." *Proc. Composite Construction IV*, Engineering Foundation, Banff, Canada.

Wheeler, A.T., Bridge, R.Q. (2000) "Thin walled steel tubes filled with high strength concrete in bending." *Proc. Composite Construction IV*, Engineering Foundation, Banff, Canada.

Winter, G. (1968) "Thin-walled structures – Theoretical solutions and test results." *Proc. IABSE Congress*, p.101-112.

Table 1 Properties of test specimens

Test Series Series	No.	b_f x d x t (mm)	L (mm)	b/t 0	s (mm)	Link ϕ (mm)	f'_c (MPa	E_c (MPa)	ε'_c ($\mu\varepsilon$)	F_y (MPa)
	C-2	450 x 450 x 9.70	2 250	23.2	225	12.7	32.7	28 000	2 250	370
1	C-3	450 x 450 x 9.70	2 250	23.2	338	12.7	32.4	28 000	2 250	370
(Small	C-4	450 x 450 x 9.70	2 250	23.2	450	12.7	31.9	28 000	2 250	370
Specimens)	C-5	450 x 450 x 9.70	2 250	23.2	225	22.2	34.3	28 000	2 250	370
	C-6	450 x 450 x 6.35	2 250	35.4	338	12.7	32.7	28 000	2 250	374
	C-7	300 x 300 x 6.35	1 500	23.6	300	12.7	31.9	31 500	2 250	374
	C-8	600 x 600 x 12.90	3 000	23.3	600	16.0	34.2	27 300	2 000	360
2	C-9	600 x 600 x 12.90	3 000	23.2	600	16.0	34.2	27 300	2 000	360
(Large	C-10	600 x 600 x 12.80	3 000	23.4	300	16.0	34.2	27 300	2 000	360
Specimens)	C-11	600 x 600 x 9.70	3 000	30.9	600	16.0	34.2	27 300	2 000	345
	C-12*	600 x 600 x 12.90	3 000	23.3	300	16.0	34.2	27 300	2 000	360
	P-1	300 x 300 x 6.50	1 500	23.6	300	12.7	36.9	29 950	2 470	390
3	P-2	300 x 300 x 6.50	1 500	23.6	300	12.7	36.9	29 950	2 470	390
(Long-Term	P-3	300 x 300 x 6.50	1 500	23.6	300	12.7	36.9	29 950	2 470	390
Specimens)	P-4	300 x 300 x 6.50	1 500	23.6	300	12.7	36.9	29 950	2 470	390
	P-5	450 x 450 x 9.60	2 350	23.2	450	12.7	30.0	29 950	2 470	345

Note: * With additional reinforcement: 4-20M longitudinal rebars, and pairs of U-stirrups 15M@300 mm.

Table 2 Properties of numerical model

Test Series	No.	b'_f x d' x t'_f	t'_w	L' = s	δ_{0m}		f'_{ce}	E_{ce}
					Mean	S.D.		
		(mm)	(mm)	(mm)	(mm)	(mm)	(MPa)	(MPa)
1	C-2	225 x 220.15 x	4.85	225	0.39	0.13	27.1	25 460
(Small	C-4	225 x 220.15 x 9.7	4.85	450	1.42	0.23	26.4	25 460
Specimens)	C-5	225 x 220.15 x 9.7	4.85	225	0.39	0.13	28.4	26 190
	C-7	150 x 146.8 x 6.4	3.20	300	0.63	0.20	27.6	29 310
	C-8	300 x 293.6 x 12.9	6.45	600	1.43	1.38	27.6	24 540
2	C-9	300 x 293.6 x 12.9	6.45	600	2.02	0.36	27.6	24 540
(Large	C-10	300 x 293.6 x 12.8	6.40	300	0.38	0.15	27.6	24 540
Specimens)	C-11	300 x 293.6 x 9.7	4.85	600	0.71	0.46	27.6	24 540
	C-12*	300 x 293.6 x 12.9	6.45	300	0.37	0.15	27.6	24 540
	P-1	150 x 146.8 x 6.5	3.25	300	0.74	0.35	31.8	27 870
3	P-2	150 x 146.8 x 6.5	3.25	300	0.58	0.27	31.8	27 870
(Long-Term	P-3	150 x 146.8 x 6.5	3.25	300	0.35	0.19	31.8	27 870
Specimens)	P-4	150 x 146.8 x 6.5	3.25	300	0.44	0.16	31.8	27 870
	P-5	225 x 220.2 x 9.6	4.80	450	0.52	0.13	24.8	22 400

Note: Steel yield stress, F_y, and concrete peak strain, ε'_c, as in specimens

Table 3 Stresses in materials according to loading sequence

Spec.	Experimental stresses			FE stresses		
	Stage 1	Stage 2		Stage 1	Stage 2	
	Steel (MPa)	Steel (MPa)	Concrete (MPa)	Steel (MPa)	Steel (MPa)	Concrete (MPa)
P-1	-	-	-	-	-	-
P-2	100	111	-	110	110	-
P-3	101	215	6.8	167	213	6.8
P-4	101	219	6.5	173	218	6.5
P-5	103	223	6.5	164	222	6.5

Table 4 **Results at peak load of plastic analyses of composite models with a concrete strength of f'_{ce}**

Test Series	Spec.	P_0 (kN)	$P_{u,fem}$ (kN)	$P_{u,exp}$ (kN)	$P_{u,exp} / P_{u,fem}$ (-)	$\varepsilon_{u,fem}$ (με)	$\varepsilon_{u,exp}$ (με)	$\varepsilon_{u,exp} / \varepsilon_{u,fem}$ (-)
1	C-2	9 938	9 889	10 100	1.02	2 500	2 306	0.92
	C-4	9 813	9 450	9 390	0.99	2 235	1 695	0.76
	C-5	10 189	10 189	10 000	0.98	2 380	2 330	0.98
	C-7	4 447	4 225	4 280	1.01	2 141	2 142	1.00
2	C-8	17 623	16 742	16 470	0.98	2 050	1 845	0.90
	C-9	17 623	16 671	16 610	1.00	2 150	1 769	0.82
	C-10	17 557	16 995	16 240	0.96	2 285	2 256	0.99
	C-11	15 308	14 206	14 930	1.05	2 090	1 810	0.87
	C-12	18 009	17 540	17 450	0.99	2 310	2 580	1.12
3	P-1	4 948	4 725	4 770	1.01	2 353	2 335	0.99
	P-2	4 948	4 716	4 670	0.99	2 717	2 730	1.01
	P-3	4 948	4 712	4 790	1.02	2 878	2 550	0.93
	P-4	4 948	4 708	4 975	1.06	3 020	2 910	1.01
	P-5	9 131	8 680	9 225	1.06	2 750	2 820	1.03
Mean*					1.00			0.95
SD*					0.03			0.09

Note: *Column P-5 not included

Table 5 Normalized load and stresses at peak load for flange, web, and concrete

No.	$P_{u,fem}/P_0$ (-)	σ_f/F_y (-)	σ_w/F_y (-)	σ_c/f'_{ce} (-)
C-2	1.00	0.97	0.96	1.02
C-4	0.96	0.88	0.95	1.02
C-5	1.00	0.97	0.96	1.03
C-7	0.95	0.87	0.87	1.02
C-8	0.95	0.86	0.94	1.01
C-9	0.95	0.85	0.95	1.00
C-10	0.97	0.92	0.94	1.01
C-11	0.93	0.75	0.94	1.00
C-12	0.97	0.92	0.94	1.01
P-1	0.96	0.88	0.88	1.02
P-2	0.95	0.87	0.91	1.01
P-3	0.95	0.87	0.93	1.00
P-4	0.95	0.85	0.94	1.01
P-5	0.95	0.86	0.97	1.00
Mean*	0.96	0.88	0.93	1.01
SD*	0.02	0.05	0.03	0.01

Note: * Analysis P-5 not included

Table 6 Sensitivity of stress efficiency ratios to residual stresses and local imperfections

Specimen	Parameter	Case 1	Case 2	Case 3	Case 4	Case 5
	$\delta_0 =$	δ_{0m}	δ_{0m}	0	$3\delta_{0m}$	$-\delta_{0m}$
	$\sigma_r =$	$\sigma_{r\,m}$	0	$\sigma_{r\,m}$	$\sigma_{r\,m}$	$\sigma_{r\,m}$
C-2	$P_{u,fem}/P_0$	1.00	1.00	1.00	0.99	1.00
d=450	σ_{fl}/F_y	0.97	0.98	0.99	0.94	0.99
s=d/2	σ_w/F_y	0.96	0.96	0.96	0.96	0.97
b/t=23	σ_c/f'_{ce}	1.02	1.02	1.02	1.02	1.02
C-4	$P_{u,fem}/P_0$	0.96	0.97	0.98	0.94	1.00
d=450	σ_{fl}/F_y	0.88	0.91	0.94	0.82	0.99
s=d	σ_w/F_y	0.95	0.95	0.96	0.95	0.96
b/t=23	σ_c/f'_{ce}	1.02	1.02	1.02	1.02	1.02
C-8	$P_{u,fem}/P_0$	0.95	0.98	0.96	0.94	0.97
d=600	σ_{fl}/F_y	0.86	0.93	0.90	0.81	0.93
s=d	σ_w/F_y	0.94	0.96	0.93	0.94	0.95
b/t=23	σ_c/f'_{ce}	1.01	1.01	1.01	1.01	1.01
C-10	$P_{u,fem}/P_0$	0.97	1.00	0.97	0.97	0.97
d=600	σ_{fl}/F_y	0.92	0.99	0.93	0.91	0.93
s=d/2	σ_w/F_y	0.94	0.97	0.94	0.94	0.94
b/t=23	σ_c/f'_{ce}	1.01	1.02	1.01	1.01	1.01
C-11	$P_{u,fem}/P_0$	0.93	0.95	0.93	0.93	0.97
d=600	σ_{fl}/F_y	0.75	0.83	0.75	0.73	0.90
s=d	σ_w/F_y	0.94	0.96	0.94	0.94	0.95
b/t=31	σ_c/f'_{ce}	1.00	1.00	1.01	1.01	1.01
P-1	$P_{u,fem}/P_0$	0.96	0.97	0.97	0.94	0.99
d=300	σ_{fl}/F_y	0.88	0.91	0.94	0.83	0.97
s=d	σ_w/F_y	0.88	0.95	0.89	0.88	0.90
b/t=23	σ_c/f'_{ce}	1.02	1.02	1.02	1.02	1.02

Table 7 Test-to-predicted ultimate load ratios

Test Series	No.				n = 2.0		n = 1.5	
		k_n (-)	λ_g (-)	$P_{u,exp}$ (kN)	$P_{u,pred}$ (kN)	$P_{u,exp} / P_{u,pred}$ (-)	$P_{u,pred}$ (kN)	$P_{u,exp} / P_{u,pred}$ (-)
1 (Small Specimens)	C-2	4.40	0.50	10 111	9 815	1.03	9 664	1.05
	C-3	2.46	0.66	9 690	9 611	1.01	9 371	1.03
	C-4	1.85	0.77	9 389	9 321	1.01	9 050	1.04
	C-5	4.40	0.50	10 040	10 075	1.00	9 925	1.01
	C-6	2.46	1.02	7 652	7 757	0.99	7 593	1.01
	C-7	1.85	0.79	4 275	4 216	1.01	4 095	1.04
2 (Large Specimens)	C-8	1.85	0.76	16 470	16 770	0.98	16 308	1.01
	C-9	1.85	0.76	16 610	16 792	0.99	16 328	1.02
	C-10	4.40	0.50	16 240	17 337	0.94	17 082	0.95
	C-11	1.85	0.99	14 930	14 259	1.05	13 940	1.07
	C-12	4.40	0.50	17 430	17 846	0.98	17 591	0.99
3 (Long-Term Specimens)	P-1	1.85	0.79	4 770	4 697	1.02	4 568	1.04
	P-2	1.85	0.79	4 670	4 697	0.99	4 568	1.02
	P-3	1.85	0.79	4 790	4 697	1.02	4 568	1.05
	P-4	1.85	0.79	4 975	4 696	1.06	4 567	1.09
	P-5	1.85	0.75	9 225	8 711	1.06	8 465	1.09
Mean*						1.004		1.028
SD*						0.03		0.03

* Specimen P-5 not included

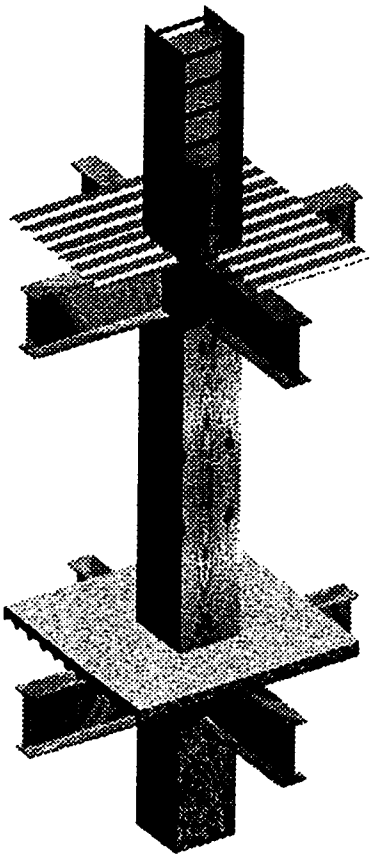

Fig. 1 Partially encased composite (PEC) column under construction

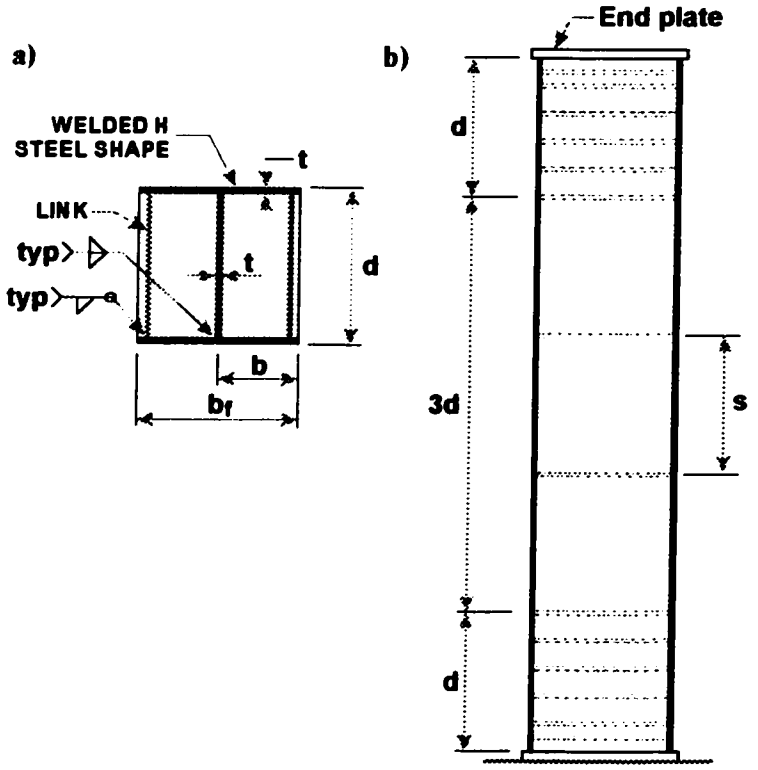

Fig. 2 Geometry of partially encased columns: (a) Cross-section; (b) Elevation of typical stub-column test specimens

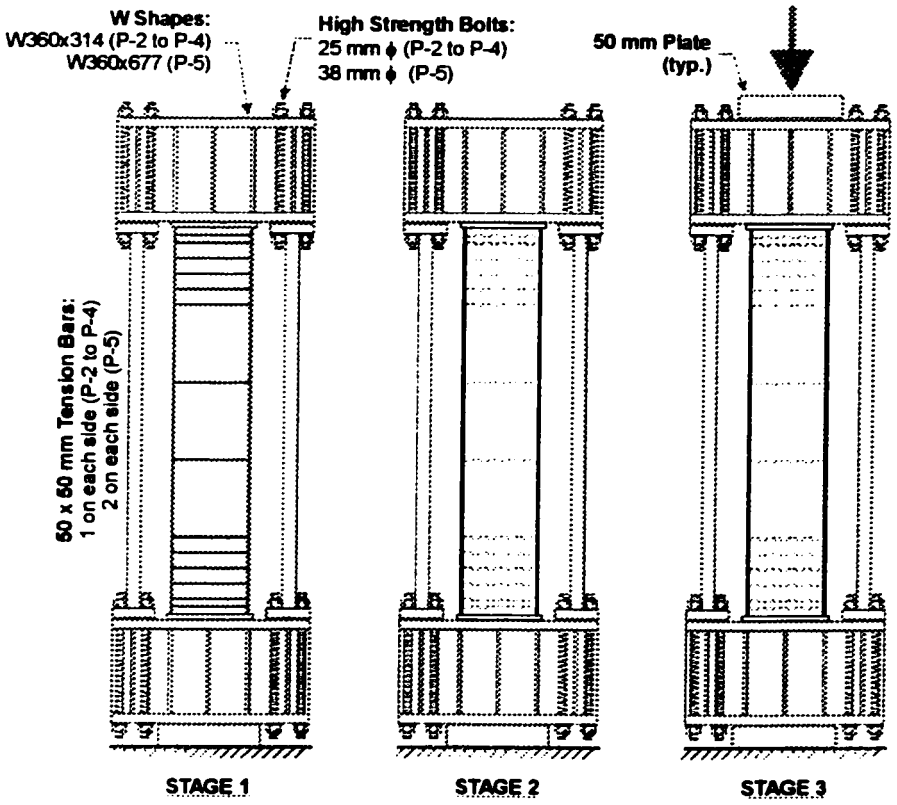

Fig. 3 Loading stages 1 to 3

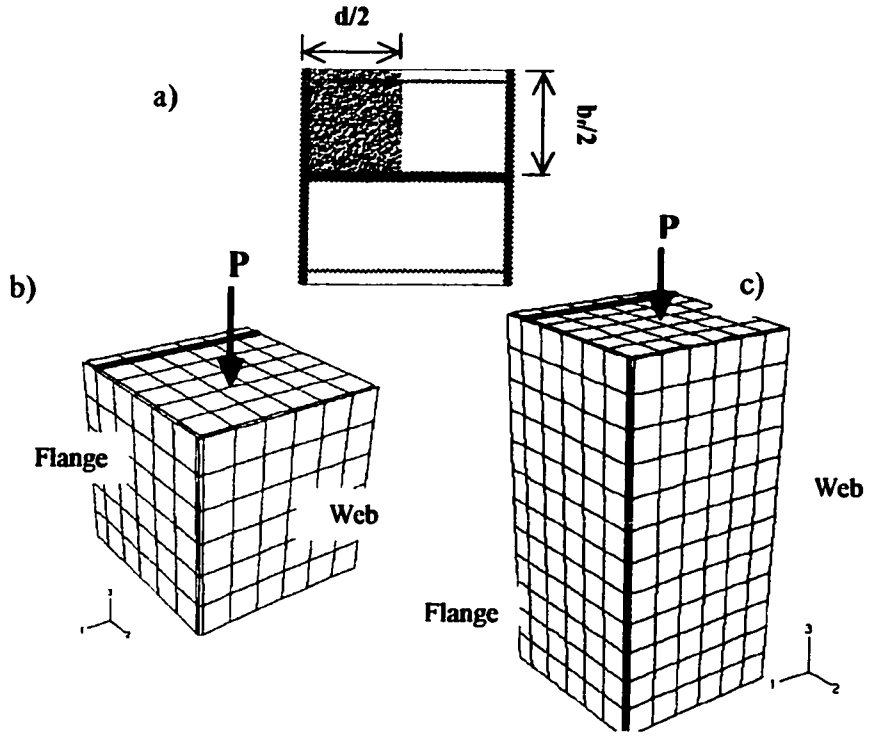

Fig. 4 Finite element models of the column: (a) Quarter cross section; (b) Specimen with s = d /2; and (c) Specimen with s = d.

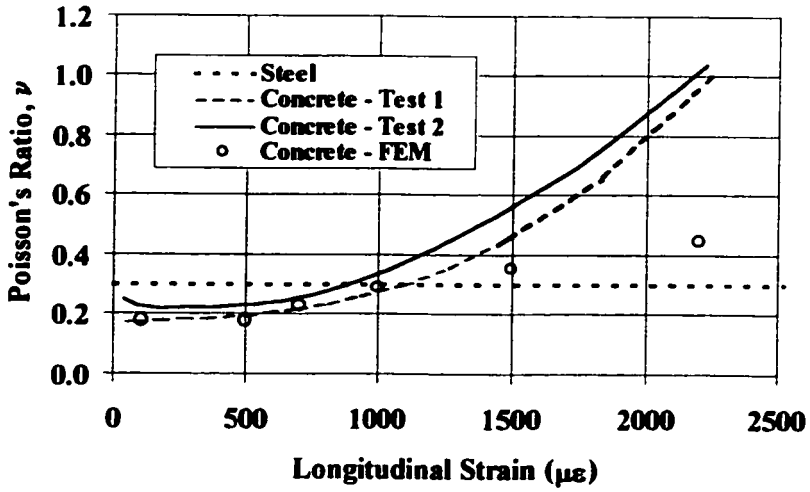

Fig. 5 Variation of the Poisson's ratio of concrete

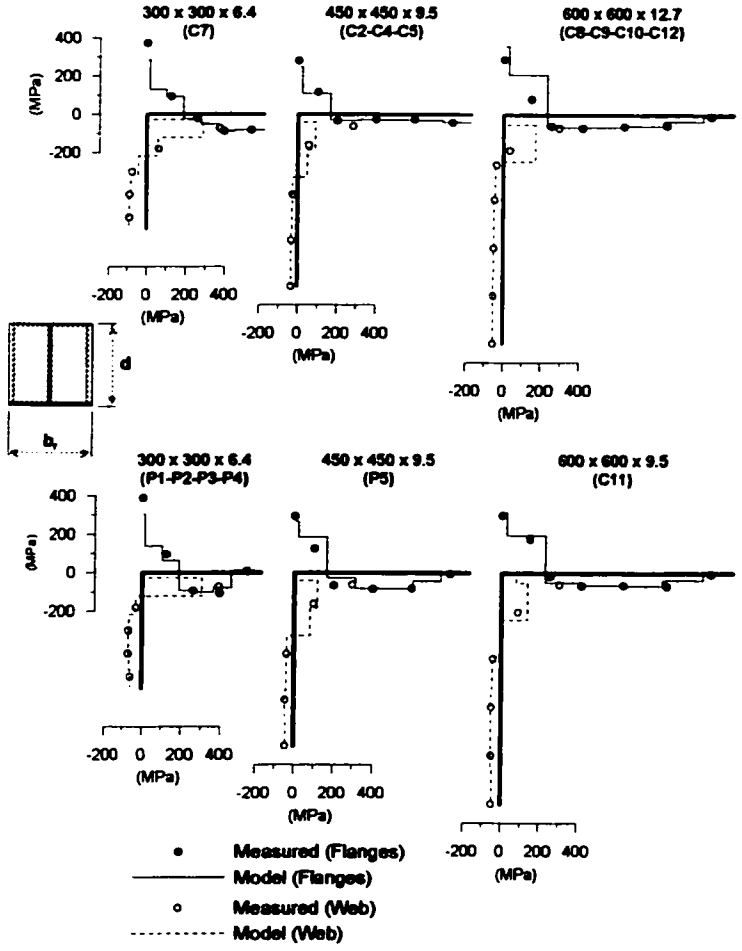

Fig. 6 Residual stresses in the steel shapes

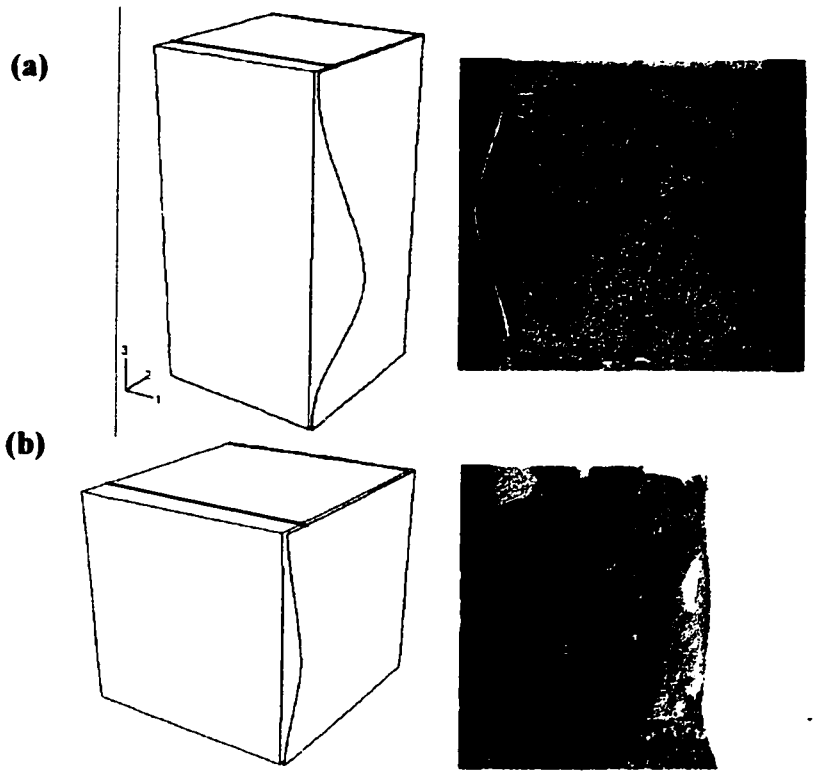

Fig. 7 Predicted and experimental failure modes for specimens with: (a) s = d; (b) s = d/2

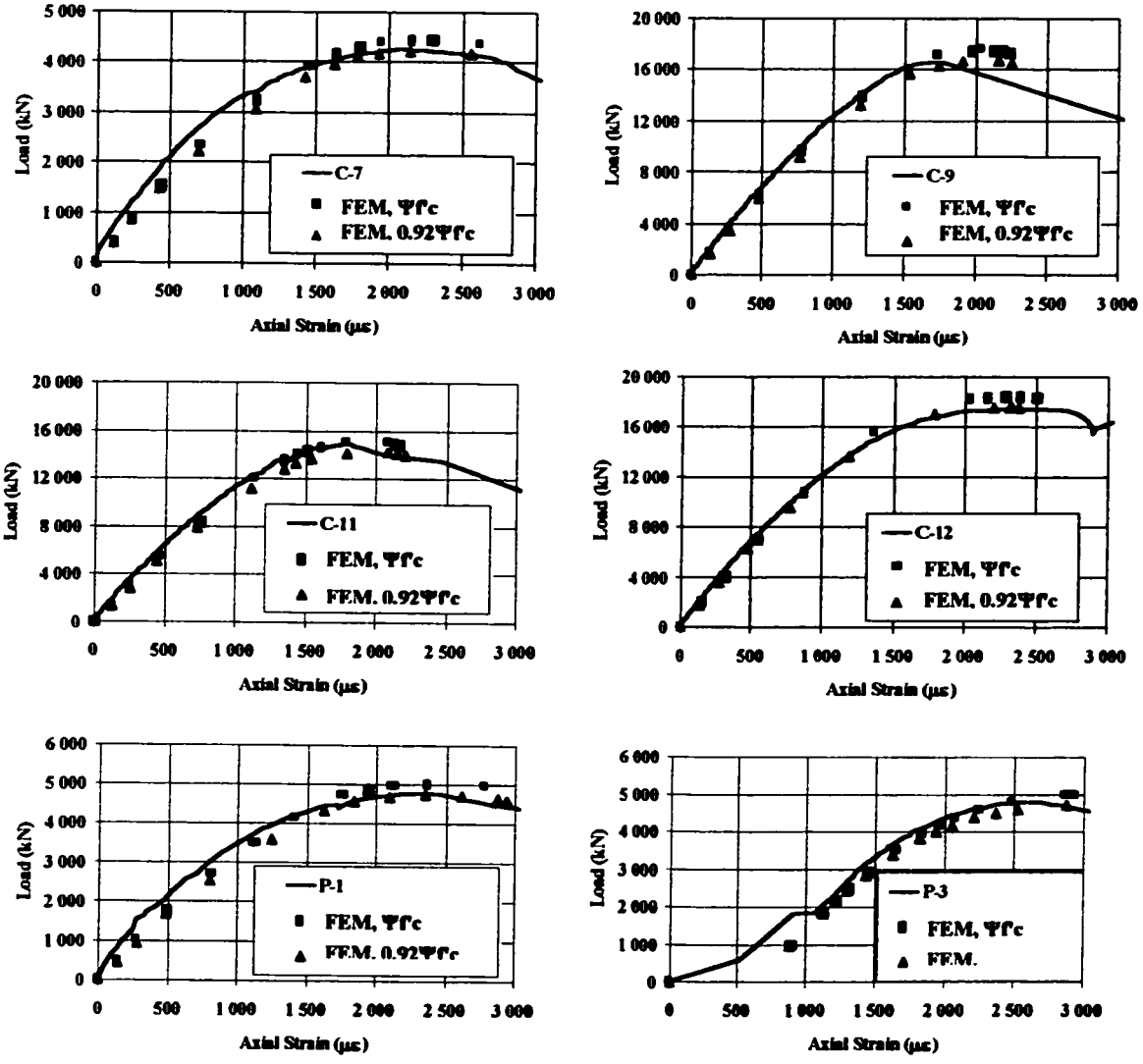

Fig. 8 Load-strain behaviour of specimens and FE models

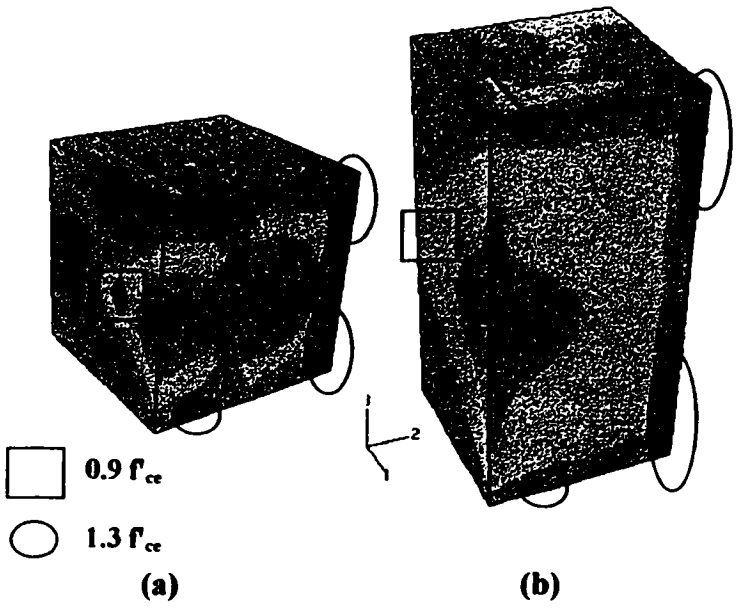

Fig. 9 Axial stresses in the concrete at peak load for specimens: (a) C-2; (b) C-4

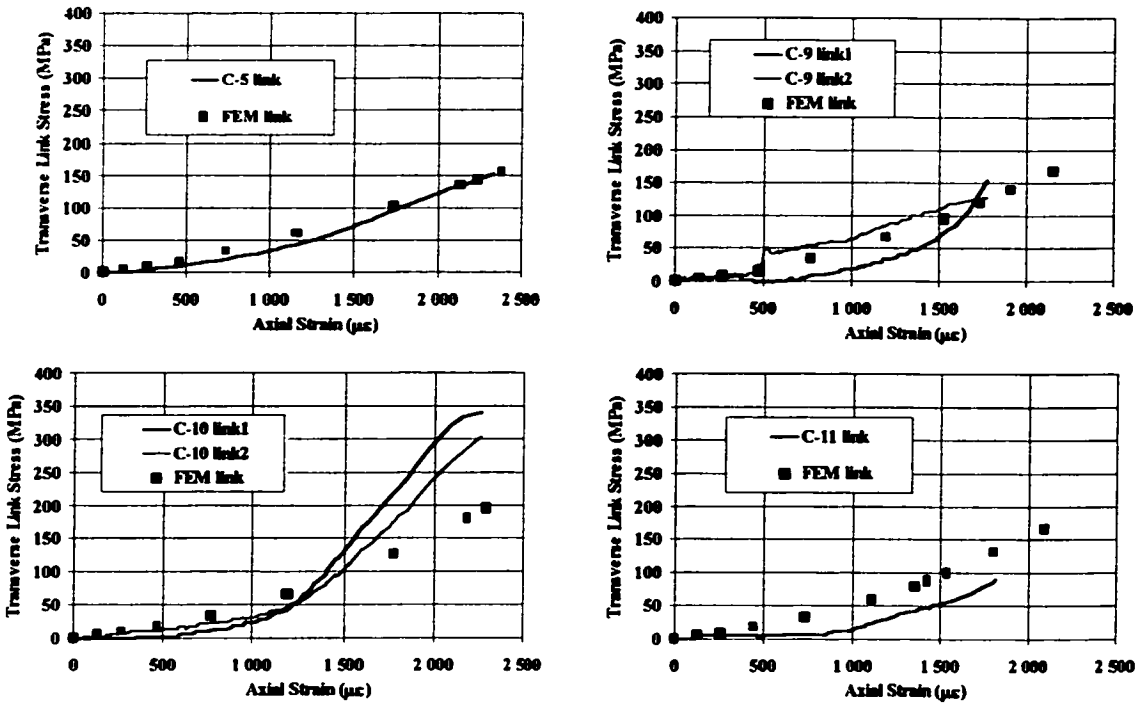

Fig. 10 Stresses in the transverse links of specimens and FE models

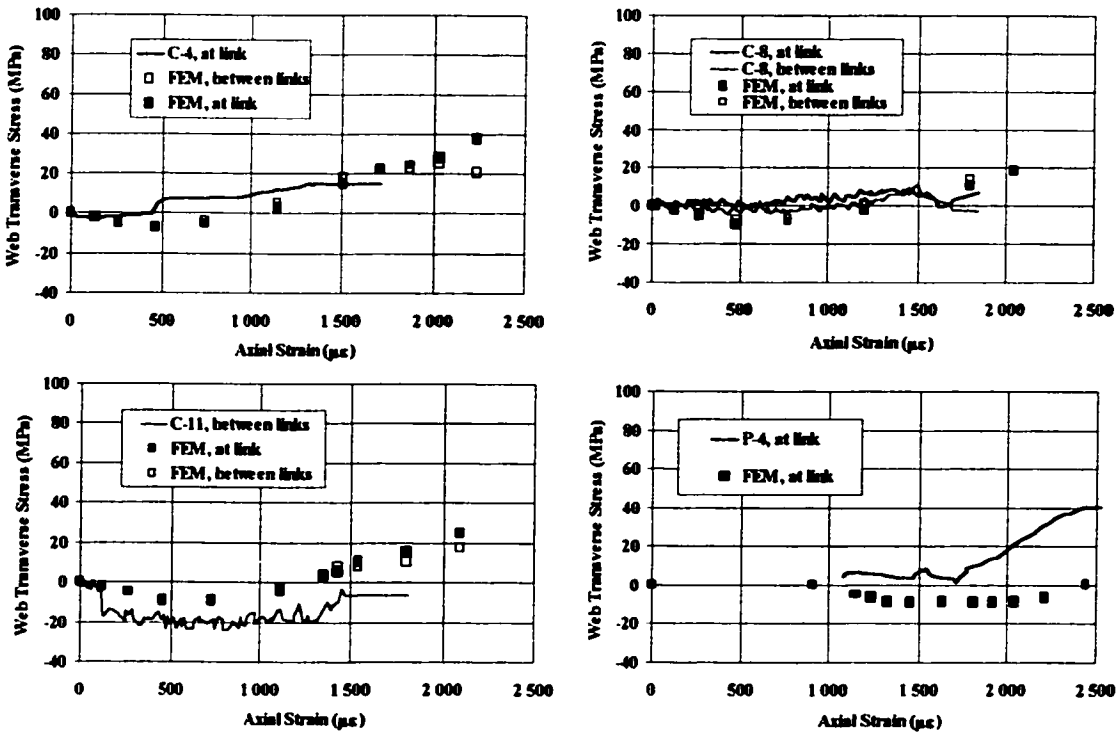

Fig. 11 Transverse stresses in the steel web of specimens and FE models

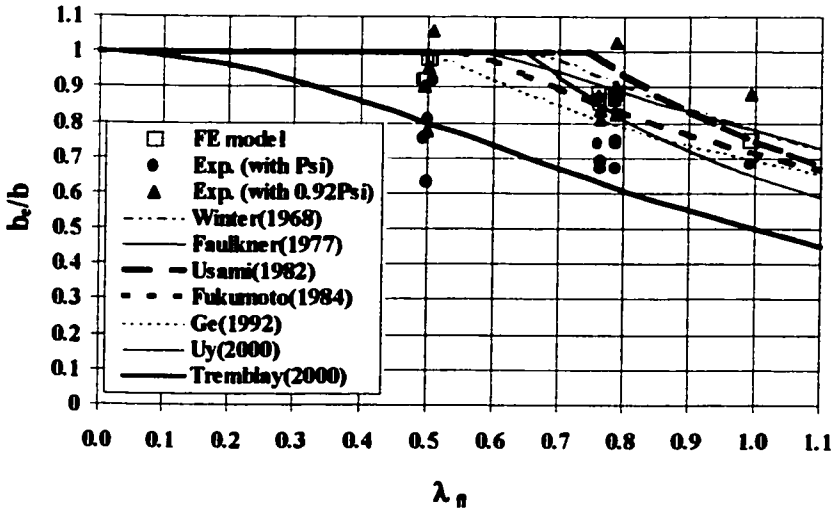

Fig. 12 Flange buckling capacity with plate slenderness

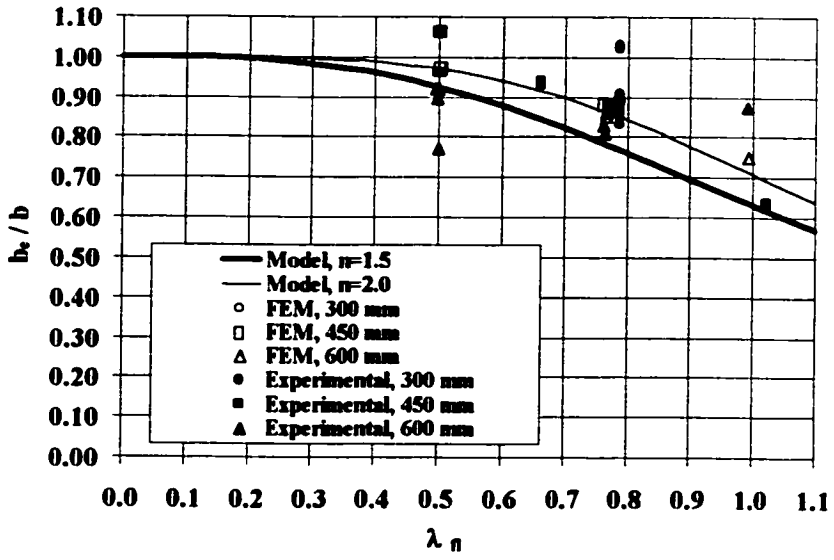

Fig. 13 Prediction model for flange effective width

Key words: composite column; built-up steel shape; local buckling; finite element models; materials behaviour; section capacity; design equations.

APPENDIX D – SAMPLE ABAQUS INPUT FILE

Input file for Specimen P-3, including local imperfections, residual stresses, and sequence of loading

```
*Heading
** Job name:P3 05
** Séquence de Chargement
** Avec défauts de rectitude et contraintes résiduelles
** Contenu édité pou impression / File edited for printing
** ----------------------------------------------------------------
**
** PART INSTANCE: rebar-HAUT
**
*System
          0.,         36.7,          300.,           1.,         36.7,
300.
*Node
       1,  -7.10543e-15,            0.
       2,       143.521,           0.
       3,        146.75,           0.
       4,       23.9202,           0.
       5,       47.8405,           0.
       6,       71.7607,           0.
       7,        95.681,           0.
       8,       119.601,           0.
       9,       145.136,           0.
      10,       11.9601,           0.
      11,       35.8804,           0.
      12,       59.8006,           0.
      13,       83.7209,           0.
      14,       107.641,           0.
      15,       131.561,           0.
*Element, type=B32
1,  1, 10,  4
2,  4, 11,  5
3,  5, 12,  6
4,  6, 13,  7
5,  7, 14,  8
6,  8, 15,  2
*Element, type=B32
7, 2, 9, 3
*Nset, nset=rebar-1._G4, generate
  1,  15,   1
*Elset, elset=rebar-1._G4, generate
 1,  7,  1
**
** SECTIONS
**
** Section: barre  Profile: armature
*Elset, elset=rebar-1._G4, generate
 1,  7,  1
*Beam Section, elset=rebar-1._G4, material=acier1, Section=rect
5.75,11.0
0,1,0
**
** PART INSTANCE: rebar-BAS
**
*System
```

```
          0.,         36.7,           0.,           1.,         36.7,
0.
*Node
      5001,  -7.10543e-15,            0.
      5002,       143.521,           0.
      5003,        146.75,           0.
      5004,       23.9202,           0.
      5005,       47.8405,           0.
      5006,       71.7607,           0.
      5007,        95.681,           0.
      5008,       119.601,           0.
      5009,       145.136,           0.
     5010,       11.9601,           0.
     5011,       35.8804,           0.
     5012,       59.8006,           0.
     5013,       83.7209,           0.
     5014,       107.641,           0.
     5015,       131.561,           0.
*Element, type=B32
5001,  5001, 5010,  5004
5002,  5004, 5011,  5005
5003,  5005, 5012,  5006
5004,  5006, 5013,  5007
5005,  5007, 5014,  5008
5006,  5008, 5015,  5002
*Element, type=B32
5007, 5002, 5009, 5003
*Nset, nset=rebar-1._G5000, generate
  5001,  5015,   1
*Elset, elset=rebar-1._G5000, generate
 5001,  5007,  1
** Section: barre  Profile: armature
*Beam Section, elset=rebar-1._G5000, material=acier1, Section=rect
5.75,11.0
0,1,0
** ----------------------------------------------------------------
**
** PART INSTANCE: aile-2
**
*System
      146.75,          0.,         75.,      146.75,          1.,
75.
      146.75, 4.73695e-17,         76.
*Node
     16,          150.,         -75.
     17,          150.,         -50.
     18,          150.,         -25.
     19,          150.,           0.
**********
    303,       18.3375,         200.
    304,            0.,        187.5
    305,       18.3375,         225.
    306,            0.,        212.5
*Element, type=S8R
```

```
 8,  16,  17,  30,  29, 120, 133, 134, 132
 9,  17,  18,  31,  30, 121, 135, 136, 133
10,  18,  19,  32,  31, 122, 137, 138, 135
11,  19,  20,  33,  32, 123, 139, 140, 137
**********
88, 102, 103, 116, 115, 275, 299, 300, 297
89, 103, 104, 117, 116, 277, 301, 302, 299
90, 104, 105, 118, 117, 279, 303, 304, 301
91, 105, 106, 119, 118, 281, 305, 306, 303
*Nset, nset=aile-2._G2, generate
  16,  306,    1
*Elset, elset=aile-2._G2, generate
  8,  91,   1
**
** SECTIONS
**
** Section: steel1
*Shell Section, elset=aile-2._G2, material=acier1, poisson=0.3
6.5, 5
** ----------------------------------------------------------------
**
** PART INSTANCE: ame-1
**
*System
          0.,         150.,         225.,           1.,         150.,
225.
          0.,         150.,         224.
*Node
    307,       146.75,         -75.
    308,       146.75,         -50.
    309,       146.75,         -25.
    310,       146.75,           0.
**********
    594,      11.9601,         200.
    595,           0.,        187.5
    596,      11.9601,         225.
    597,           0.,        212.5
*Element, type=S8R
 92, 307, 308, 321, 320, 411, 424, 425, 423
 93, 308, 309, 322, 321, 412, 426, 427, 424
 94, 309, 310, 323, 322, 413, 428, 429, 426
 95, 310, 311, 324, 323, 414, 430, 431, 428
**********
172, 393, 394, 407, 406, 566, 590, 591, 588
173, 394, 395, 408, 407, 568, 592, 593, 590
174, 395, 396, 409, 408, 570, 594, 595, 592
175, 396, 397, 410, 409, 572, 596, 597, 594
*Nset, nset=ame-1._G2, generate
 307,  597,    1
*Elset, elset=ame-1._G2, generate
  92,  175,    1
**
** SECTIONS
**
```

```
** Section: steel2
*Shell Section, elset=ame-1._G2, material=acier1,POISSON=0.3
3.25, 5
** ----------------------------------------------------------------
**
** PART INSTANCE: cube-1
**
*System
       215.3,      146.75,         300.,       215.3,      145.75,
300.
       214.3,      146.75,         300.
*Node
    598,       146.65,         71.8,           0.
    599,      146.667,       95.7167,          0.
    600,      146.683,       119.633,          0.
    601,        146.7,        143.55,          0.
**************************
   2911,       11.005,       191.383,         300.
   2912,           0.,         215.3,        287.5
   2913,           0.,       203.342,         300.
   2914,      11.0063,         215.3,         300.
*Element, type=C3D20R
176,  689,  690,  697,  696,  598,  599,  606,  605, 1398, 1412, 1413,
1410, 1235, 1242, 1243,
     1241, 1397, 1399, 1414, 1411
177,  690,  691,  698,  697,  599,  600,  607,  606, 1400, 1415, 1416,
1412, 1236, 1244, 1245,
     1242, 1399, 1401, 1417, 1414
178,  691,  692,  699,  698,  600,  601,  608,  607, 1402, 1418, 1419,
1415, 1237, 1246, 1247,
     1244, 1401, 1403, 1420, 1417
179,  692,  693,  700,  699,  601,  602,  609,  608, 1404, 1421, 1422,
1418, 1238, 1248, 1249,
     1246, 1403, 1405, 1423, 1420
************************
604, 1223, 1224, 1231, 1230, 1132, 1133, 1140, 1139, 2884, 2903, 2904,
2900, 2631, 2650, 2651,
     2647, 2882, 2885, 2905, 2902
605, 1224, 1225, 1232, 1231, 1133, 1134, 1141, 1140, 2887, 2906, 2907,
2903, 2634, 2653, 2654,
     2650, 2885, 2888, 2908, 2905
606, 1225, 1226, 1233, 1232, 1134, 1135, 1142, 1141, 2890, 2909, 2910,
2906, 2637, 2656, 2657,
     2653, 2888, 2891, 2911, 2908
607, 1226, 1227, 1234, 1233, 1135, 1136, 1143, 1142, 2893, 2912, 2913,
2909, 2640, 2659, 2660,
     2656, 2891, 2894, 2914, 2911
*Nset, nset=cube-1._G2, generate
  598,  2914,     1
*Elset, elset=cube-1._G2, generate
 176,  607,    1
**
** SECTIONS
**
```

```
** Section: concrete
*Solid Section, elset=cube-1._G2, material=beton
1.,
** *************** DEBUT DU BLOC INPUT
**
*System
*Nset, nset=BCSet_A
 1144, 1145, 1146, 1147, 1148, 1149, 1150, 1151, 1152, 1153, 1154,
1155, 1156, 1157, 1158, 1159
 1160, 1161, 1162, 1163, 1164, 1165, 1166, 1167, 1168, 1169, 1170,
1171, 1172, 1173, 1174, 1175
************************
2870, 2872, 2873, 2875, 2877, 2878, 2880, 2881, 2883, 2884, 2886, 2887,
2889, 2890, 2892, 2893
 2895, 2897, 2898, 2900, 2901, 2903, 2904, 2906, 2907, 2909, 2910,
2912, 2913
*Elset, elset=BCSet_A, generate
 536,  607,    1
*Nset, nset=BCSet_B
 1150, 1157, 1164, 1171, 1178, 1185, 1192, 1199, 1206, 1213, 1220,
1227, 1234, 2692, 2712, 2732
 2752, 2772, 2792, 2812, 2832, 2852, 2872, 2892, 2912
*Elset, elset=BCSet_B, generate
 541,  607,    6
*Nset, nset=BCSet_C
 1228, 1229, 1230, 1231, 1232, 1233, 1234, 2898, 2901, 2904, 2907,
2910, 2913
*Elset, elset=BCSet_C, generate
 602,  607,    1
*Nset, nset=BCSet_D
 1234,
*Nset, nset=BCSet_E
  688,  779,  870,  961, 1052, 1143, 1234, 1649, 1902, 2155, 2408,
2661, 2914
*Elset, elset=BCSet_E, generate
 247,  607,   72
*Nset, nset=BCSet_F
  604,  611,  618,  625,  632,  639,  646,  653,  660,  667,  674,
681,  688,  695,  702,  709
************************
 2794, 2812, 2814, 2832, 2834, 2852, 2854, 2872, 2874, 2892, 2894,
2912, 2914
*Elset, elset=BCSet_F, generate
 181,  607,    6
*Nset, nset=BCSet-G_ame, generate
 307,  597,    1
*Nset, nset=BCSet-G_aile
 17, 18, 19, 20, 21, 22, 23,24,25,26,27,28,120,
121,122,123,124,125,126,127,128,129,130,131
*Nset, nset=BCSet-G
BCSet-G_ame, BCSet-G_aile
*Elset, elset=BCSet-G, generate
  92,  175,    1
*Nset, nset=BCSet-H
```

```
 398, 399, 400, 401, 402, 403, 404, 405, 406, 407, 408, 409, 410, 575,
577, 579
 581, 583, 585, 587, 589, 591, 593, 595, 597
*Elset, elset=BCSet-H, generate
 164,  175,    1
*Nset, nset=BCSet_I
16,319,446, 332, 345, 358, 371, 384, 397, 410, 471, 496, 521, 546, 571,
596
*Elset, elset=BCSet_I, generate
 115,  175,   12
*Nset, nset=BCSet_J
 410,
*Nset, nset=BCSet_K
  28,155,41,  54,  67,  80,  93, 106, 119, 180, 205, 230, 255, 280, 305
*Elset, elset=BCSet_K, generate
 31,  91,  12
*Nset, nset=BCSet_L
  16,132,29,  42,  55,  68,  81,  94, 107, 157, 182, 207, 232, 257, 282
*Elset, elset=BCSet_L, generate
 20,  80,  12
*Nset, nset=BCSet_M
  682,  683,  684,  685,  686,  687,  688,  773,  774,  775,  776,
777,  778,  779,  864,  865
*****************************
2901, 2902, 2904, 2905, 2907
 2908, 2910, 2911, 2913, 2914
*Elset, elset=BCSet_M
 242, 243, 244, 245, 246, 247, 314, 315, 316, 317, 318, 319, 386, 387,
388, 389
 390, 391, 458, 459, 460, 461, 462, 463, 530, 531, 532, 533, 534, 535,
602, 603
 604, 605, 606, 607
*Nset, nset=BCSet_Nhaut
 1
*Nset, nset=BCSet_Nbas
 5001
*Nset, nset=Set_Rebar
  1,  2,  4,  5,  6,  7,  8, 10, 11, 12, 13, 14, 15
*Elset, elset=Set_Rebar, generate
 1,  6,  1
*Nset, nset=Set_Reb_Gap
 3,
*Nset, nset=Set_Cube_Face_Ame
 1144, 1145, 1146, 1147, 1148, 1149, 1150, 1151, 1152, 1153, 1154,
1155, 1156, 1157, 1158, 1159
*****************************
2887, 2889, 2890, 2892, 2893
 2895, 2897, 2898, 2900, 2901, 2903, 2904, 2906, 2907, 2909, 2910,
2912, 2913
*Elset, elset=Set_Cube_Face_Ame, generate
 536,  607,    1
*Nset, nset=Set_Cube_Face_Aile
  598,  605,  612,  619,  626,  633,  640,  647,  654,  661,  668,
675,  682,  689,  696,  703
```

```
**************************
2776, 2795, 2796, 2815, 2816, 2835, 2836, 2855, 2856, 2875, 2876, 2895,
2896
*Elset, elset=Set_Cube_Face_Aile, generate
 176,  602,    6
*Nset, nset=Set_Ame, generate
 307,  597,    1
*Elset, elset=Set_Ame, generate
  92,  175,    1
*Nset, nset=Set_Aile, generate
  16,  306,    1
*Elset, elset=Set_Aile, generate
  8,  91,   1
*Nset, nset=Set_Aile_Cote_Ame
  16,  17,  18,  19,  20,  21,  22,  23,  24,  25,  26,  27,  28, 120,
121, 122
 123, 124, 125, 126, 127, 128, 129, 130, 131
*Elset, elset=Set_Aile_Cote_Ame, generate
  8,  19,   1
*Nset, nset=Set_Ame_Cote_Aile
 307, 308, 309, 310, 311, 312, 313, 314, 315, 316, 317, 318, 319, 411,
412, 413
 414, 415, 416, 417, 418, 419, 420, 421, 422
*Elset, elset=Set_Ame_Cote_Aile, generate
  92,  103,    1
*Nset, nset=Set_Aile_Cote_Sup
  41,  54,  67,  80,  93, 106, 119, 180, 205, 230, 255, 280, 305
*Elset, elset=Set_Aile_Cote_Sup, generate
 31,  91,  12
*Nset, nset=Set_Ame_Cote_Sup
 320, 333, 346, 359, 372, 385, 398, 448, 473, 498, 523, 548, 573
*Elset, elset=Set_Ame_Cote_Sup, generate
 104,  164,   12
*Nset, nset=Set_Cube_Face_Sup
  598,  599,  600,  601,  602,  603,  604,  689,  690,  691,  692,
693,  694,  695,  780,  781
**************************
2665, 2666, 2667, 2668, 2669
 2670, 2671, 2672, 2673, 2674
*Elset, elset=Set_Cube_Face_Sup
 176, 177, 178, 179, 180, 181, 248, 249, 250, 251, 252, 253, 320, 321,
322, 323
 324, 325, 392, 393, 394, 395, 396, 397, 464, 465, 466, 467, 468, 469,
536, 537
 538, 539, 540, 541
*Nset, nset=_G194
 307,
**
**------------------------------ MATERIALS
**
*Material, name=acier1
*ELASTIC
200E3, 0.3
*PLASTIC
```

```
390,0
400, 0.015
500, 0.05
550, 0.15
500, 0.25
**
*Material, name=beton
*ELASTIC
27870, 0.18
*CONCRETE
12.74,0.000000
13.72,0.000008
17.81,0.000061
21.26,0.000137
24.13,0.000234
25.37,0.000290
27.46,0.000415
29.08,0.000556
30.29,0.000713
30.75,0.000796
30.95,0.000839
31.13,0.000883
31.28,0.000927
31.42,0.000973
31.64,0.001072
31.71,0.001112
31.77,0.001160
31.86,0.001327
31.81,0.001458
31.57,0.001667
31.38,0.001774
31.16,0.001882
31.05,0.001930
30.61,0.002102
30.29,0.002213
29.95,0.002325
29.58,0.002438
29.20,0.002552
28.81,0.002666
28.40,0.002781
27.98,0.002896
27.55,0.003011
27.12,0.003127
26.68,0.003243
26.24,0.003359
25.79,0.003474
25.35,0.003590
24.90,0.003706
24.46,0.003822
24.02,0.003938
23.59,0.004054
23.15,0.004169
**
*FAILURE RATIOS
```

```
1.16,0.09,1.27
*TENSION STIFFENING, TYPE=DISPLACEMENT
0.05
**
**
** ------------------ RESSORTS AILE/BETON
**
*ELEMENT,TYPE=SPRING2,ELSET=SPRINGS_VOILEMENT
1501,598,119
1502,1241,306
1503,605,118
1504,1254,304
**************************
1750,2875,136
1751,1221,30
1752,2895,134
1753,1228,29
**
*SPRING,ELSET=SPRINGS_VOILEMENT,nonlinear
1,1
-1e-5,-1
-1e-4,-1e-4
0.0,0.0
1,1e-4
100,1e-2
1e5,1
**
******************************** COUPLAGE DE l'AME ET DU BETON
*ELEMENT,TYPE=SPRING2,ELSET=SPRINGS_AME
7001,1144,320
7002,2663,448
7003,1145,333
7004,2665,473
**************************
7250,2910,571
7251,1233,397
7252,2913,596
7253,1234,410
**
*SPRING,ELSET=SPRINGS_AME,nonlinear
1,1
-1e12,-1
0.0,0.0
1e12,1
**
************************************************************************
COUPLAGE DE L'AILE et de L'AME A LA SOUDURE
**
*ELEMENT,TYPE=SPRING2,ELSET=SPRINGS_ame_aile11
6000,28,307
6001,131,411
6002,27,308
6003,130,412
**********************
```

```
6021,121,421
6022,17,318
6023,120,422
6024,16,319
**
*SPRING,ELSET=SPRINGS_ame_aile11,nonlinear
1,1
-1e12,-1
0.0,0.0
1e12,1
**
**
*ELEMENT,TYPE=SPRING2,ELSET=SPRINGS_ame_aile33
6101,131,411
6102,27,308
6103,130,412
6104,26,309
6105,129,413
6106,25,310
6107,128,414
6108,24,311
6109,127,415
6110,23,312
6111,126,416
6112,22,313
6113,125,417
6114,21,314
6115,124,418
6116,20,315
6117,123,419
6118,19,316
6119,122,420
6120,18,317
6121,121,421
6122,17,318
6123,120,422
**
*SPRING,ELSET=SPRINGS_ame_aile33,nonlinear
3,3
-1e12,-1
0.0,0.0
1e12,1
**
**********************************************************************
COUPLAGE DU LIEN / AILE : DIR33
*ELEMENT,TYPE=SPRING2,ELSET=SPRINGS_lien_haut33
3101,1,80
3102,10,80
3103,4,80
3104,11,80
3105,5,80
3106,12,80
3107,6,80
3108,13,80
```

```
3109,7,80
3110,14,80
3111,8,80
3112,15,80
3113,2,80
3114,9,80
**
*SPRING,ELSET=SPRINGS_lien_haut33,nonlinear
3,3
-1e12,-1
0.0,0.0
1e12,1
**
**************************************************************************
COUPLAGE DU LIEN / AILE : DIR22
*ELEMENT,TYPE=SPRING2,ELSET=SPRINGS_LIENS_AILE22
3601,5001,94
3602,5010,94
3603,5004,94
3604,5011,94
3605,5005,94
3606,5012,94
3607,5006,94
3608,5013,94
3609,5007,94
3610,5014,94
3611,5008,94
3612,5015,94
3613,5002,94
3614,5009,94
**
3501,1,106
3502,10,106
3503,4,106
3504,11,106
3505,5,106
3506,12,106
3507,6,106
3508,13,106
3509,7,106
3510,14,106
3511,8,106
3512,15,106
3513,2,106
3516,9,106
**
*SPRING,ELSET=SPRINGS_LIENS_AILE22,nonlinear
2,2
-1e12,-1
0.0,0.0
1e12,1
**
**************************************************************************
*** COUPLAGE LIEN / AILE a la soudure: 11 a 66
```

```
**
*ELEMENT,TYPE=SPRING2,ELSET=SPRINGS_LIENHAUT_AILE11
3301,3,106
*SPRING,ELSET=SPRINGS_LIENHAUT_AILE11,nonlinear
1,1
-1e12,-1
0.0,0.0
1e12,1
**
*ELEMENT,TYPE=SPRING2,ELSET=SPRINGS_LIENHAUT_AILE22
3302,3,106
*SPRING,ELSET=SPRINGS_LIENHAUT_AILE22,nonlinear
2,2
-1e12,-1
0.0,0.0
1e12,1
**
*ELEMENT,TYPE=SPRING2,ELSET=SPRINGS_LIENHAUT_AILE33
3303,3,106
*SPRING,ELSET=SPRINGS_LIENHAUT_AILE33,nonlinear
3,3
-1e12,-1
0.0,0.0
1e12,1
**
*ELEMENT,TYPE=SPRING2,ELSET=SPRINGS_LIENHAUT_AILE44
3304,3,106
*SPRING,ELSET=SPRINGS_LIENHAUT_AILE44,nonlinear
4,4
-1e12,-1
0.0,0.0
1e12,1
**
*ELEMENT,TYPE=SPRING2,ELSET=SPRINGS_LIENHAUT_AILE55
3305,3,106
*SPRING,ELSET=SPRINGS_LIENHAUT_AILE55,nonlinear
5,5
-1e12,-1
0.0,0.0
1e12,1
**
*ELEMENT,TYPE=SPRING2,ELSET=SPRINGS_LIENHAUT_AILE66
3306,3,106
*SPRING,ELSET=SPRINGS_LIENHAUT_AILE66,nonlinear
6,6
-1e12,-1
0.0,0.0
1e12,1
**
**
**
*ELEMENT,TYPE=SPRING2,ELSET=SPRINGS_LIENBAS_AILE11
3401,5003,94
*SPRING,ELSET=SPRINGS_LIENBAS_AILE11,nonlinear
```

```
1,1
-1e12,-1
0.0,0.0
1e12,1
**
*ELEMENT,TYPE=SPRING2,ELSET=SPRINGS_LIENBAS_AILE22
3402,5003,94
*SPRING,ELSET=SPRINGS_LIENBAS_AILE22,nonlinear
2,2
-1e12,-1
0.0,0.0
1e12,1
**
*ELEMENT,TYPE=SPRING2,ELSET=SPRINGS_LIENBAS_AILE33
3403,5003,94
*SPRING,ELSET=SPRINGS_LIENBAS_AILE33,nonlinear
3,3
-1e12,-1
0.0,0.0
1e12,1
**
**
*ELEMENT,TYPE=SPRING2,ELSET=SPRINGS_LIENBAS_AILE44
3404,5003,94
*SPRING,ELSET=SPRINGS_LIENBAS_AILE44,nonlinear
4,4
-1e12,-1
0.0,0.0
1e12,1
**
*ELEMENT,TYPE=SPRING2,ELSET=SPRINGS_LIENBAS_AILE55
3405,5003,94
*SPRING,ELSET=SPRINGS_LIENBAS_AILE55,nonlinear
5,5
-1e12,-1
0.0,0.0
1e12,1
**
*ELEMENT,TYPE=SPRING2,ELSET=SPRINGS_LIENBAS_AILE66
3406,5003,94
*SPRING,ELSET=SPRINGS_LIENBAS_AILE66,nonlinear
6,6
-1e12,-1
0.0,0.0
1e12,1
**
**********************************************************************
COUPLAGE DU LIEN ET DU BETON : DIR 11
**
*ELEMENT,TYPE=SPRING2,ELSET=SPRINGS_lien_haut11
3001,1,695
3002,10,1408
3003,4,694
3004,11,1406
```

```
3005,5,693
3006,12,1404
3007,6,692
3008,13,1402
3009,7,691
3010,14,1400
3011,8,690
3012,15,1398
3013,2,689
**
*SPRING,ELSET=SPRINGS_lien_haut11,nonlinear
1,1
-1e12,-1
0.0,0.0
1e12,1
**
**
*ELEMENT,TYPE=SPRING2,ELSET=SPRINGS_lien_bas11
3201,5001,779
3202,5010,1648
3203,5004,778
3204,5011,1645
3205,5005,777
3206,5012,1642
3207,5006,776
3208,5013,1639
3209,5007,775
3210,5014,1636
3211,5008,774
3212,5015,1633
3213,5002,773
**
*SPRING,ELSET=SPRINGS_lien_bas11,nonlinear
1,1
-1e12,-1
0.0,0.0
1e12,1
**
**
**------------------ SUPPL. BOUNDARY COND.
*Boundary
cube-1._G2,4,6
**
** BC: BC-A Type: Displacement
*Boundary
BCSet_A, 2, 2
** BC: BC-B Type: Displacement
*Boundary
BCSet_B, 1, 1
BCSet_B, 2, 2
** BC: BC-C Type: Displacement
*Boundary
BCSet_C, 2, 2
BCSet_C, 3, 3
```

```
** BC: BC-D Type: Displacement
*Boundary
BCSet_D, 1, 1
BCSet_D, 2, 2
BCSet_D, 3, 3
** BC: BC-E Type: Displacement
*Boundary
BCSet_E, 1, 1
BCSet_E, 3, 3
** BC: BC-F Type: Displacement
*Boundary
BCSet_F, 1, 1
** BC: BC-G Type: Displacement
*Boundary
BCSet-G, 2, 2
BCSet-G, 4, 4
BCSet-G, 5, 5
BCSet-G, 6, 6
** BC: BC-H Type: Displacement
*Boundary
BCSet-H, 1, 1
BCSet-H, 2, 2
BCSet-H, 4, 4
BCSet-H, 5, 5
BCSet-H, 6, 6
** BC: BC-I Type: Displacement
*Boundary
BCSet_I, 2, 2
BCSet_I, 3, 3
BCSet_I, 4, 4
BCSet_I, 5, 5
BCSet_I, 6, 6
** BC: BC-J Type: Displacement
*Boundary
BCSet_J, 1, 1
BCSet_J, 2, 2
BCSet_J, 3, 3
BCSet_J, 4, 4
BCSet_J, 5, 5
BCSet_J, 6, 6
** BC: BC-K Type: Displacement
*Boundary
BCSet_K, 4, 4
BCSet_K, 5, 5
**BCSet_K, 6, 6
** BC: BC-L Type: Displacement
*Boundary
BCSet_L, 3, 3
BCSet_L, 4, 4
BCSet_L, 5, 5
**BCSet_L, 6, 6
** BC: BC-M Type: Displacement
*Boundary
BCSet_M, 3, 3
```

```
rebar-1._G5000,3,3
** BC: BC-N Type: Displacement
*Boundary
BCSet_Nhaut, 1, 1
BCSet_Nhaut, 4, 4
BCSet_Nhaut, 5, 5
BCSet_Nhaut, 6, 6
*Boundary
BCSet_Nbas, 1, 1
BCSet_Nbas, 3, 3
BCSet_Nbas, 4, 4
BCSet_Nbas, 5, 5
BCSet_Nbas, 6, 6
**
*Boundary
rebar-1._G4,4,5
rebar-1._G5000,4,5
**
**
**----------------------------couplage sommet
**
*Nset, nset=Set_Cube_Face_Sup3
  598,  599,  600,  601,  602,  603,  689,  690,  691,  692,  693,
694,  780,  781
  782,  783,  784,  785,  871,  872,  873,  875,  876,  962,  963,
**************************
 2414, 2415, 2416, 2417, 2418, 2419, 2420, 2662, 2664, 2666, 2668,
 2670, 2672,
**874
**
*KINEMATIC COUPLING,REF NODE=874
Set_Cube_Face_Sup3,3
**
*ELEMENT,TYPE=SPRING2,ELSET=SPRINGS_beton33
8001,874,1144
8002,874,1145
8003,874,1146
8004,874,1147
8005,874,1148
8006,874,1149
8007,874,1150
8008,874,2663
8009,874,2665
8010,874,2667
8011,874,2669
8012,874,2671
8013,874,2673
8014,874,1059
8015,874,968
8016,874,877
8017,874,786
8018,874,695
8019,874,604
8020,874,2674
```

```
8021,874,2421
8022,874,2168
8023,874,1915
8024,874,1662
8025,874,1409
**
*SPRING,ELSET=SPRINGS_beton33,nonlinear
3,3
-1e12,-1
0.0,0.0
1e12,1
**
*ELEMENT,TYPE=SPRING2,ELSET=SPRINGS_acier33
8101,80,28
8102,80,155
8103,80,41
8104,80,180
8105,80,54
8106,80,205
8107,80,67
8108,80,230
8109,80,359
8110,80,255
8111,80,93
8112,80,280
8113,80,106
8114,80,305
8115,80,119
8116,80,307
8117,80,423
8118,80,320
8119,80,448
8120,80,333
8121,80,473
8122,80,346
8123,80,498
8124,80,523
8125,80,372
8126,80,548
8127,80,385
8128,80,573
8129,80,398
**
*SPRING,ELSET=SPRINGS_acier33,nonlinear
3,3
-1e12,-1
0.0,0.0
1e12,1
**
**
*ELEMENT,TYPE=SPRING2,ELSET=SPRINGS_TOP33
8200,80,874
**
*SPRING,ELSET=SPRINGS_TOP33,nonlinear
```

```
3,3
-1e12,-1
0.0,0.0
1e12,1
**
** ------------------------- IMPERFECTIONS
**
*IMPERFECTION,  file=P1_ac_03buk, step=2
1, 0.35
**
**--------------------------INITIAL CONDITIONS
*INITIAL CONDITIONS,TYPE=STRESS,USER
**
** ---------------------------STEP: Step-1
**
*STEP
remove elements
*STATIC
*MODEL CHANGE,REMOVE
**aile-2._G2,
**SPRINGS_acier33,
**
**rebar-1._G4,rebar-1._G5000,
**SPRINGS_lien_haut33,SPRINGS_LIENS_AILE22,
**SPRINGS_LIENHAUT_AILE11,SPRINGS_LIENHAUT_AILE22,SPRINGS_LIENHAUT_AILE
33,
**SPRINGS_LIENHAUT_AILE44,SPRINGS_LIENHAUT_AILE55,SPRINGS_LIENHAUT_AILE
66,
**SPRINGS_LIENBAS_AILE11,SPRINGS_LIENBAS_AILE22,SPRINGS_LIENBAS_AILE33,
**SPRINGS_LIENBAS_AILE44,SPRINGS_LIENBAS_AILE55,SPRINGS_LIENBAS_AILE66,
**
**ame-1._G2,
**SPRINGS_ame_aile11,SPRINGS_ame_aile33,
**
**cube-1._G2,SPRINGS_beton33,
SPRINGS_AME,
SPRINGS_voilement,
SPRINGS_lien_bas11,SPRINGS_lien_haut11,
SPRINGS_TOP33,
**
** OUTPUT REQUESTS
**
*Restart, write, frequency=1
*El Print, frequency=1,POSITION=AVERAGED AT NODES
1,2,3,4,5
S11,s22,s33,e11,e22,e33
*End Step
**
**
*STEP,nlgeom,INC=2
loading step1
*static
1,1
*Cload
```

```
80, 3, -238e3
**
**
** OUTPUT REQUESTS
**
*Restart, write, frequency=1
*El Print, frequency=1,POSITION=AVERAGED AT NODES
1,2,3,4,5
S11,s22,s33,mises,e11,e22,e33
*node print, totals=yes, nset=rebar-1._G4
*node print, totals=yes, nset=rebar-1._G5000
*node print, totals=yes, nset=aile-2._G2
*node print, totals=yes, nset=ame-1._G2
*node print, totals=yes, nset=cube-1._G2
*End Step
**
**
**
*STEP
add elements
*STATIC
*MODEL CHANGE,ADD
**aile-2._G2,
**SPRINGS_acier33,
**
**rebar-1._G4,rebar-1._G5000,
**SPRINGS_lien_haut33,SPRINGS_LIENS_AILE22,
**SPRINGS_LIENHAUT_AILE11,SPRINGS_LIENHAUT_AILE22,SPRINGS_LIENHAUT_AILE
33,
**SPRINGS_LIENHAUT_AILE44,SPRINGS_LIENHAUT_AILE55,SPRINGS_LIENHAUT_AILE
66,
**SPRINGS_LIENBAS_AILE11,SPRINGS_LIENBAS_AILE22,SPRINGS_LIENBAS_AILE33,
**SPRINGS_LIENBAS_AILE44,SPRINGS_LIENBAS_AILE55,SPRINGS_LIENBAS_AILE66,
**
**ame-1._G2,
**SPRINGS_ame_aile11,SPRINGS_ame_aile33,
**
**cube-1._G2,SPRINGS_beton33,
SPRINGS_AME,
SPRINGS_voilement,
SPRINGS_lien_bas11,SPRINGS_lien_haut11,
SPRINGS_TOP33,
**
** OUTPUT REQUESTS
**
*Restart, write, frequency=1
*El Print, frequency=1,POSITION=AVERAGED AT NODES
1,2,3,4,5
S11,s22,s33,e11,e22,e33
*End Step
**
**
**
*STEP,nlgeom,INC=2
```

```
loading step2
*static
1,1
*Cload
67, 3, -214e3
**
**
** OUTPUT REQUESTS
**
*Restart, write, frequency=1
*El Print, frequency=1,POSITION=AVERAGED AT NODES
1,2,3,4,5
S11,s22,s33,mises,e11,e22,e33
*node print, totals=yes, nset=rebar-1._G4
*node print, totals=yes, nset=rebar-1._G5000
*node print, totals=yes, nset=aile-2._G2
*node print, totals=yes, nset=ame-1._G2
*node print, totals=yes, nset=cube-1._G2
*End Step
**
**
**
*STEP,NLGEOM,INC=20
loading step3
*static,riks
0.1,1
*Cload
93, 3, -784e3
**
**
** OUTPUT REQUESTS
**
*Restart, write, frequency=1
*El Print, frequency=1,POSITION=AVERAGED AT NODES
1,2,3,4,5
S11,s22,s33,mises,e11,e22,e33
*node print, totals=yes, nset=rebar-1._G4
*node print, totals=yes, nset=rebar-1._G5000
*node print, totals=yes, nset=aile-2._G2
*node print, totals=yes, nset=ame-1._G2
*node print, totals=yes, nset=cube-1._G2
*End Step
**
**
*USER SUBROUTINES
      SUBROUTINE SIGINI(SIGMA,COORDS,NTENS,NCRDS,NOEL,NPT,LAYER,
     1 KSPT,LREBAR,REBARN)
C
      INCLUDE 'ABA_PARAM.INC'
C
      DIMENSION SIGMA(NTENS),COORDS(NCRDS),RES(4),VAL(28)
      INTEGER COL
      CHARACTER*8 REBARN
C
```

```
      VAL(1) =10
      VAL(2) =10
      VAL(3) =-80.2
      VAL(4) =-80.2
      VAL(5) =-100.8
      VAL(6) =-100.8
      VAL(7) =-92
      VAL(8) =-92
      VAL(9) =65.2
      VAL(10) =65.2
      VAL(11) =139.8
      VAL(12) =139.8
      VAL(13) =304.1
      VAL(14) =304.1
      VAL(15) =0
      VAL(16) =0
      VAL(17) =304.1
      VAL(18) =304.1
      VAL(19) =-32
      VAL(20) =-32
      VAL(21) =-64.8
      VAL(22) =-64.8
      VAL(23) =-70.7
      VAL(24) =-70.7
      VAL(25) =-65.3
      VAL(26) =-65.3
      VAL(27) =-60
      VAL(28) =-60
      IF((NOEL .GE. 8).AND.(NOEL .LE. 91)) THEN
         DO 100 I=1,3
           SIGMA(I) = 0.0
100      CONTINUE
         COL = 7 - (NOEL - 8)/12
         RES(1) = VAL (2*COL-1)
         RES(2) = VAL (2*COL)
         RES(3) = VAL (2*COL-1)
         RES(4) = VAL (2*COL)
         DO 110 J=1,4
            IF (NPT .EQ. J) THEN
               SIGMA(1) = RES(J)
            ENDIF
110      CONTINUE
         WRITE (6,1000) NOEL,NPT,(SIGMA(K),K=1,3)
      ENDIF
      IF((NOEL .GE. 92).AND.(NOEL .LE. 175)) THEN
         DO 120 I=1,3
           SIGMA(I) = 0.0
120      CONTINUE
         COL = 8 + (NOEL - 92)/12
         RES(1) = VAL (2*COL-1)
         RES(2) = VAL (2*COL)
         RES(3) = VAL (2*COL-1)
         RES(4) = VAL (2*COL)
         DO 130 Z=1,4
```

```
            IF (NPT .EQ. Z) THEN
               SIGMA(2) = RES(Z)
            ENDIF
130       CONTINUE
          WRITE (6,1000) NOEL,NPT,(SIGMA(K),K=1,3)
1000      FORMAT (T5,'NOEL,NPT:',2I10,3F10.3)
      ENDIF
C
      RETURN
      END
************************** FIN DU BLOC INPUT
```